BOLLETTINO DI GEOFISICA TEORICA ED APPLICATA VOL. 41, N. 3-4, PP. 243-313; SEP.-DEC. 2000

Formalized representation of isoseismal uncertainty for Italian earthquakes

T.L. KRONROD[1,2], G.M. MOLCHAN[1,2], V.M. PODGAETSKAYA[1] and G.F. PANZA[2,3]

[1] *International Institute of Earthquake Prediction Theory and Mathematical Geophysics, Russian Academy of Sciences, Moscow, Russia*
[2] *The Abdus Salam International Centre for theoretical Physics, SAND Group, Trieste, Italy*
[3] *Department of Earth Sciences, University of Trieste, Italy*

(Received February 23, 2001; accepted November 28, 2001)

Abstract - A unique macroseismic data base, in the form of Intensity Data Point (IDP) maps, is available for some of the seismic events which have occurred in Italy since 461 A.C. The problem of the reconstruction of the isoseismal shape imposes rigorous requirements on the quality of intensity data. We present here a collection of 55 IDP maps in isolines which, to various degrees, meet our quality requirements to analyze the shape problem. Our generalization of an IDP map in isolines is unconventional, and is based on the new approach. The methodology, along with the smoothing method for IDP maps (Modified Polynomial Filtering, MPF), uses the Diffused Boundary (DB) method, which visualizes the uncertainty of isoseismal boundaries. We define a quantitative measure of the isoseismal uncertainty and classify the isoseismals for all selected events. The presented collection of isoseismals can be used for comparison between observed and theoretical isoseismals. This comparison involves simultaneous testing of crustal and source models. The collection gives a sufficiently accurate idea of the quality of the isoseismals of Italian earthquakes; it can be useful for space local control of the intensity measurements as well.

1. Introduction

Macroseismic data, Intensity Data Point (IDP) maps, are essential for analyses and calculations of the seismic hazard. Compared to instrumental observations used for the purpose, they cover a larger area and a longer record of damaging seismic events. The situation in Italy is unique in this respect. Here, two macroseismic data bases are now available: CFTI by Boschi et

Corresponding author: T.L. Kronrod; International Institute of Earthquake Prediction Theory, Warshavskoe sh., 79, k.2 Moscow 113556, Russia; e-mail: kronrod@mitp.ru

al. (1997, 2000) and DOM by Monachesi and Stucchi (1997). The first data base, CFTI-2 (1997), contains 31 000 intensity data for 460 earthquakes from 461 A.C. to 1990, the second one contains more than 37 000 intensity data for 904 earthquakes from 950 to 1980.

Macroseismic data are used to derive quantitative information on earthquake source parameters, namely, magnitude, the length and orientation of the source for large magnitude events (see, e.g., Karnik, 1969; Shebalin, 1972; Johnston, 1996; Gasperini et al., 1999; Sirovich and Pettenati, 1999). When used for seismic hazard purposes, macroseismic data can yield regional correlation equations connecting intensity of shaking I, magnitude M and the logarithm of the hypocentral distance D (macroseismic mean field equation in the terminology of Shebalin, (1972). The result is an average intensity field I(g) having circular or oval (for extended sources) isoseismals (see, e.g., Gusev and Shumilina, 2000). The isolines of actual intensity maps, as seen in regional atlases and journal papers, are much more complex. The generalization of IDP maps is certainly affected by the data processing methods or by the author's preconceptions, the noise presented in the data, and the site effects. However, these are not the only differences between the actual I-maps and (I, M, D)-relations, as shown by specific examples (Molchan et al., 2002) and indirectly by synthetic isoseismals. Engineering work relies on peak characteristics of the wave field in the period range 1-10 s expressed in terms of displacement, velocity or acceleration (call it A(g)). Theoretical calculations of these characteristics derived by normal mode summation (Panza, 1985; Florsch et al., 1991) corroborate that the isolines of A(g) have complex shapes in the zone near the source (within 200 km). Depending on the source mechanism, they may have 2 to 4 lobes (Panza et al., 1991). Burger et al. (1987) show a partial violation of the monotone behaviour in the peak acceleration field at distances of 60-120 km from the earthquake source due to the competitive effect of direct S waves and those post-critically reflected at the Moho.

The relation between I(g) and theoretical fields A(g) is not quite clear. For their comparisons, in addition to parameters of the mean field, one consistency criterion could be the shape similarity between A and I. For this reason we produce a collection of IDP maps in a form that would make it possible to draw inferences about the shape of at least a single isoseismal of I(g) at $I > \mathrm{IV}$ level. We propose to not deal with the first isoseismals, because A(g) fields are poorly modelled near the epicenter, neither at the periphery with high rank isoseismals $\mathrm{R} = I_0 - I$ (I_0 is the epicentral intensity), because they degenerate into ovals of little informational value.

We thus come to the following problem: how can one see the shape of an isoseismal in an IDP map? Two methods have been developed to deal with the problem (Molchan et al., 2002); they are briefly explained in the body of the paper. The first (MPF) is one of the averaging techniques applied to IDP maps and is a modification of the so-called local polynomial filtering method put forward by De Rubeis et al. (1992) and Tosi et al. (1995). The modification was designed to control the local maximum error in the filtered I-data and to take into account the spatial distribution of site-intensity pairs (IDP). The MPF method reduces the noise component in the data, but smoothes the isoseismal shape. Similar to any smoothing technique, it does not carry any information about the local uncertainty of an isoseismal, while this is essential for the comparisons between theoretical continuous fields with the discrete-value observations. These difficulties are overcome by the second, the Diffused Boundary (DB) method. The DB method

constructs an isoline as a boundary zone of variable width that reflects the local uncertainty of the relevant isoline. The relative contribution of the boundary zone to the total area of the isoseismal is an integral parameter that characterizes the quality of the isoseismal boundary. For this reason, we are using this quantity to derive a 5-unit classification of isolines, the first class corresponding to the highest quality.

In the present study, we selected 55 earthquakes from the CFTI-2 and DOM data bases. Their spatial distribution and the parameters (date, location, magnitude, and the number of intensity data) are given in Appendix. The intensity maps in isolines obtained by the MPF and DB methods make up Appendix. Because of the difficulties related to a black-and-white representation of DB isoseismals, Appendix contains, as a rule, the best isoseismals (classes 1 to 4). The selection of events has also been influenced by our own requirements on the quality of isoseismals and the publication limits. Naturally, this collection can be expanded or reduced depending on our objectives. To guarantee the reproducibility of the results obtained from intensity maps, we specify all the parameters of the MPF and DB methods that are not universal.

Whatever the goals we aim to achieve are, the maps presented in Appendix B provide an idea of the uncertainty of the isoseismals of good quality for Italy. Mapping the uncertainty is a new element in the presentation of macroseismic data. The first attempt to use MPF, DB and synthetic isoseismals for the analysis of isoseismal shape can be found in Molchan et al. (2002).

2. Smoothing technique: MPF method

The generalization of IDP maps should take into account the following features present in macroseismic data: the measurement sites form an irregular set of points that depends on the distribution of the population in the area; the observed I values involve a noise component, which is due to the statistical nature of intensity, to the measurement errors and to local effects; intensity scales are discrete. To reduce the noise component in the observations De Rubeis et al. (1992) suggested a smoothing procedure, specifically, the local polynomial filtering (PF). This method is based on the assumption that the macroseismic field can be well fitted locally with a polynomial of degree two, $P_2(g)$. The fit of the field at a given point g_0 is found by considering a circle $B(g_0,R)$ centred at g_0 and having radius R. If $P_2(g)$ approximates the I-data in $B(g_0,R)$ with minimal squared error, then the polynomial at the center of the circle is taken to be the desired estimate $\hat{I}(g_0)$ of the intensity field at g_0. It is usually assumed that an isoseismal of level I is an external contour enclosing areas of reliably determined intensities I. Therefore, the area where $\hat{I}(g) \geq I-\Delta I/2$ is regarded herein after as the isoseismal of level I, ΔI being the discretization interval of the intensity scale. The PF method involves a constant radius R, which is a parameter to be estimated. When the measurement sites are distributed uniformly, the decision to do so is natural. However, it is not the case for the actual density of observations. As a result, complex segments of an isoseismal boundary well constrained by data will be unjustifiably oversmoothed by the PF method.

Therefore, the smoothing parameter R in the Modified PF method is variable and it is adapted to the local structure of the intensity data. This is done as follows. The field $\hat{I}(g)$ is

computed on a grid with step $\Delta g = 3 \div 5$ km. For every point g_0 of the grid the radius R is chosen within the set $\{R_k = kd,\ k \geq 1\}$ with the condition $R \leq \overline{R} = min\ (D/4, R_0)$, where D is the diameter of the set of all measurement sites and R_0 is a regional parameter. In particular, $R_0 = 70$ km and $d = 10$ km for the events considered here ($d = \Delta g$ is better). We will try values of R_k in increasing order. To control the upper bound of the variance of the random component in the estimate of $\hat{I}(g)$ we find the first area $B(g_0,R)$ that contains at least $n_p = 6$ m observation sites; m is the average number of measurements per each unknown coefficient of the polynomial $P_2(g)$. Typically, $m = 2 \div 4$ and $n_p = 12 \div 24$. If the n_p–condition is not fulfilled for the largest $R = \overline{R}$, the point g_0 is not considered.

Bearing in mind that I takes discrete values, in each intensity zone of constant level it is natural to take R as large as possible. For this reason we impose the extra requirement that the number of different intensity values in the circle $B(g_0,R)$ should not be below a threshold $n_I > 1$. The value of the threshold n_I depends on the noise level in the intensity data; here we used $n_I = 3$. Near the epicenter, where the deterministic component of the intensity field is rapidly varying, the n_I-restriction is very likely to be satisfied for small R. At the periphery of an IDP map, the n_I-restriction makes R larger. This restriction is removed, once R has reached its limiting value $\overline{R}$.

An obvious bias in the estimates of the local trend of $P_2(g)$ occurs at the periphery of an IDP map where the observation sites that occur in the area $B(g_0, R)$ are seen from g_0 at an angle $\varphi < 180°$. Then g_0 is a point where the field $I(g)$ has to be extrapolated, i.e., it is a location where the fit $P_2(g_0)$ is not constrained by observations. An additional threshold for the angle φ, $\varphi \geq \varphi_0$, is then used to exclude such effects. This increases the radius R and, if the value $\overline{R}$ is exceeded, the point is not considered; for our collection $\varphi_0 = 200°$.

Overall, the merit of the MPF technique is that it does not involve a priori restrictions on the shape and connectedness of the isoseismals; it partly suppresses the noise and local perturbations in the observations and takes into account the space distribution of measurement sites. The use of filtering techniques is natural with respect to continuous fields. But the intensity takes integer values, in our case in the range from III to IX, and there may be only 2 or 3 different values in the vicinity of the boundary between two intensities. Therefore, the initial assumption that the intensity field can be well fitted with a polynomial is violated near intensity boundaries. As a result, the interpretation of the shape of isoseismals remains problematical owing to the possible smoothing-out of details. One then needs additional methods that would incorporate the local uncertainty of the isoseismals.

3. Diffused Boundary (DB) method

The analysis of the shape of an isoseismal requires the visualization of its local uncertainty. Speaking in terms of mathematical statistics, we have to replace a point estimation of an isoline by interval estimation. The local thickness or uncertainty of an isoline must depend on the local geometry of the measurement sites and on the noise component the data involved. Our solution essentially relies on the fact that the intensity scale is discrete. We assume that the isoseismal

zones of level I, G_I, are simply connected and monotonic. The connectedness assumption is not absolutely indispensable, as we shall see.

To explain the principles of the DB concept let us start from the one-dimensional case of intensity data. Isoseismals on a line make a set of embedded intervals with intensity $\geq I$, that are increasing with decreasing I. For a given intensity level, we must separate points of two types on the line: "+" with intensity $\geq I$ and "0" with intensity $< I$ (Fig. 1a). When the observations are error-free, a cluster of pluses lies between two clusters of zeroes. (By a cluster on a line we mean a nonempty sequence of identical characters that cannot be expanded without adding a different character.) The true boundary of level I is covered by two intervals, Δ_- and Δ_+, that separate the clusters and supply all available information on the boundary uncertainty, no smoothing techniques being able to improve the boundary between "+" and "0".

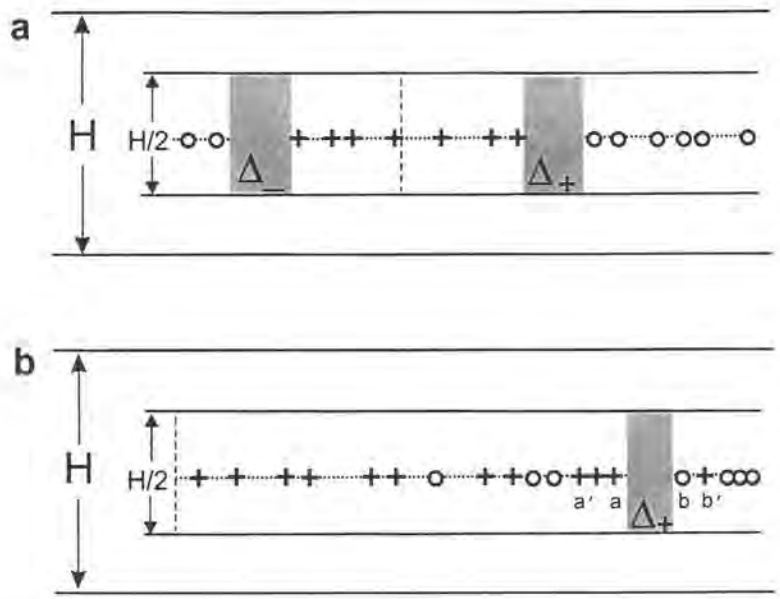

Fig. 1 - Illustration of the DB method: (a) Local Diffused Boundary (LDB) (shadow zone) for the data without noise. Dashed and dotted lines are the axes of the strip; (b) the same as in (a) for noisy data.

When intensity observations contain noise, the pattern is more complex: some pluses percolate into the zeroes zone and conversely (see Fig. 1b). For simplicity Fig. 1b presents only the right semi-axis which starts from the barycenter of the pluses. In view of possible errors in the observations we allow some pluses, up to the amount $\varepsilon\%$ of the total number of pluses on the semiaxis, to be considered as erroneous. Keeping in mind the definition of isoseismals (see previous section), we are primarily interested in the outer boundary of pluses. For this reason, the first candidates to be classified as erroneous will be those pluses farthest from the center. Under these new conditions the interval, say Δ_+, is specified uniquely by the following requirements. It is the interval (a, b) which separates the pluses cluster contained in the interval [a', a] and the zeroes cluster contained in the interval [b, b') (see Fig.1b). We assume that $I(\infty) = 0$, so that the point "∞" always belongs to the set of measurements, and we require that in

the interval (a, ∞) the number of pluses is ≤ ε% of all pluses on the semiaxis, and > ε% in the interval [a', ∞).

Let us consider the example shown in Fig. 1b. Here two pluses of the twelve available, marked with arrows, could be removed at the level ε = 20%. We remove only one plus (the rightmost one) because the other belongs to a cluster (a', a) containing 3 pluses and can be removed only together with the cluster. The removal of the cluster (3 pluses) violates our rule on the Δ-threshold since (1 + 3) / 12 > 20%. The resulting boundary Δ_+ is shown in Fig. 1b. Thus, a distant cluster of pluses cannot be classified as erroneous, unless it is comparatively small, and as a rule it is preserved as a whole, when its size is evidence that the observed intensity is a genuine effect.

We now turn to the real two-dimensional case. The local uncertainty of an isoseismal in the 2-D case can be obtained by inspection of the *I*-points in the vicinity of each straight line traced on the IDP map. The traces of G_I on any cross-section of the intensity field will inherit the connectedness and monotonicity of the intensity field; therefore, to find an intensity boundary we may use the criteria defined in the 1-D case.

Let us consider a strip across an IDP map. The strip is specified by the distance, r, of its axis L from the epicenter, by the direction, φ, of that axis, and by the width, H, which plays the role of a smoothing parameter. Projecting all points lying in this strip onto its major axis, we get a 1-D variant of the problem. Figure 1 now illustrates the decisions about the boundary between the observations that fall into the strip. Since the strip is two-dimensional, we consider two rectangles of size H/2 x $\Delta_\pm$ (see Fig. 1) as the local boundary of level *I* along the straight line (r, φ). This rectangle is called the Local Diffused Boundary (LDB), and its indicator function, having the values 1 for points of the rectangle and 0 otherwise, will be termed LDB-function.

Evidently, a single LDB can be unstable due to the strong dependence on the choice of ε. However, sorting out all possible sections (r, φ) of the IDP map, we obtain a 2-D family of local boundaries, the Diffused Boundary (DB), for a given intensity. The new object, DB, is more stable and supplies information on the uncertainty of G_I at any point of the space, in any direction, while a number of overlapping LDB elements at a point can be interpreted as a local measure of the reliability for the diffused boundary.

The visualization of DB can be made with two different methods. With one method only LDB axes are plotted in the IDP map with some discretization of (r, φ). The emerging picture looks like a thorny "hedgehog". This visualization will therefore be called a "thorny" diffused boundary (TDB). The other method takes into account the fraction of overlapping LDB elements at each point, n (g). The area where n (g) > p *max* n (g), 0 < p < 1, is considered to be the p-diffused boundary (p-DB) of G_I. The p-DB representation extracts such parts of the intensity boundary, which are better provided by the data. When an isoseismal G_I is not convex or not simply connected, the DB-function can be underestimated due to the boundary points of G_I, which are internal with respect to the convex hull of G_I. The reason is that we take into consideration only two (the left- and right most) boundary points of G_I in any cross-section of the IDP map.

The main DB parameters and their typical values for the selected earthquakes:

– strip width H = 20 ÷ 40 km; the smaller the density of measurement sites with given intensity

I-1, the greater should H for the isoseismal of level I be;
- $\varepsilon = 5 \div 15\%$, typically $\varepsilon = 5\%$; the larger the noise in the intensity data, the greater should the parameter ε be;
- threshold $p = .15 \div .30$; the value $p = 1/3$ follows from the theoretical analysis by Molchan et al. (2002);
- each strip axis L is specified by the distance, r, from the epicenter and by the direction φ; the parameters (r, φ) of the line are discretized with steps $\Delta r = 0.1$ H and $\Delta\varphi = 5°$, respectively.

Unlike the conventional isolines, diffused boundaries for adjacent intensities may partly coincide. Whatever their causes, cases of this kind should prompt a deeper analysis of the data. One example is the 3/04/1898 Valle del Parma earthquake. The DBs for I = V and I = IV based on the DOM data largely overlap. The new version of data in CFTI-3 (2000) made the isoseismal area of level I = IV to become larger by a factor of 4.5, and the overlap disappeared (see Appendix).

4. The quality of an isoseismal

The DB method gives the possibility to introduce a crude quantitative measure of the uncertainty in the isoseismal boundaries. Let's suppose that the DB method gives a connected boundary of G_I, considering both inner and outer boundaries of DB as a possible boundary of G_I, we get two areas of size Q_- and Q_+, respectively. The quantity

$$q = \frac{1}{2}\frac{Q_+ - Q_-}{\sqrt{Q_+ Q_-}} \tag{1}$$

is zero when DB has zero thickness. To introduce a scale of the DB quality we assume that our areas are similar, with the similarity coefficient k. Then $Q_+ = k^2 Q_-$ and $q = (k - k^{-1}) / 2$. According to Shebalin (1972), on average, one has $k = 2$ for two adjacent isoseismals. For this reason, a DB with $q \geq (2 - 1/2) / 2 = 0.75$ can be considered unsatisfactory. For k = 1.25; 1.5; 1.75 and 2, we obtain, respectively, q = 0.22; 0.42; 0.59 and 0.75. Table 1 gives the following 5-class scale of the isoseismal quality.

Table 1 - Scale of the isoseismal quality.

q	[0, .22]	(0.22, 0.42]	(0.42, 0.59]	(0.59, 0.75)	≥ 0.75
class	1	2	3	4	5

This scale is used in Appendix and to assess the isoseismal quality of the selected Italian earthquakes. About half of the selected isoseismals have the quality class 1 or 2. Our experience shows that the formal classification of the IDP maps proposed here is in sufficiently good agreement with the intuitive assessments of quality based on DB maps.

5. Collection of isoseismals

The appendix contains a collection of isoseismals for 55 earthquakes. The macroseismic data are taken from the DOM, CFTI-2 data bases and from publications in the Bolletino Macrosismico, 1988-1995 (7 events). The MPF and DB methods described above have been applied to each intensity map in order to compare the methods and to visualize the resolution of an isoseismal. For 19 events we have both the CFTI-2 and DOM variants of intensity data. We choose the data base which has the greater number of measurements for an event. There are four difficult cases for which the number of measurements for the two versions of IDP maps are approximately equal but the generalized IDP maps are not similar. In such cases, we show in Appendix two variants of the generalised IDP maps. When this study had been completed, the CFTI-3 data base, where new data had been added and intensities partly revised, became available to us. Substantial modifications have occurred for 12 of the 28 events. All of these are included in Appendix based on the CFTI-3 data.

The selected collection of isoseismals is designed for testing how theoretical models can explain spatial strong motion patterns. Although the DBs of isoseismals are frequently locally blurred, they can have expressive enough shapes as a whole. To illustrate it, we focus on the isoseismals I = IV, 6/27/1898, Rieti; I = V, 9/13/1989, Pasubio; I = VI, 21/08/1962, Irpinia (DOM data set); I = V, 4/26/1917, Monterchi-Citerna. They all have non-standard cross-shaped forms. A detailed analysis of the shape of this type for I = VI, 10/18/1936, Bosco Cansiglio and the relation it bears to the source parameters can be found in Molchan et al. (2002).

The collection contains cases where the DBs at adjacent levels overlap and this phenomenon may imply serious observational errors as we have seen in the case of the 3/04/1898 Valle del Parma earthquake (section 3). This kind of information is impossible to derive from smoothed intensity maps. Thus the DB-maps can be useful for the revision of the intensity data.

6. Area statistics of MPF isoseismals

Below we give the linear orthogonal regression equations of the log isoseismal area of level I (log Q_I) versus magnitude, which characterize the MPF isoseismals on the average. Relations like these are used in seismic risk assessments (Caputo et al., 1974). They are also important for comparing the mean macroseismic field with its instrumental analogues derived from observations or from theoretical calculations. The mean I(g) field is usually given by a linear regression equation connecting I, M and log D, D being the hypocentral distance. The depth of shallow earthquakes is poorly constrained, and the shape of their isoseismals is far from being a circle, which adds more scatter to the regression equation. For this reason the variable 2log D is replaced with log (Q_I / π) (Caputo et al., 1973). The isoseismals of small area should be eliminated from the data to avoid large errors caused by the depth uncertainty. Below we require that $Q_I > 100$ km^2.

We consider a data set of Q_I based on the MPF isoseismals of 78 Italian events, including the 55 selected in Appendix. The sample includes closed isoseismals only. Therefore, our data

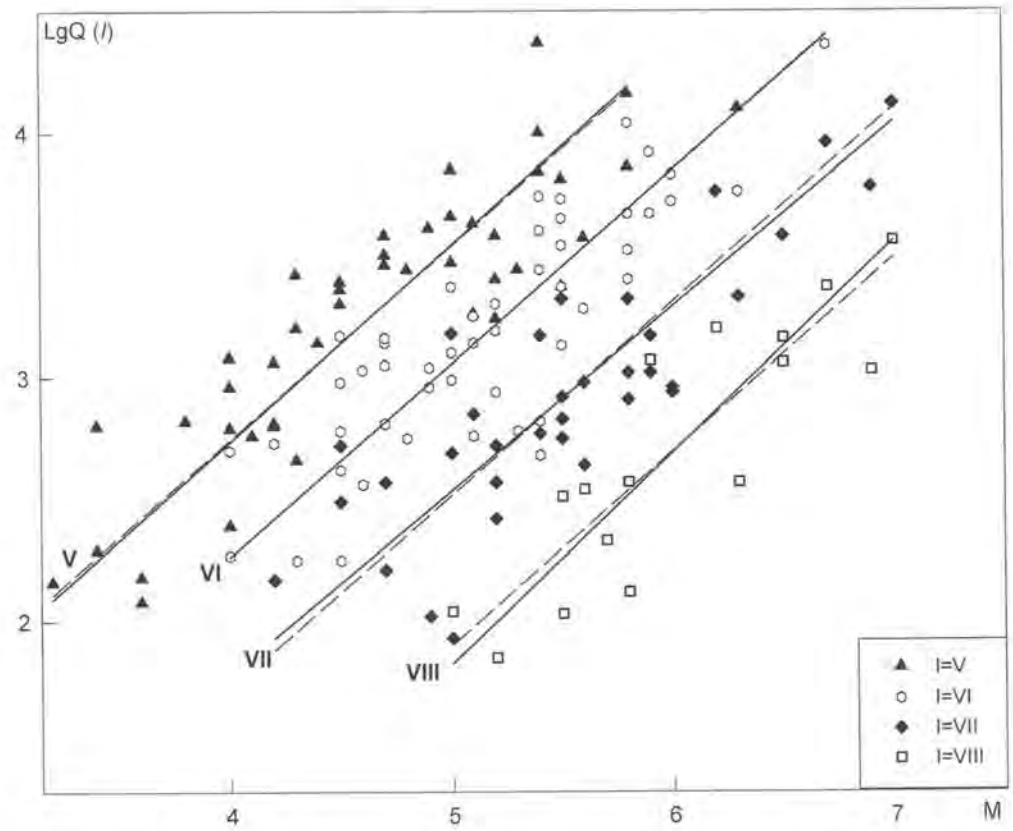

Fig. 2 - Linear orthogonal regressions of log Q_I versus magnitude M for MPF isoseismals of level *I*. Here *I* = V, VI, VII, VIII; Q_I is isoseismal area; *a priori* the standard errors in log Q_I and M are 0.2 and 0.25 respectively

set $\{Q_I\}$ is non-representative for $I \leq$ IV. To the pre-1992 earthquakes the unified M_L magnitudes have been assigned as reported in the Camassi and Stucchi catalogue [NT411]; the magnitudes for later events, M_L and M_d, are taken from the Bolletino Macrosismico of ING. The raw data and the regression lines are shown in Fig. 2, the parameters of the orthogonal regressions $\log Q_I = a_I + b_I M$ for *I* = V-VIII are listed in Table 2. The regressions were calculated with the assumption that M and logQ have standard errors $\sigma_M = 0.25$ and $\sigma_Q = 0.2$, respectively. The error $\sigma_Q = 0.2$ is quite reasonable because the expected value of $\log (Q_I/Q_{I+1})$ is log4 = 0.6 by Shebalin (1972). Table 2 shows the summary squared residual

$$\chi_I^2 = \sum_k \frac{(\log Q_I (M_k) - a - bM_k)^2}{\sigma_Q^2 + b^2 \sigma_M^2} \qquad (2)$$

for each *I*. The normalized deviation of the residual $\Delta = (\chi^2 - n') / \sqrt{2n'}$, $n' = n - 2$, where n is the number of data in the sample for intensity *I*, gives a possibility of judging on the agreement between the data and the linear model, including the convention about the errors σ_M and σ_Q. In our case Δ = -0.8, -0.2, 0.5 and -0.3 for *I*=V, VI, VII and VIII, respectively. Recalling that Δ is approximately normally distributed, these values indicate good agreement.

Table 2 - Parameters of the orthogonal regression log Q= a+bM.

I	n	a	b	χ^2	a_Σ
V	43	-0.49	.80	35.7	-0.43
VI	49	-0.90	.79	45.2	-0.91
VII	34	-1.24	.75	35.9	-1.45
VIII	15	-2.50	.86	12.1	-2.06
		Total b: b_Σ=	.79		

Our data are in good agreement with the assumption of equal slopes b_I (the hypothesis H_0). The relevant estimates of a and b in Table 2 are marked with the subscript Σ. The hypothesis H_0 can be tested by the statistic $\mathbf{T} = \chi^2_\Sigma - \Sigma\chi^2_I$, where χ^2_Σ is the total squared residual under H_0 (Wilks, 1962). The quantity **T** is approximately distributed as chi-square with n = 8 - 5 = 3 degrees of freedom, when H_0 is true. Its observed value **T** = 1.0 is in favour of H_0.

The above regression analysis has revealed the following isoseismals with abnormally large areas: I = VIII, 9/05/1950 Gran Sasso, M = 5.6; I = VI, 5/15/1961 Lodigiano, M = 4.9; I = VI-VIII, 2/06/1971 Tuscania, M = 4.2; I = V and VI, 1/08/1988 Apennino Lucania, M = 4.1. These data have not been included in the final calculation; they deserve a special study.

The column a_Σ of Table 2 shows that $\log (Q_I / Q_{I+1}) \cong 0.54$, i.e. $\log Q_I \cong 2.3 + b_\Sigma M - 0.54I$ for $Q_I > 100$ km^2. This equation is recalculated in the equation of Shebalin (1972): $I = \beta M - \nu \log D + c$, with the physical parameters (β, ν, c) = (1.46, 3.7, 3.34). They are close to Shebalin's universal parameters (1.5, 3.5, 3.0). In addition, the estimates $b_\Sigma = 0.8$ and $\log(Q_{VII} / Q_{VIII}) \cong 0.5$ were derived by Caputo et al. (1973, 1974) from a collection of hand-drawn isoseismal maps for Italian earthquakes by different authors. These comparisons show that MPF and hand techniques are equivalent to describing the mean intensity field.

7. Discussion and conclusion

Any statistical analysis starts by visualizing the data. Computer technologies have considerably simplified the process, so that an IDP map can be inspected even on top of the background topography. Nevertheless, intensity maps are rather complicated because of the presence of space gaps in observations, space irregularity of the observation sites, as well as noise in the measurements (gaps are due to administrative borders, the coastline and unpopulated areas). For this reason the next possible phase in the visualization consists in an elementary processing of IDP maps in order to reduce the noise component in the observations. Smoothing, as applied to I(g), is frequently sufficient to recover some earthquake source parameters or to estimate the mean field (I, M, logD) for the area of study. This is, however, insufficient to infer isoseismal shapes. The shape problem arises at once, when one asks about how the space intensity patterns can be explained from a theoretical point of view. We focus attention on the isoseismal shape, because the intensity scale is discrete, while the instrumental analogues of I are continuous. There is a preconception that macroseismic isoseismals have

trivial oval shapes in the absence of noise and site effects and "the source anisotropy due to the radiation pattern is almost never seen in the isoseismals" (Gusev and Shumilina, 2000). The present paper shows rather expressive examples of cross-shaped isoseismals, expected for earthquakes of strike-slip type. Note, this type of earthquake is non-typical for the Italian region.

The relation between isoseismals and earthquake source parameters has been studied insufficiently, because no IDP maps in large enough amounts and, of good quality, have been available up to now, while no one has aimed at recovering the isoseismal shape. We therefore propose two approaches to visualize isoseismals, one of which (DB method) demonstrates the uncertainty of isolines. The problem of a visualization of this kind has long been felt, but so far no practical solution has been found. The DB method is a first step in that direction but we believe that the visualization problem of isoseismals deserves further study. In our opinion, the quality of the DBs reflects the present state of macroseismic data rather than methodological defects (though certainly, there are some weak points in the methodology). We estimate that the good quality of an isoseismal for Italy can be characterized quantitatively as follows: the similarity coefficient k between the inner and outer «confidence» boundaries of an isoseismal is $k = 1.2\text{-}1.5$ (class two in our classification). Theoretical ground motion fields are continuous, hence their isolines for close levels are similar. The same thing is partially observed for intensity observations and for the outline of a DB. For this reason values $k > 1.2$ for an isoseismal do not exclude the testing of the isoseismal against the syntethic data.

The present collection of isoseismals can be used for comparison between observed and theoretical isoseismals. This comparison involves the simultaneous testing of crustal and source models. The collection gives a sufficiently accurate idea of the quality of the Italian earthquke isoseismals. The intensity data in the places of strong overlapping of the DBs for different I deserves careful revision. On the whole, we consider the modern Italian macroseismic database as a challenge for seismologists to explain the intensity patterns collected in Appendix.

Acknowledgments. Remarks by two anonymous reviewers and by the Publishing Editor D. Slejko have been very helpful in revising this paper. Our work is supported by grants: ISTC (project 1293-99); NATO SfP 972266; USNSF: EAR 9804859; the Russian Foundation for Basic Research (00-05-64097); and Italian MURST, 2000 funds, Active deformation at the northern boundary of Adria.

Appendix: Selected Italian earthquakes

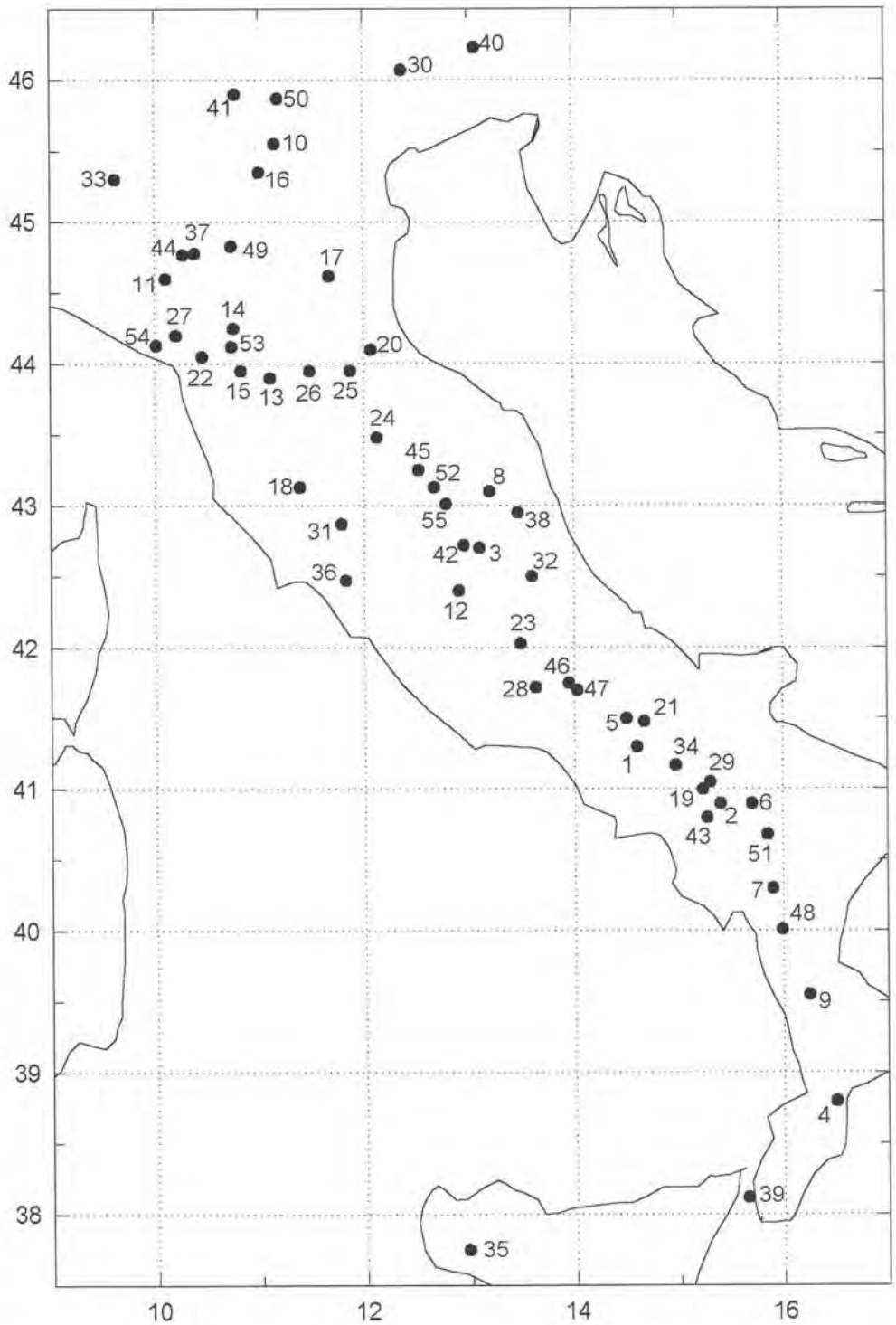

Fig. A - Epicenters of the selected earthquakes. *Epicenter:* solid circle and ordinal number in Table A1.

Table A1 - Parameters of selected earthquakes.
Epicenter (latitude Nord, longitude East), *Depth* (h) and *Magnitude* (M). Non-marked h and M are taken from the catalogue [NT411]. The *superscripts of* h *or* M specify additional references: [P], [CS], [BM] and [CMT]. The *subscripts of* M specify the type of magnitude: macroseismic (m), local (L), duration (d) and moment magnitude (w).
Macroseismic data: N_{obs} is the total number of data points with numerical intensity values or NoFelt type.
Ref (References): * is [DOM], 2 is [CFTI-2], 3 is [CFTI-3].
Quality of isoseismals: each pair of Roman and Arabic numbers indicates the intensity level of an isoseismal area and the quality class of its DB-boundary, according to the classification given in Table 1. The symbol «–» means incompleteness of DBs.

	Earthquake				Macroseismic data			Quality of isoseismals
	Date	Epicenter	h	M	I_{max}	N_{obs}	Ref	Intensiy level-quality class
1.	1688.06.05	41.3 14.6		7.3_m	XI	154	*	X-2, IX-2
2.	1694.09.08	40.9 15.4		7.0_m	XI	200	*	X-3, IX-2
					X	248	3	X-3, IX-2, VIII-3
3.	1703.01.14	42.7 13.1		6.7_m	X	216	*	X-4
4.	1783.03.28	38.8 16.5	18^P	6.7_m	XI	317	*	X-4, IX-3
5.	1805.07.26	41.5 14.5	10^P	6.7_m	X	209	3	IX-3, VIII-2
6.	1851.08.14	40.9 15.7		6.4_m	X	97	2	VII-4
7.	1857.12.16	40.3 15.9	$5\text{-}25^P$	7.0_m	XI	305	*	X-3, IX-2
8.	1873.03.12	43.1 13.2	20^P	5.2_m	IX	189	2	VII-4, VI-3
9.	1887.12.03	39.55 16.25	4^P	5.9_m	IX	141	2	–
10.	1891.06.07	45.55 11.15	40^P	5.5_m	VIII	262	*	VII-4, VI-3
11.	1898.03.04	44.6 10.1	5^P	4.7_m	VII-VIII	302	3	VI-3, V-3, IV-2
					VII	229	*	
12.	1898.06.27	42.4 12.9	$5\text{-}25^P$	5.2_m	VIII	181	*	VI-3
13.	1899.06.26	43.9 11.1	23^P	5.0_m	VII-VIII	114	*	VI-4, V-2
14.	1904.06.10	44.25 10.75	5-25	5.2	VII	87	2	–
15.	1904.11.17	43.95 10.82	5	5.0_m	VII	193	*	V-3, IV-2
16.	1907.04.25	45.35 11.00	10	4.5	VI	134	*	VI-4, V-3
17.	1909.01.13	44.62 11.67	25	5.4	VI-VII	797	*	VI-3
18.	1909.08.25	43.13 11.38	10^P	5.1	VIII	276	2	VII-3, VI-2
19.	1910.06.07	41.00 15.23	9	5.9	IX	352	2	VI-2
20.	1911.02.19	44.10 12.07	5	5.2	VII	173	2	VI-3
21.	1913.10.04	41.48 14.67	12	5.2	VIII	204	*	VI-3, V-2
22.	1914.10.27	44.05 10.45	28	5.8	VII	617	*	VII-2
23.	1915.01.13	42.03 13.49	8	7.0	XI	1026	2	(X,IX,VIII,VII)-2
24.	1917.04.26	43.48 12.12	2	5.6	IX-X	133	3	VII-4, VI-2, V-3
25.	1918.11.10	43.95 11.87	12	5.8	IX	188	3	VII-2, VI-3, V-2
26.	1919.06.29	43.95 11.48	5	6.3	X	560	3	VI-2
27.	1920.09.07	44.20 10.20	18	6.5	X	740	3	VIII-2, VII-3
28.	1922.12.29	41.72 13.63	5	5.5	VII	99	*	VII-4, VI-3
29.	1930.07.23	41.05 15.30	35	6.7	X	500	3	VIII-3, (VII,VI)-2
30.	1936.10.18	46.07 12.37	18	5.8	IX	263	*	–

	Earthquake				Macroseismic data			Quality of isoseismals
	Date	Epicenter	h	M	I_{max}	N_{obs}	Ref	Intensiy level-quality class
31.	1940.10.16	42.87 11.78	20	5.1	VII-VIII	106	*	VI-4, V-3
32.	1950.09.05	42.50 13.60	3	5.6	VIII	136	*	VIII-2, VII-2
33.	1951.05.15	45.30 9.62	12	4.9	VI	121	*	VI-3
34.	1962.08.21	41.17 14.97	40	6.2	IX	196	*	VII-2
					IX	261	3	VII-2
35.	1968.01.15	37.75 12.97	44	5.9	X	162	3	VIII-4
36.	1971.02.06	42.47 11.82	2	4.2	VIII-IX	89	*	VI-2
37.	1971.07.15	44.78 10.38	12	5.4	VIII	230	3	(VII,VI)-4, V-3
38.	1972.11.26	42.95 13.47	25-60	4.8	VIII	70	*	VII-2
39.	1975.01.16	38.12 15.65	21^{P}	4.7^{P}_{L}	VII-VIII	372	2	VII-3
40.	1976.05.06	46.23 13.07	17	6.5	X	514	3	(IX, VIII)-2
					IX-X	742	*	(IX, VIII)-2
41.	1976.12.13	45.90 10.77	20^{P}	4.4^{P}_{L}	VII	128	*	V-2, IV-2
42.	1979.09.19	42.72 12.95	6	5.9	VIII-IX	688	2	VIII-3, (VII,VI)-2, V-1
43.	1980.11.23	40.80 15.27	18	6.9	X	1316	2	VIII-2, VII-2
44.	1983.11.09	44.77 10.27	35	5.0^{CS}_{L}	VII	831	2	VI-2, V-2
45.	1984.04.29	43.25 12.52	9^{CS}	5.2^{CS}_{L}	VIII	580	2	VII-2
46.	1984.05.07	41.75 13.95	11^{CS}	5.8^{CS}_{L}	VIII	904	2	VII-1, VI-1
47.	1984.05.11	41.70 14.03	10^{CS}	5.3^{CS}_{L}	VII	342	2	VI-1
48.	1988.01.08	40.12 16.03	5^{CS}	4.0^{CS}_{d}	VII	112	[BM]	VI-2
49.	1988.03.15	44.83 10.73		4.1^{CS}_{d}	VI-VII	159	[BM]	V-2, IV-1
50.	1989.09.13	45.87 11.18	2^{CS}	4.4^{CS}_{L}	VI-VII	779	[BM]	V-2
51.	1990.05.05	40.73 15.63	10	5.8^{CMT}_{w}	VII-VIII	1372	[BM]	VI-2
52.	1993.06.05	43.13 12.67	8^{CS}	4.5^{CS}_{d}	VI	326	[BM]	V-3, IV-1
53.	1995.08.24	44.12 10.73	10^{CS}	4.3^{CS}_{d}	V-VI	187	[BM]	V-3, IV-2
54.	1995.10.10	44.13 10.01	5^{CS}	4.6^{BM}_{d}	VII	330	[BM]	VI-4, V-2
55.	1997.09.26	43.08 12.78	15^{CMT}	6.0^{CMT}_{w}	IX	869	3	VIII-4, VI-2

Collection of IDP maps in isolines

Each map is based on an intensity data set specified in Table A1; if the specification is double-valued (four cases) the data set is specified in the figure. The maps are drawn in the Lambert projection with the median latitude at the epicenter.

Geographical Names are given in the transcription of data sources (DOM, CFTI, BM, NT411).

Title: date, location, magnitude, epicenter (latitude Nord, longitude East), focal depth (km).

Upper map(s): IDP map with isoseismals drawn with the MPF method *(bold lines* – integer *I*, *thin lines* – half-integer *I*).

np, dg: filtering parameters, n_p and Δg, are explained in the text; they may depend on the isoseismal intensity level.

I-$I_{filtered}$: range of residuals $I(g)$-$\hat{I}(g)$, where $I(g)$ and $\hat{I}(g)$ refer to observed and smoothed IDP maps, respectively.

Lower map(s): diffused boundaries for some levels of intensity, *I*. (There are three exceptions, 03/28/1783 Calabria, 11/23/1980 Irpinia and 05/05/1980 Basilicata, for which we show more detailed MPF's isolines as well.)

DB parameters: H, ε, *p* (see text).

For a fixed level of intensity two types of visualization of DB are used: thorny DB (TDB) or p-DB, as indicated in each figure. DBs for different levels are depicted using different notations. In the cases of complicated partial superimposition of DBs we give, in addition, a vector of intensity levels, say (I_1, I_2, I_3 ...), which determines the order of overlapping: I_1 covers I_2, I_3; ... I_2 covers I_3... and so on.
Near a coast line DB may contain semi-infinite LDB elements opened in the direction of the sea. To simplify the DB pictures we omit all unbounded LDB elements. As a result our DBs may be open.

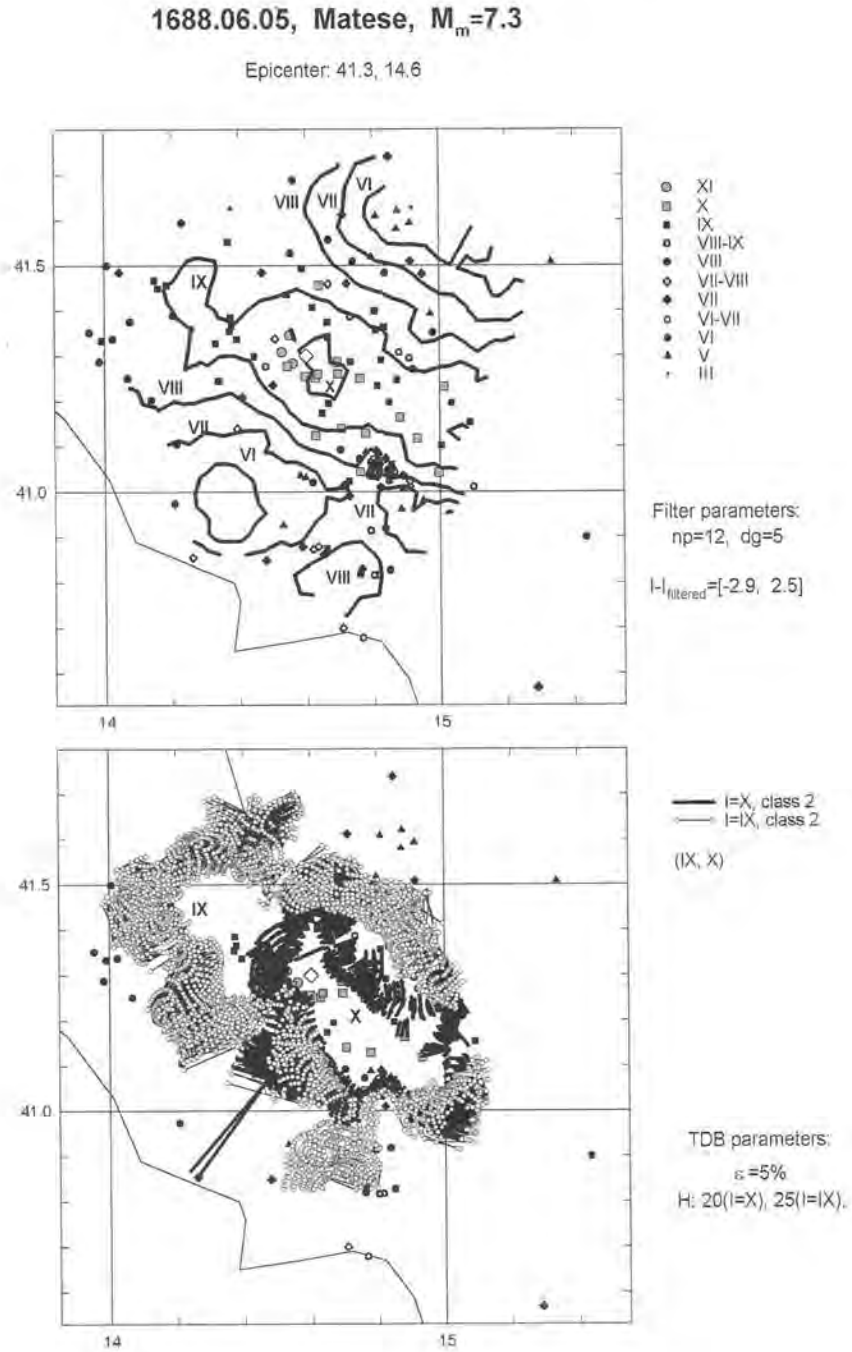

Fig. A-1

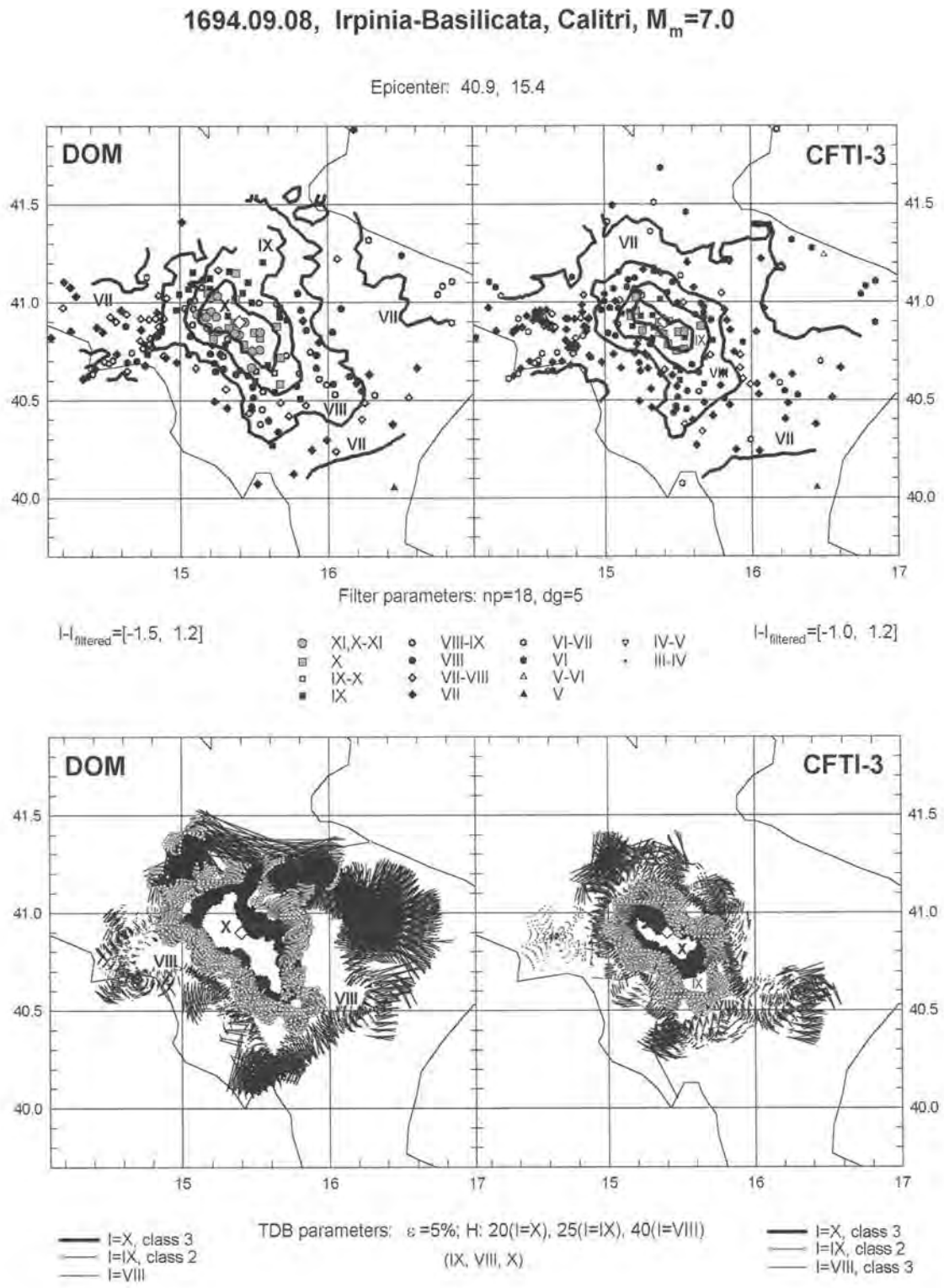
1694.09.08, Irpinia-Basilicata, Calitri, M_m=7.0
Epicenter: 40.9, 15.4
DOM
CFTI-3
41.5
41.0
40.5
40.0
15
16
17
IX
VII
VIII
Filter parameters: np=18, dg=5
I-I filtered=[-1.5, 1.2]
I-I filtered=[-1.0, 1.2]
XI,X-XI
X
IX-X
IX
VIII-IX
VIII
VII-VIII
VII
VI-VII
VI
V-VI
V
IV-V
III-IV
TDB parameters: ε=5%; H: 20(I=X), 25(I=IX), 40(I=VIII)
(IX, VIII, X)
I=X, class 3
I=IX, class 2
I=VIII
I=X, class 3
I=IX, class 2
I=VIII, class 3

Fig. A-2

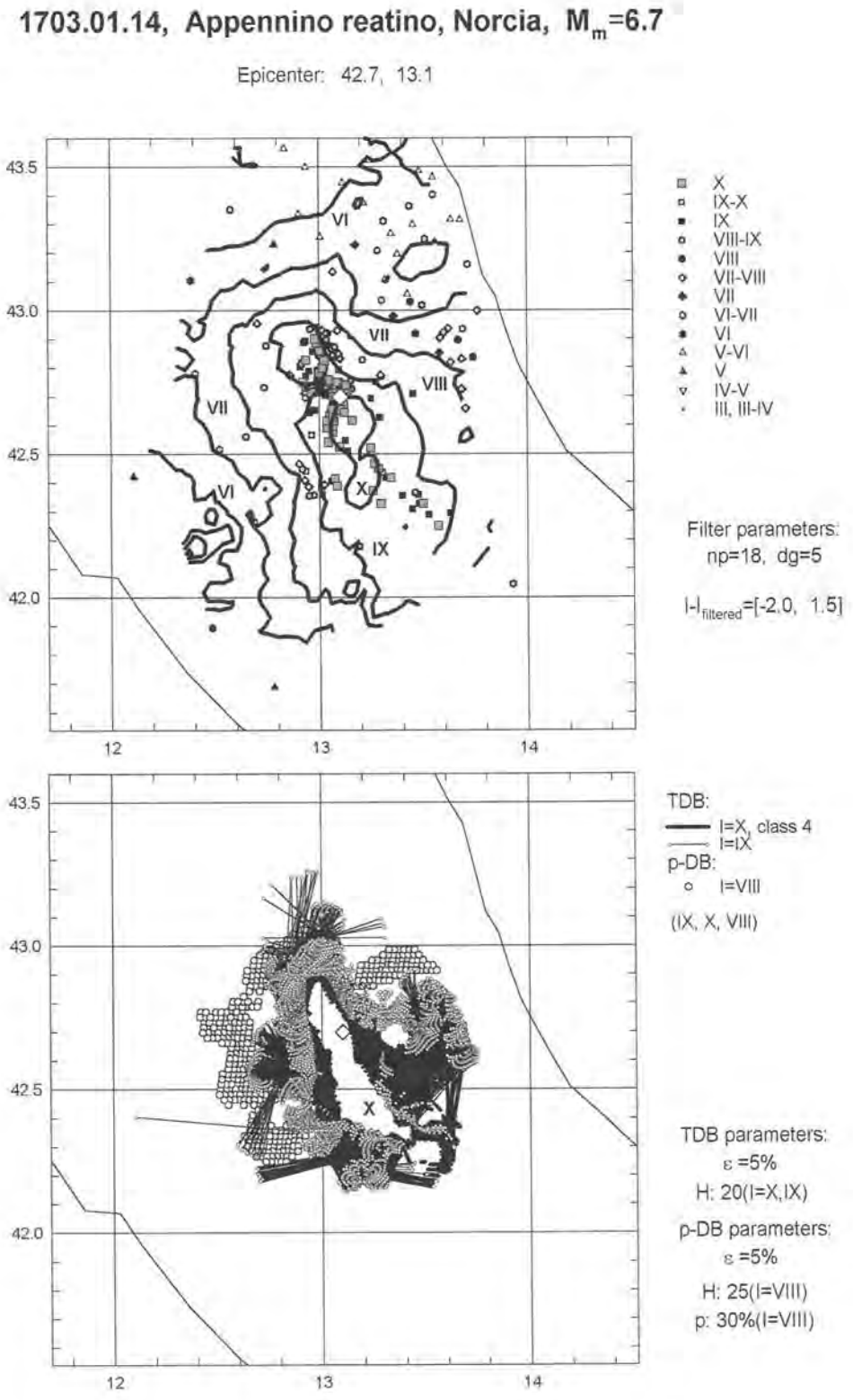
1703.01.14, Appennino reatino, Norcia, M_m=6.7
Epicenter: 42.7, 13.1
43.5
43.0
42.5
42.0
12
13
14
VI
VII
VIII
X
IX
X
IX-X
IX
VIII-IX
VIII
VII-VIII
VII
VI-VII
VI
V-VI
V
IV-V
III, III-IV
Filter parameters:
np=18, dg=5
$I-I_{filtered}$=[-2.0, 1.5]
TDB:
I=X, class 4
I=IX
p-DB:
I=VIII
(IX, X, VIII)
TDB parameters:
ε =5%
H: 20(I=X,IX)
p-DB parameters:
ε =5%
H: 25(I=VIII)
p: 30%(I=VIII)

Fig. A-3

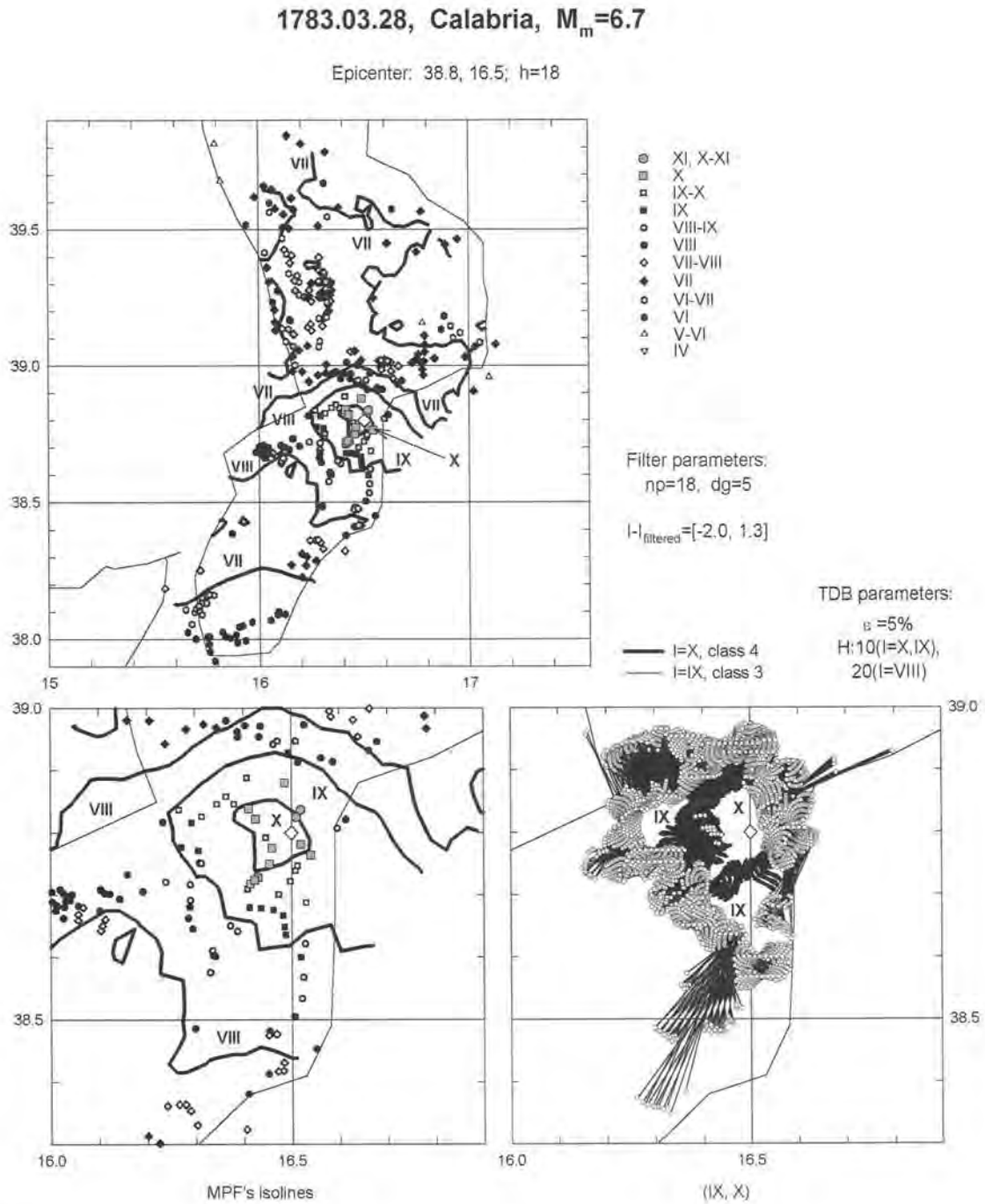
1783.03.28, Calabria, M_m=6.7
Epicenter: 38.8, 16.5; h=18
XI, X-XI
X
IX-X
IX
VIII-IX
VIII
VII-VIII
VII
VI-VII
VI
V-VI
IV
Filter parameters:
np=18, dg=5
$I-I_{filtered}$=[-2.0, 1.3]
TDB parameters:
ε =5%
H:10(I=X,IX),
20(I=VIII)
I=X, class 4
I=IX, class 3
MPF's isolines
(IX, X)

Fig. A-4

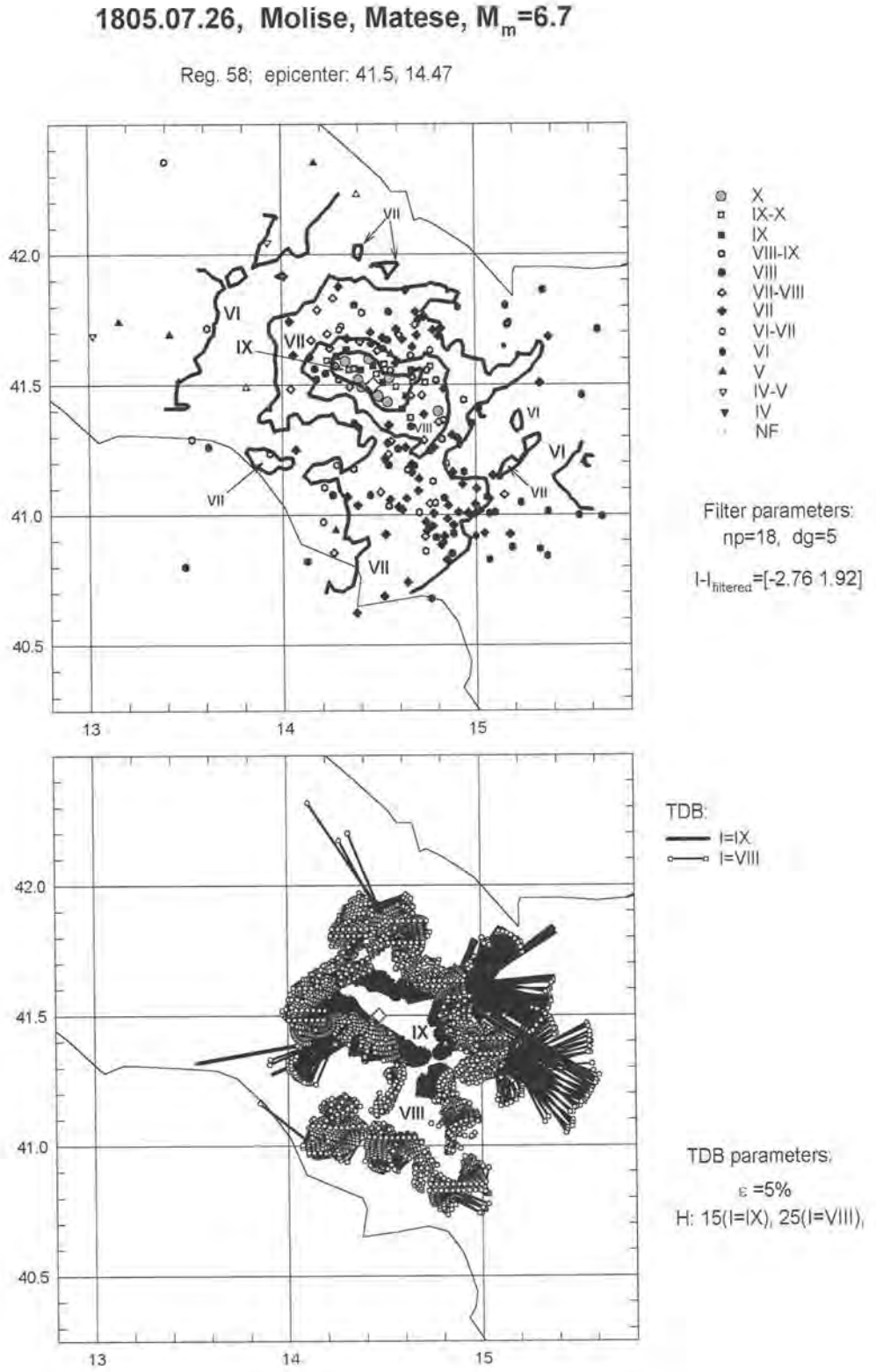
1805.07.26, Molise, Matese, M_m=6.7
Reg. 58; epicenter: 41.5, 14.47
X
IX-X
IX
VIII-IX
VIII
VII-VIII
VII
VI-VII
VI
V
IV-V
IV
NF
Filter parameters:
np=18, dg=5
$I-I_{filtered}$=[-2.76 1.92]
TDB:
I=IX
I=VIII
TDB parameters:
ε =5%
H: 15(I=IX), 25(I=VIII),
42.0
41.5
41.0
40.5
13
14
15

Fig. A-5

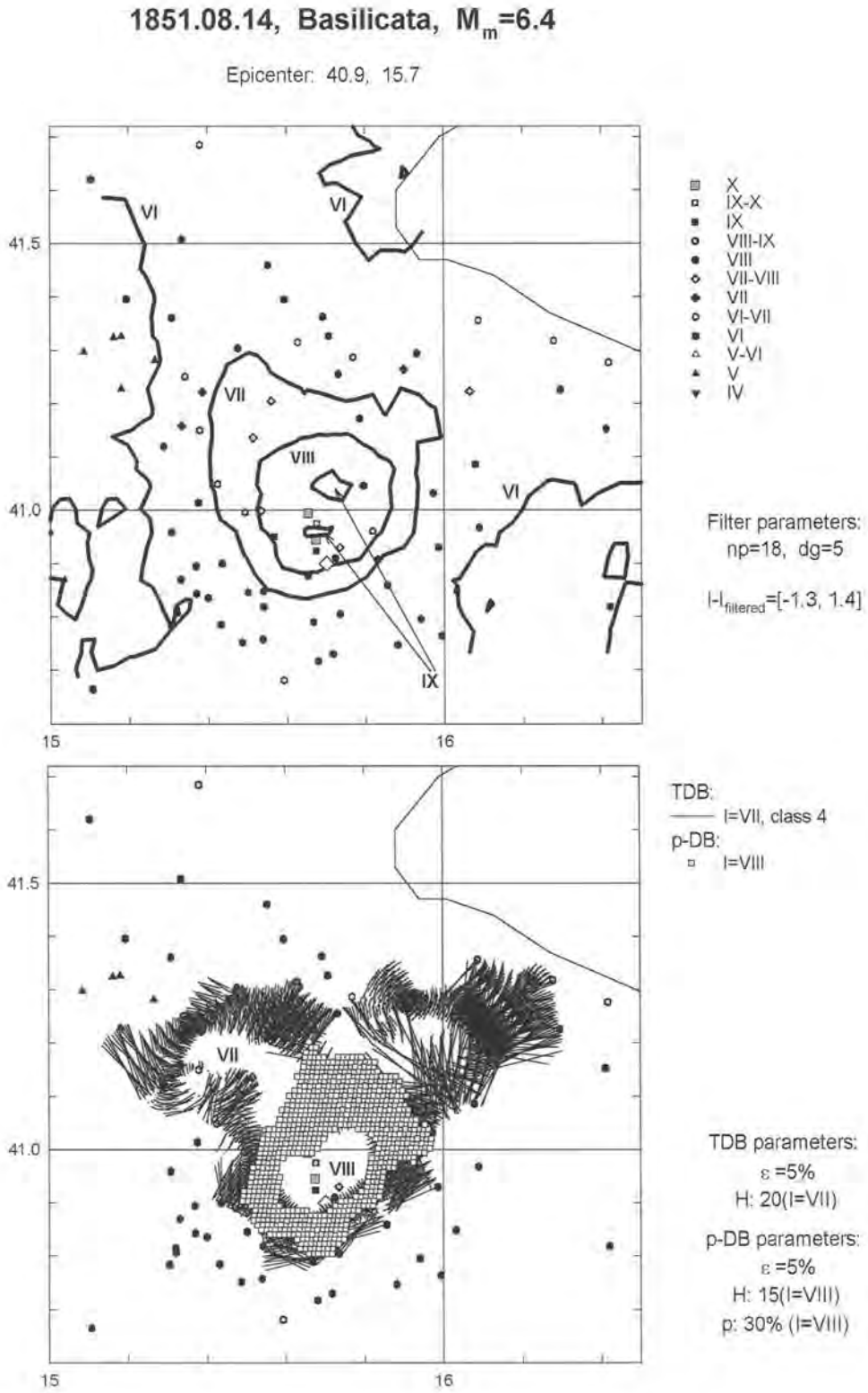
1851.08.14, Basilicata, M_m=6.4
Epicenter: 40.9, 15.7
41.5
41.0
15
16
VI
VII
VIII
IX
X
IX-X
IX
VIII-IX
VIII
VII-VIII
VII
VI-VII
VI
V-VI
V
IV
Filter parameters:
np=18, dg=5
$I-I_{filtered}$=[-1.3, 1.4]
TDB:
I=VII, class 4
p-DB:
I=VIII
TDB parameters:
ε =5%
H: 20(I=VII)
p-DB parameters:
ε =5%
H: 15(I=VIII)
p: 30% (I=VIII)

Fig. A-6

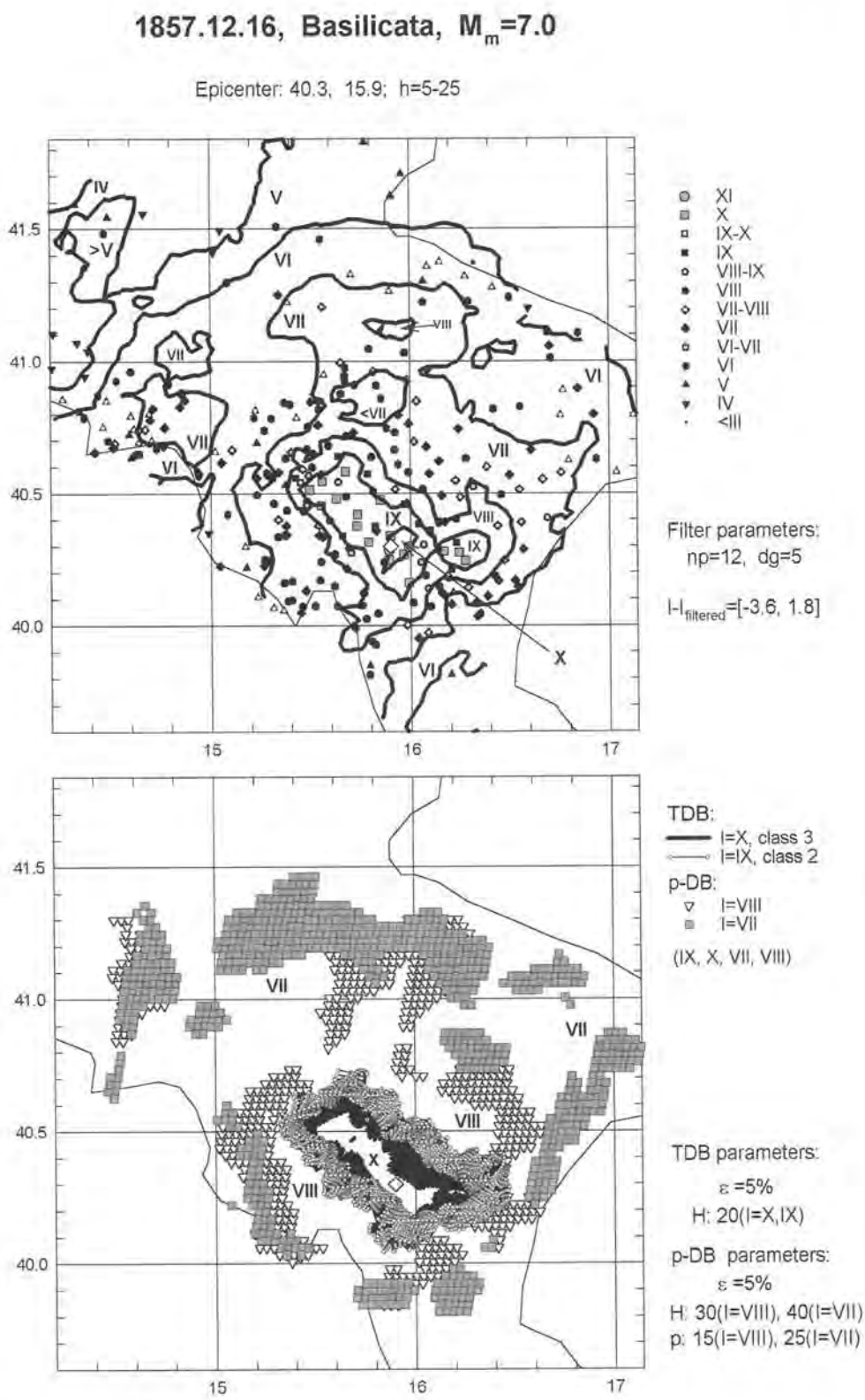
1857.12.16, Basilicata, M_m=7.0
Epicenter: 40.3, 15.9; h=5-25
XI
X
IX-X
IX
VIII-IX
VIII
VII-VIII
VII
VI-VII
VI
V
IV
<III
Filter parameters:
np=12, dg=5
$I\text{-}I_{filtered}$=[-3.6, 1.8]
TDB:
I=X, class 3
I=IX, class 2
p-DB:
I=VIII
I=VII
(IX, X, VII, VIII)
TDB parameters:
ε =5%
H: 20(I=X,IX)
p-DB parameters:
ε =5%
H: 30(I=VIII), 40(I=VII)
p: 15(I=VIII), 25(I=VII)
41.5
41.0
40.5
40.0
15
16
17

Fig. A-7

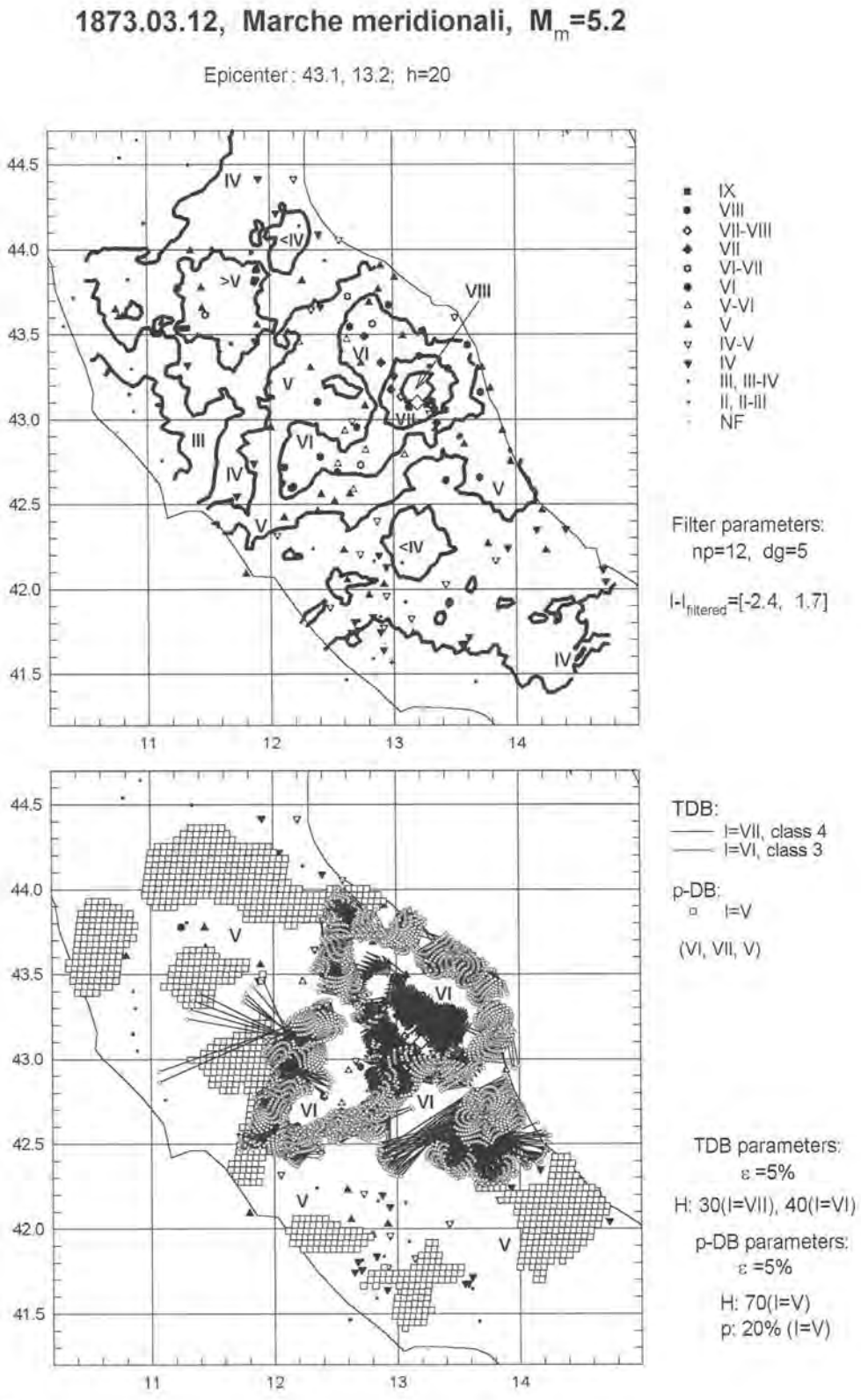
1873.03.12, Marche meridionali, M_m=5.2
Epicenter: 43.1, 13.2; h=20
IX
VIII
VII-VIII
VII
VI-VII
VI
V-VI
V
IV-V
IV
III, III-IV
II, II-III
NF
Filter parameters:
np=12, dg=5
$I-I_{filtered}$=[-2.4, 1.7]
TDB:
I=VII, class 4
I=VI, class 3
p-DB:
I=V
(VI, VII, V)
TDB parameters:
ε =5%
H: 30(I=VII), 40(I=VI)
p-DB parameters:
ε =5%
H: 70(I=V)
p: 20% (I=V)

Fig. A-8

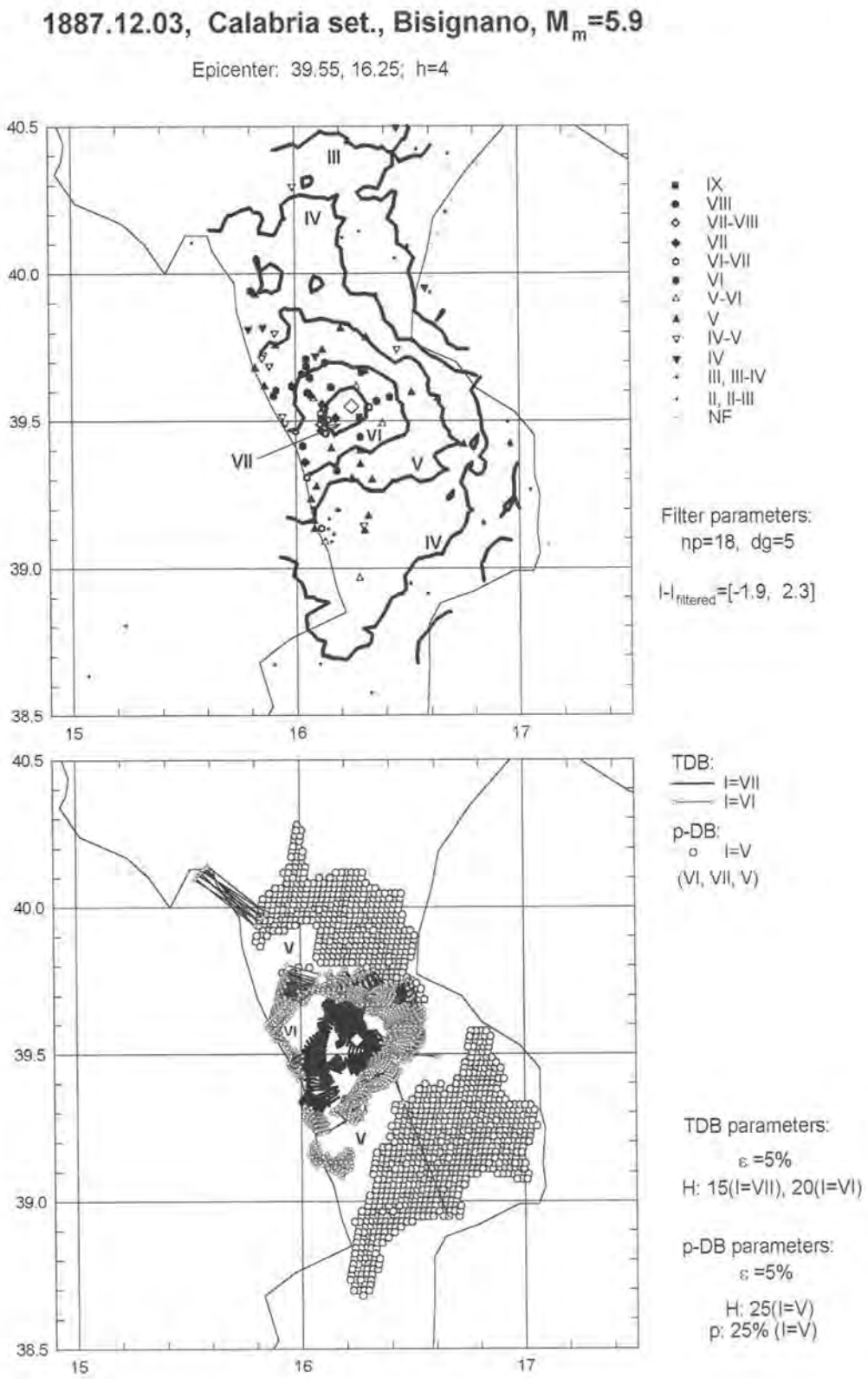
1887.12.03, Calabria set., Bisignano, M_m=5.9
Epicenter: 39.55, 16.25; h=4
40.5
40.0
39.5
39.0
38.5
15
16
17
III
IV
VII
VI
V
IV
IX
VIII
VII-VIII
VII
VI-VII
VI
V-VI
V
IV-V
IV
III, III-IV
II, II-III
NF
Filter parameters:
np=18, dg=5
$I-I_{filtered}$=[-1.9, 2.3]
TDB:
I=VII
I=VI
p-DB:
I=V
(VI, VII, V)
TDB parameters:
ε =5%
H: 15(I=VII), 20(I=VI)
p-DB parameters:
ε =5%
H: 25(I=V)
p: 25% (I=V)

Fig. A-9

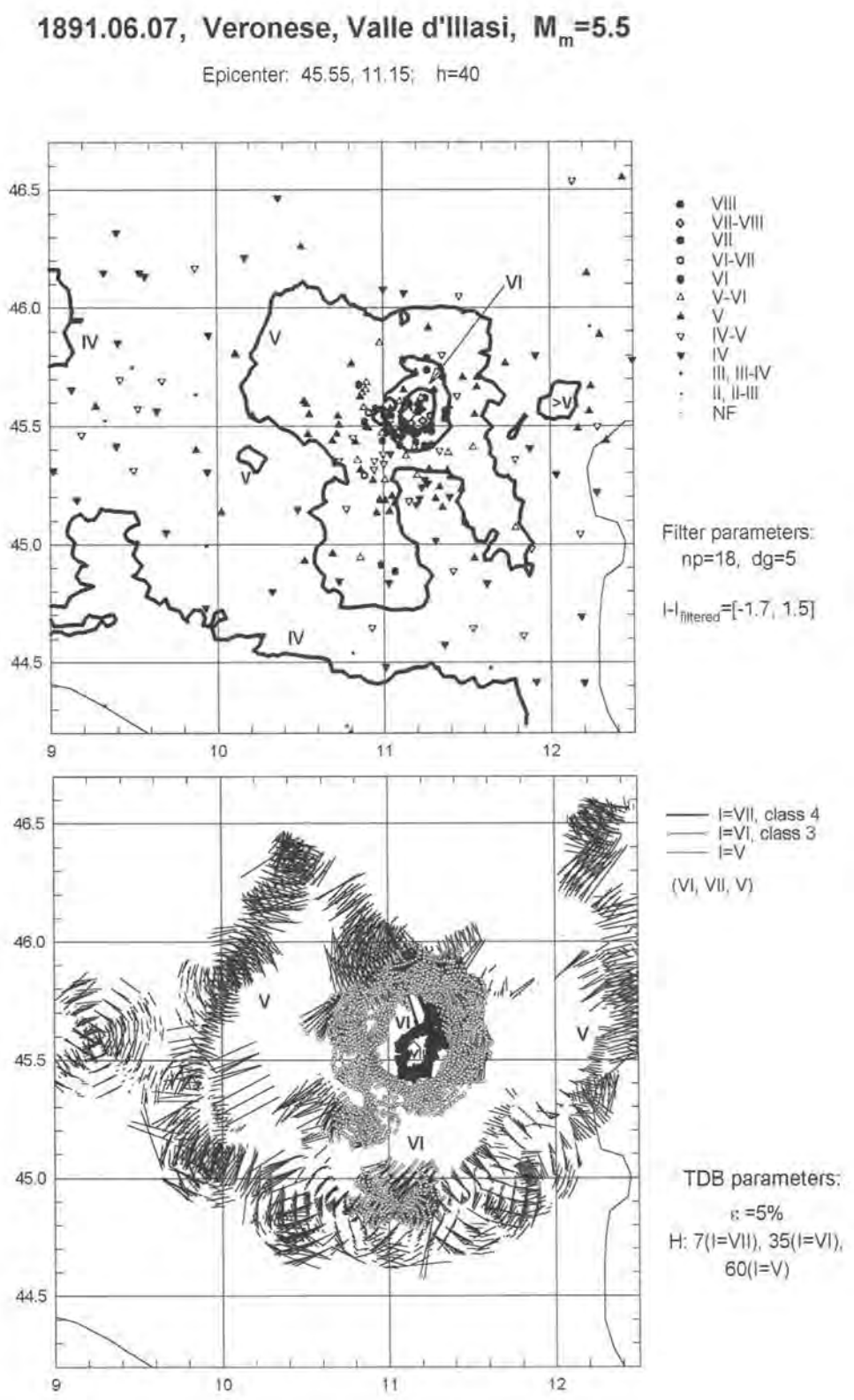
1891.06.07, Veronese, Valle d'Illasi, M_m=5.5
Epicenter: 45.55, 11.15; h=40
VIII
VII-VIII
VII
VI-VII
VI
V-VI
V
IV-V
IV
III, III-IV
II, II-III
NF
Filter parameters:
np=18, dg=5
$I-I_{filtered}$=[-1.7, 1.5]
I=VII, class 4
I=VI, class 3
I=V
(VI, VII, V)
TDB parameters:
ε =5%
H: 7(I=VII), 35(I=VI), 60(I=V)

Fig. A-10

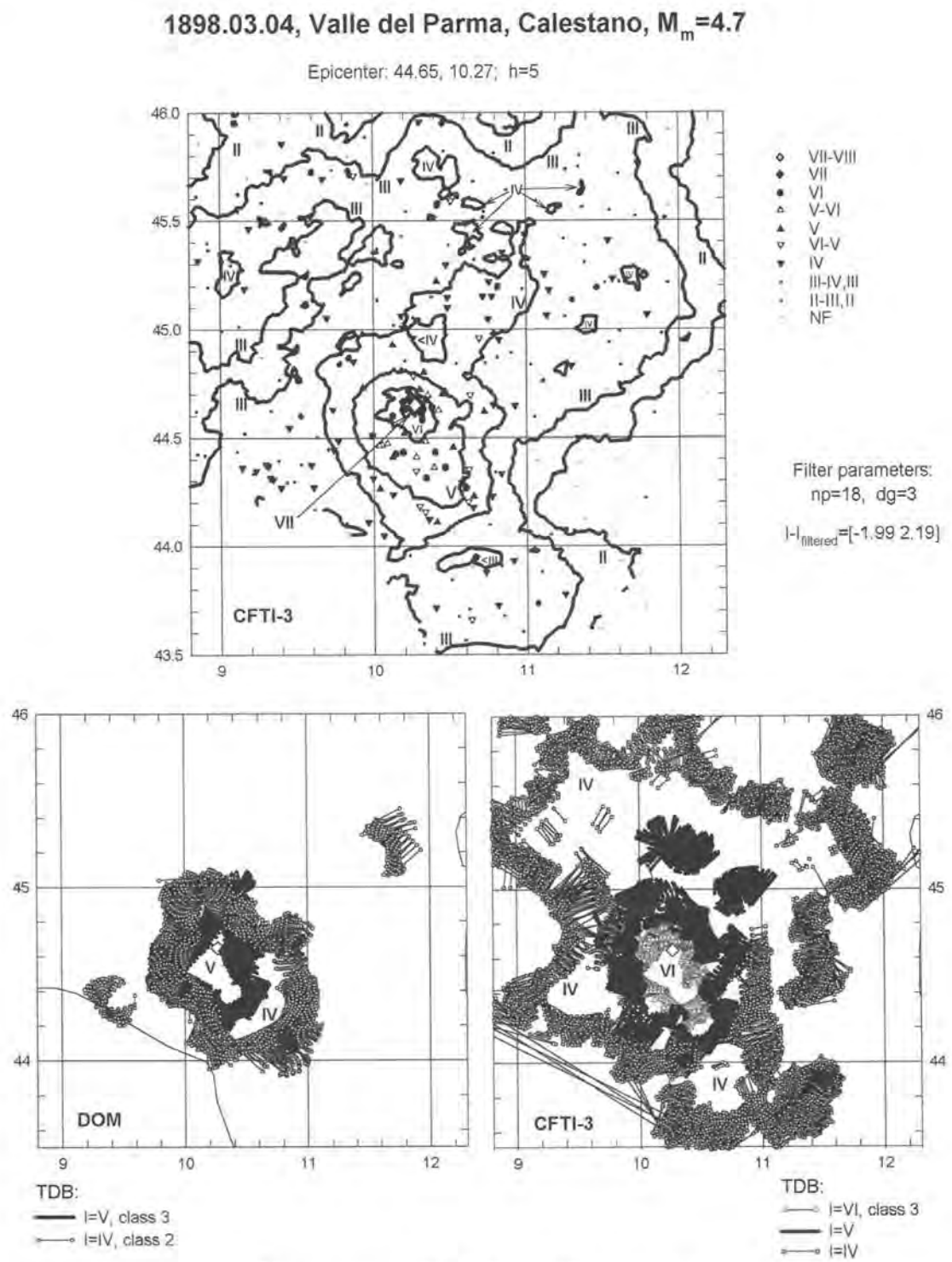
1898.03.04, Valle del Parma, Calestano, M_m=4.7
Epicenter: 44.65, 10.27; h=5
CFTI-3
VII-VIII
VII
VI
V-VI
V
VI-V
IV
III-IV,III
II-III,II
NF
Filter parameters:
np=18, dg=3
$I-I_{filtered}$=[-1.99 2.19]
DOM
CFTI-3
TDB:
I=V, class 3
I=IV, class 2
TDB:
I=VI, class 3
I=V
I=IV
TDB parameters: ε =5%, H: 25(I=VI), 30(I=V), 40(I=IV)

Fig. A-11

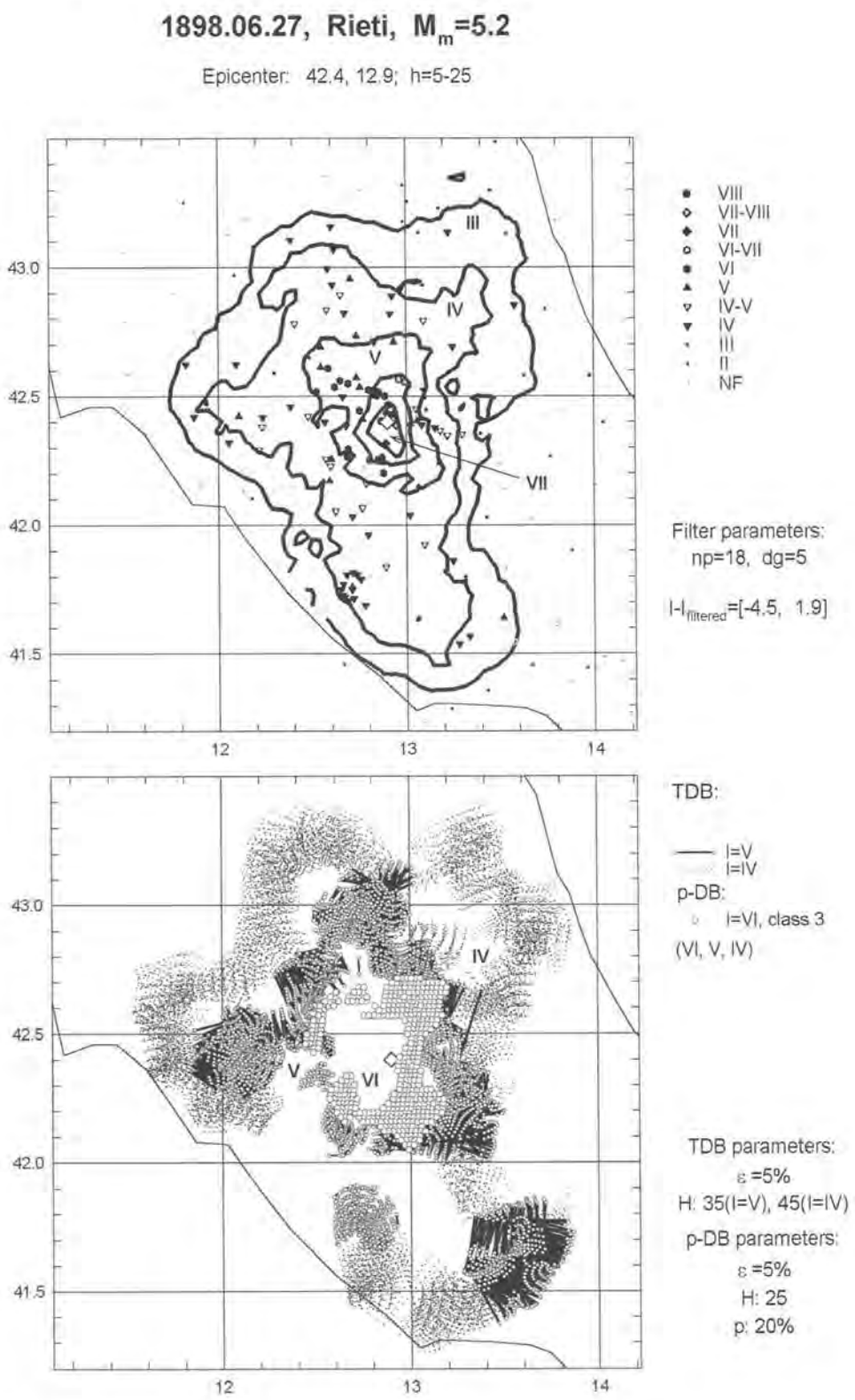
1898.06.27, Rieti, M_m=5.2
Epicenter: 42.4, 12.9; h=5-25
VIII
VII-VIII
VII
VI-VII
VI
V
IV-V
IV
III
II
NF
III
IV
V
VII
43.0
42.5
42.0
41.5
12
13
14
Filter parameters:
np=18, dg=5
$I-I_{filtered}$=[-4.5, 1.9]
TDB:
I=V
I=IV
p-DB:
I=VI, class 3
(VI, V, IV)
I
IV
V
VI
TDB parameters:
ε =5%
H: 35(I=V), 45(I=IV)
p-DB parameters:
ε =5%
H: 25
p: 20%

Fig. A-12

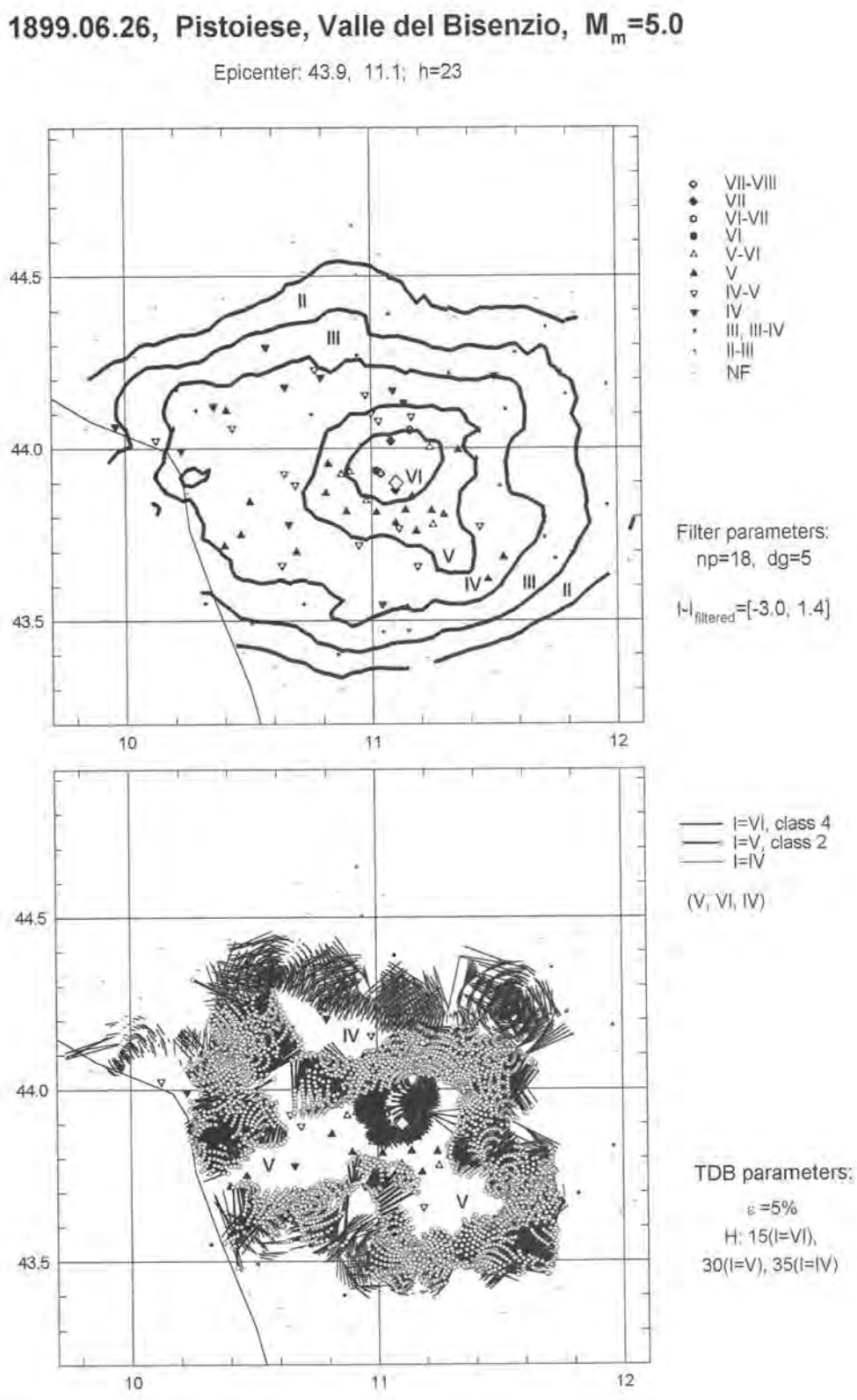
1899.06.26, Pistoiese, Valle del Bisenzio, M_m=5.0
Epicenter: 43.9, 11.1; h=23
VII-VIII
VII
VI-VII
VI
V-VI
V
IV-V
IV
III, III-IV
II-III
NF
Filter parameters:
np=18, dg=5
I-I filtered=[-3.0, 1.4]
I=VI, class 4
I=V, class 2
I=IV
(V, VI, IV)
TDB parameters:
ε=5%
H: 15(I=VI),
30(I=V), 35(I=IV)
44.5
44.0
43.5
10
11
12

Fig. A-13

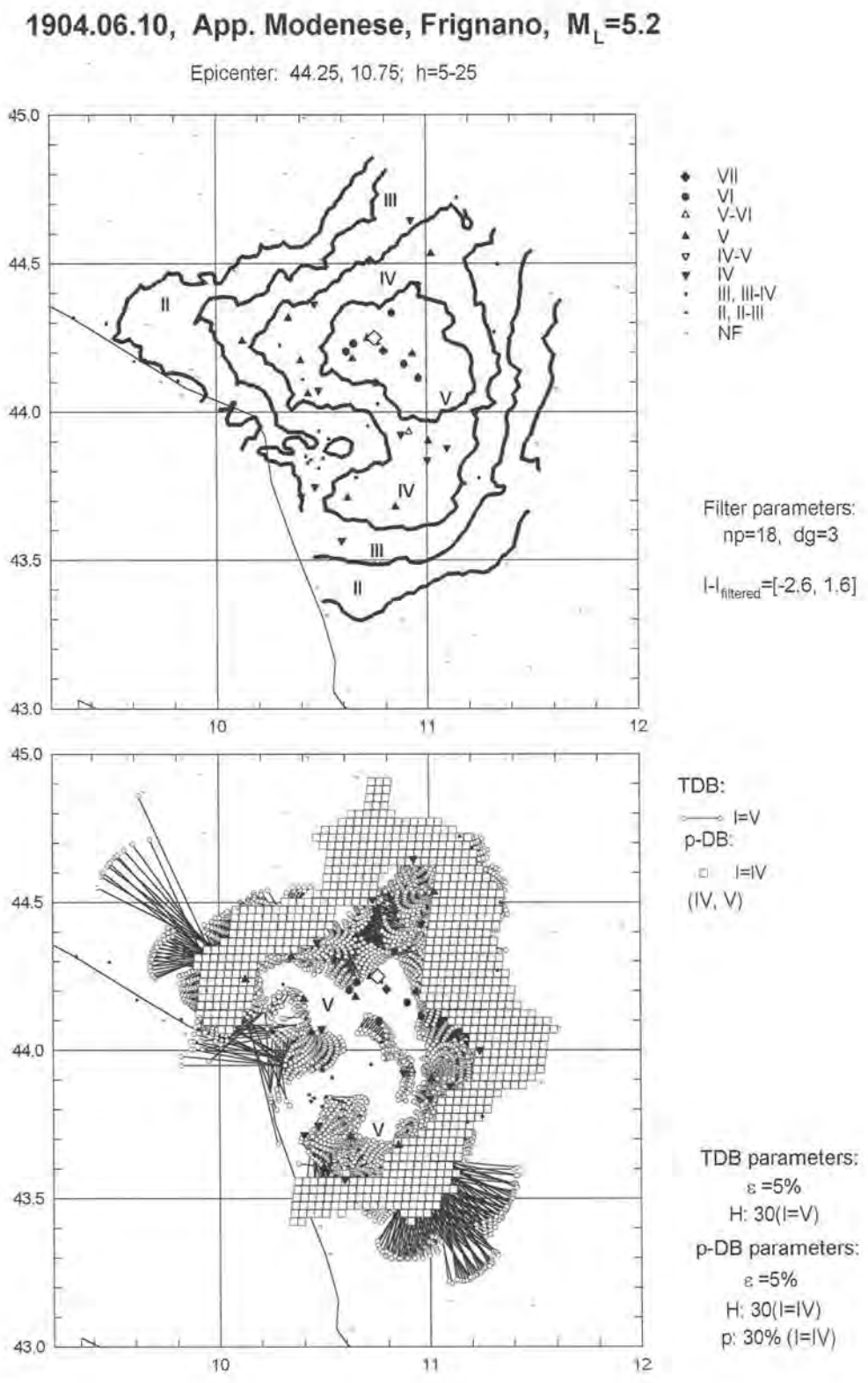
1904.06.10, App. Modenese, Frignano, M_L=5.2
Epicenter: 44.25, 10.75; h=5-25
45.0
44.5
44.0
43.5
43.0
10
11
12
III
IV
II
V
VII
VI
V-VI
V
IV-V
IV
III, III-IV
II, II-III
NF
Filter parameters:
np=18, dg=3
$I-I_{filtered}$=[-2.6, 1.6]
TDB:
I=V
p-DB:
I=IV
(IV, V)
TDB parameters:
ε =5%
H: 30(I=V)
p-DB parameters:
ε =5%
H: 30(I=IV)
p: 30% (I=IV)

Fig. A-14

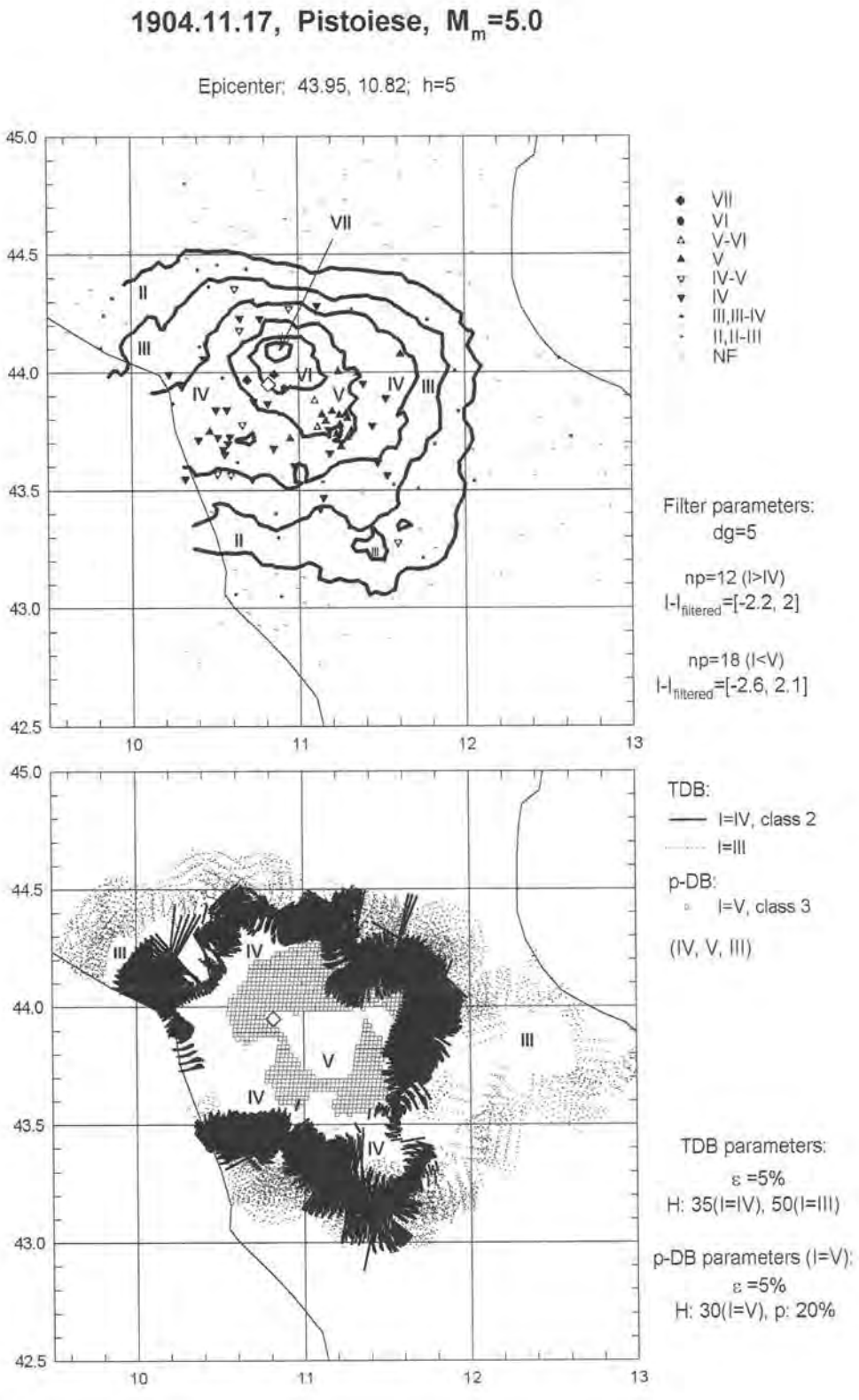
1904.11.17, Pistoiese, M_m=5.0
Epicenter: 43.95, 10.82; h=5
VII
VI
V-VI
V
IV-V
IV
III,III-IV
II,II-III
NF
Filter parameters:
dg=5
np=12 (I>IV)
$I-I_{filtered}$=[-2.2, 2]
np=18 (I<V)
$I-I_{filtered}$=[-2.6, 2.1]
TDB:
I=IV, class 2
I=III
p-DB:
I=V, class 3
(IV, V, III)
TDB parameters:
ε =5%
H: 35(I=IV), 50(I=III)
p-DB parameters (I=V):
ε =5%
H: 30(I=V), p: 20%
45.0
44.5
44.0
43.5
43.0
42.5
10
11
12
13

Fig. A-15

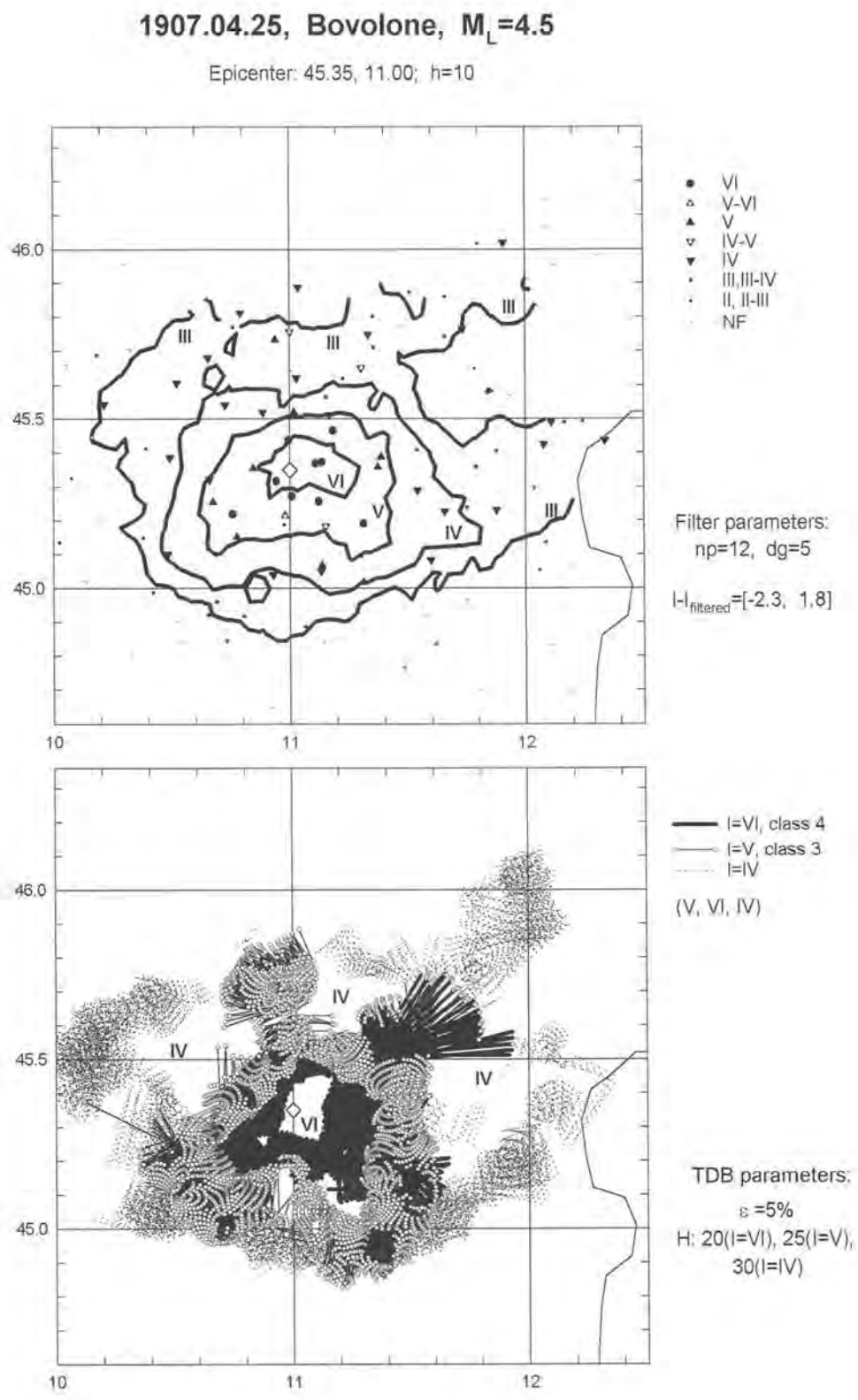
1907.04.25, Bovolone, M_L=4.5
Epicenter: 45.35, 11.00; h=10
VI
V-VI
V
IV-V
IV
III,III-IV
II, II-III
NF
Filter parameters:
np=12, dg=5
$I-I_{filtered}$=[-2.3, 1.8]
I=VI, class 4
I=V, class 3
I=IV
(V, VI, IV)
TDB parameters:
ε =5%
H: 20(I=VI), 25(I=V),
30(I=IV)
46.0
45.5
45.0
10
11
12

Fig. A-16

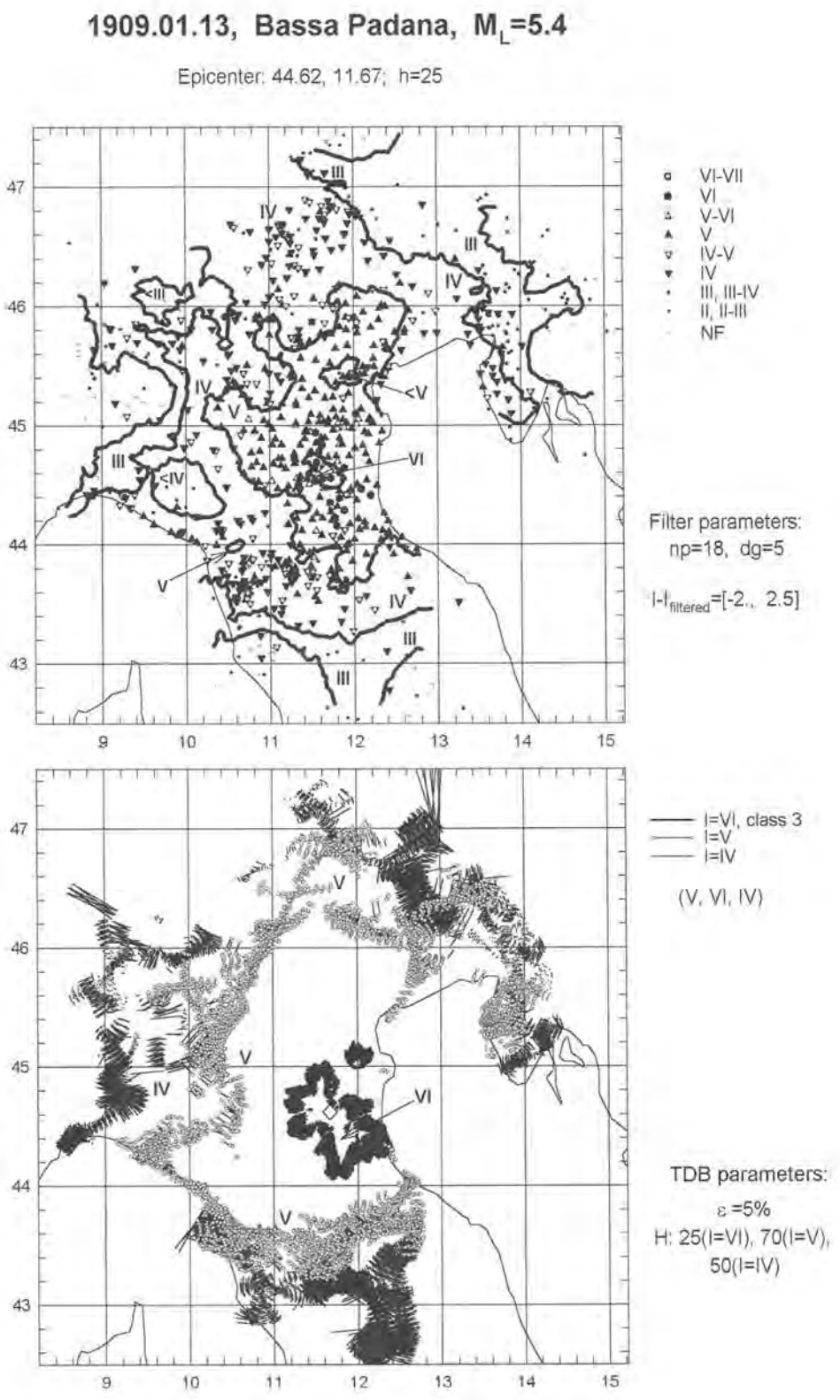
1909.01.13, Bassa Padana, M_L=5.4
Epicenter: 44.62, 11.67; h=25
VI-VII
VI
V-VI
V
IV-V
IV
III, III-IV
II, II-III
NF
Filter parameters:
np=18, dg=5
$I-I_{filtered}$=[-2., 2.5]
I=VI, class 3
I=V
I=IV
(V, VI, IV)
TDB parameters:
ε=5%
H: 25(I=VI), 70(I=V),
50(I=IV)
47
46
45
44
43
9
10
11
12
13
14
15

Fig. A-17

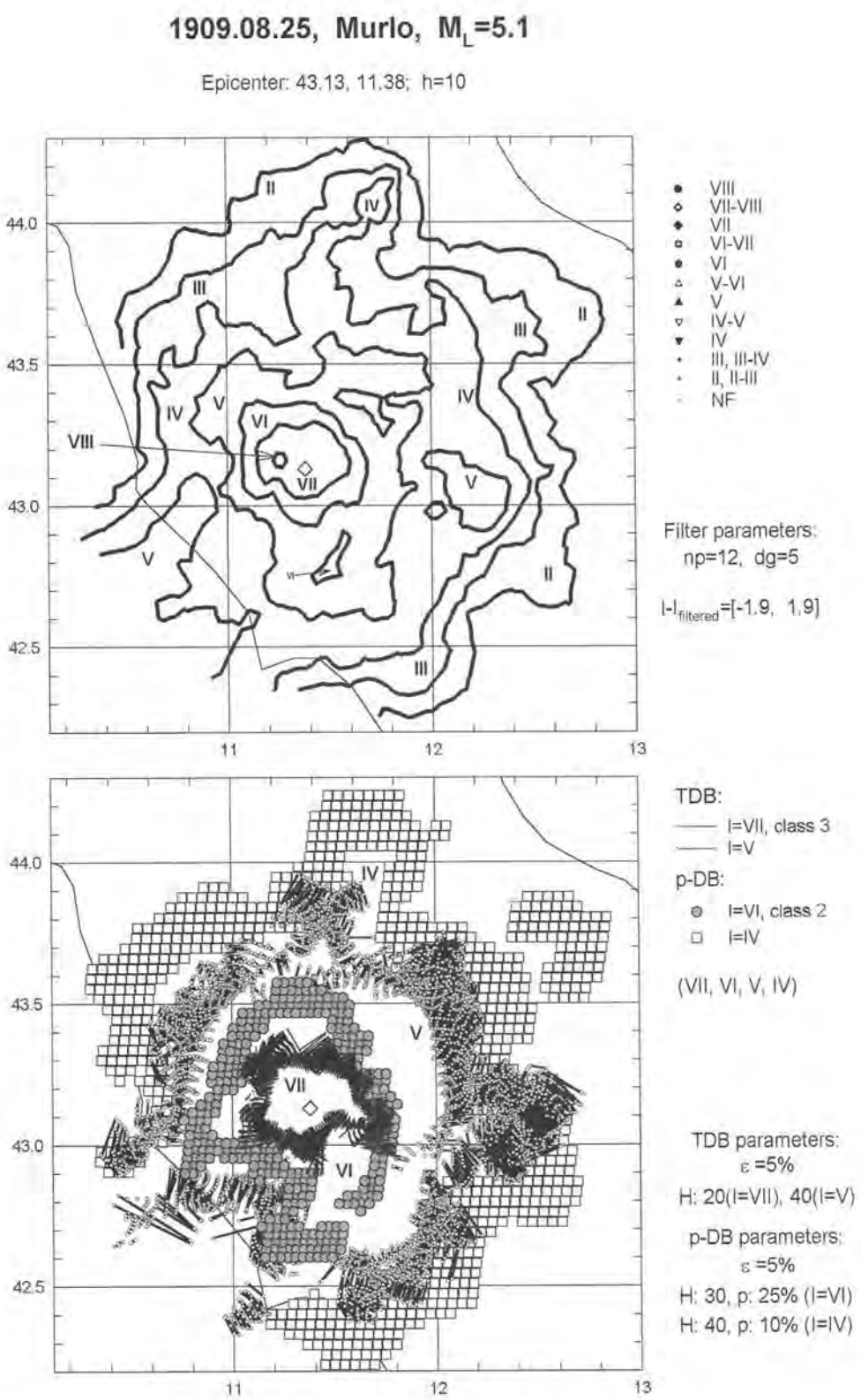
1909.08.25, Murlo, M_L=5.1
Epicenter: 43.13, 11.38; h=10
VIII
VII-VIII
VII
VI-VII
VI
V-VI
V
IV-V
IV
III, III-IV
II, II-III
NF
Filter parameters:
np=12, dg=5
$I-I_{filtered}$=[-1.9, 1.9]
TDB:
I=VII, class 3
I=V
p-DB:
I=VI, class 2
I=IV
(VII, VI, V, IV)
TDB parameters:
ε =5%
H: 20(I=VII), 40(I=V)
p-DB parameters:
ε =5%
H: 30, p: 25% (I=VI)
H: 40, p: 10% (I=IV)
44.0
43.5
43.0
42.5
11
12
13

Fig. A-18

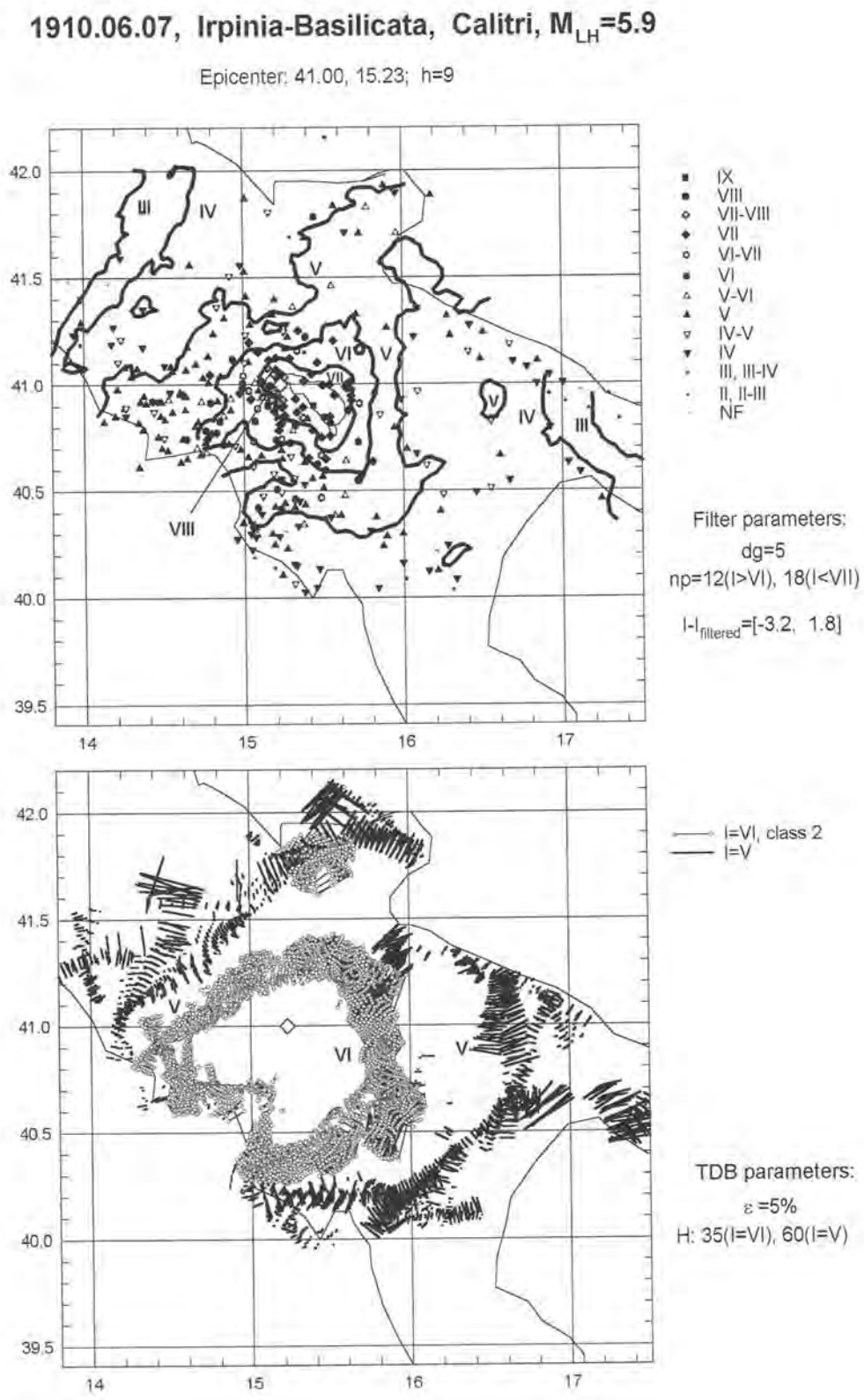
1910.06.07, Irpinia-Basilicata, Calitri, M_{LH}=5.9
Epicenter: 41.00, 15.23; h=9
IX
VIII
VII-VIII
VII
VI-VII
VI
V-VI
V
IV-V
IV
III, III-IV
II, II-III
NF
Filter parameters:
dg=5
np=12(I>VI), 18(I<VII)
$I-I_{filtered}$=[-3.2, 1.8]
I=VI, class 2
I=V
TDB parameters:
ε =5%
H: 35(I=VI), 60(I=V)
42.0
41.5
41.0
40.5
40.0
39.5
14
15
16
17

Fig. A-19

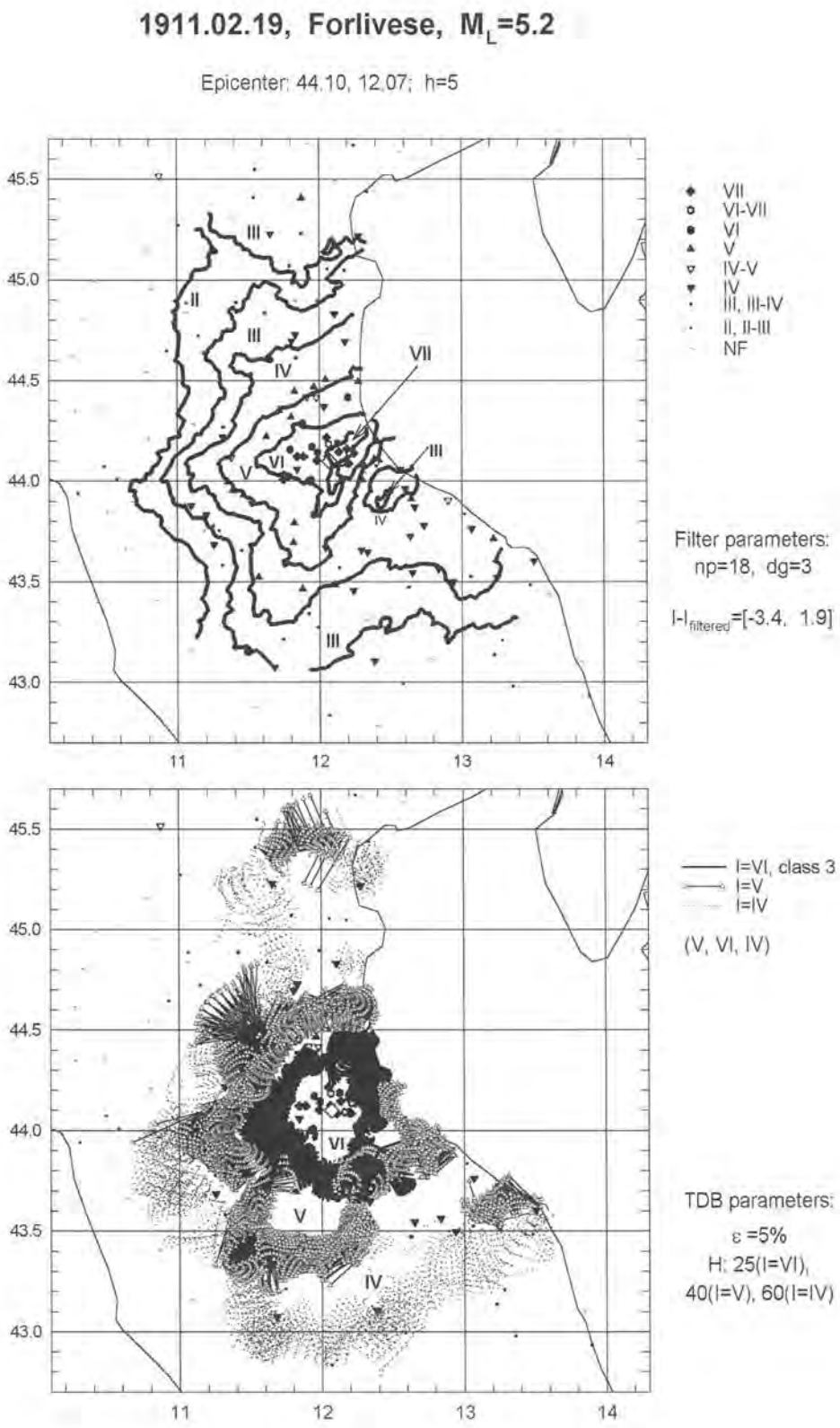
1911.02.19, Forlivese, M_L=5.2
Epicenter: 44.10, 12.07; h=5
VII
VI-VII
VI
V
IV-V
IV
III, III-IV
II, II-III
NF
Filter parameters:
np=18, dg=3
$I-I_{filtered}$=[-3.4, 1.9]
I=VI, class 3
I=V
I=IV
(V, VI, IV)
TDB parameters:
ε =5%
H: 25(I=VI),
40(I=V), 60(I=IV)
45.5
45.0
44.5
44.0
43.5
43.0
11
12
13
14

Fig. A-20

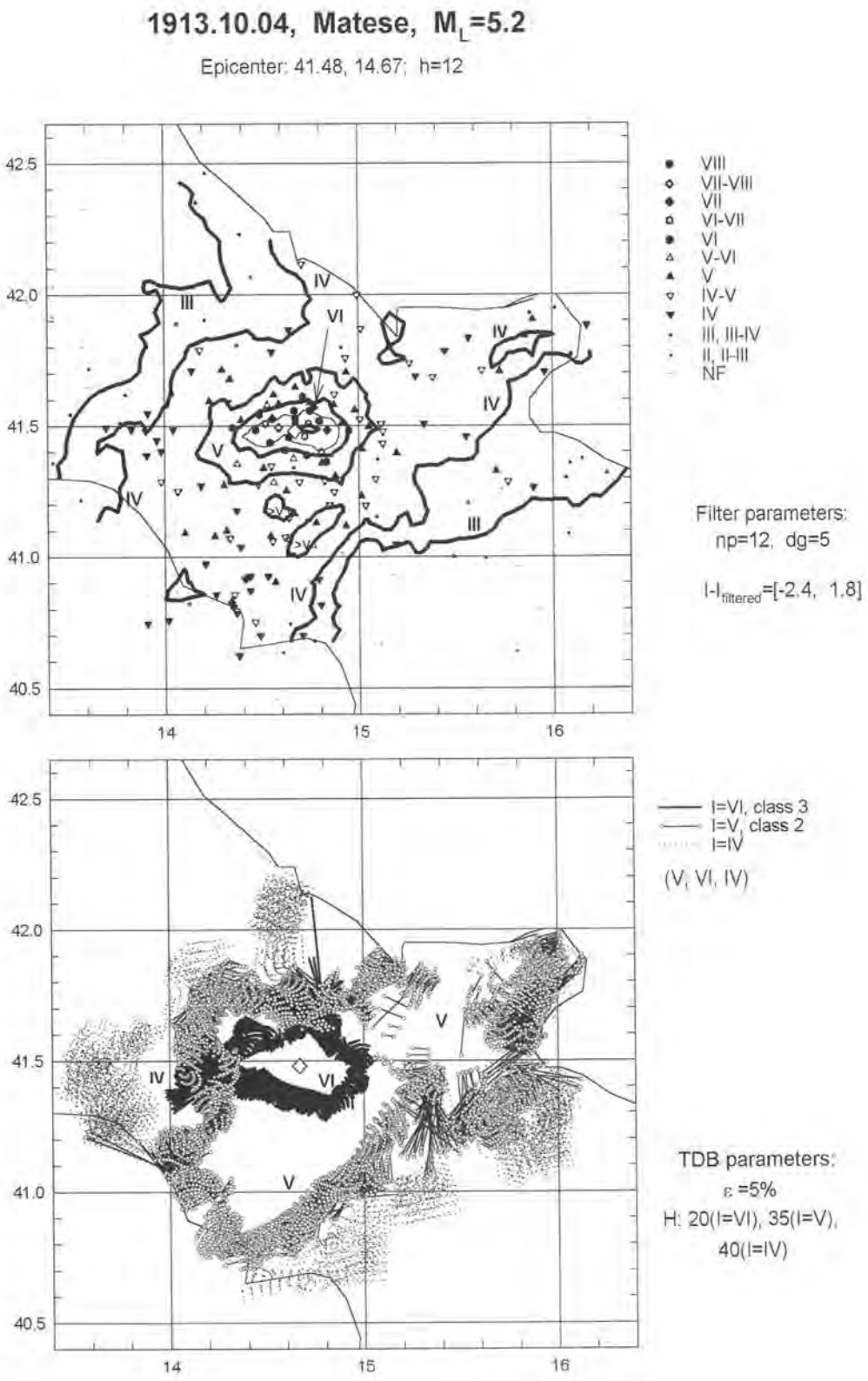
1913.10.04, Matese, M_L=5.2
Epicenter: 41.48, 14.67; h=12
VIII
VII-VIII
VII
VI-VII
VI
V-VI
V
IV-V
IV
III, III-IV
II, II-III
NF
Filter parameters:
np=12, dg=5
$I-I_{filtered}$=[-2.4, 1.8]
I=VI, class 3
I=V, class 2
I=IV
(V, VI, IV)
TDB parameters:
ε =5%
H: 20(I=VI), 35(I=V),
40(I=IV)
42.5
42.0
41.5
41.0
40.5
14
15
16

Fig. A-21

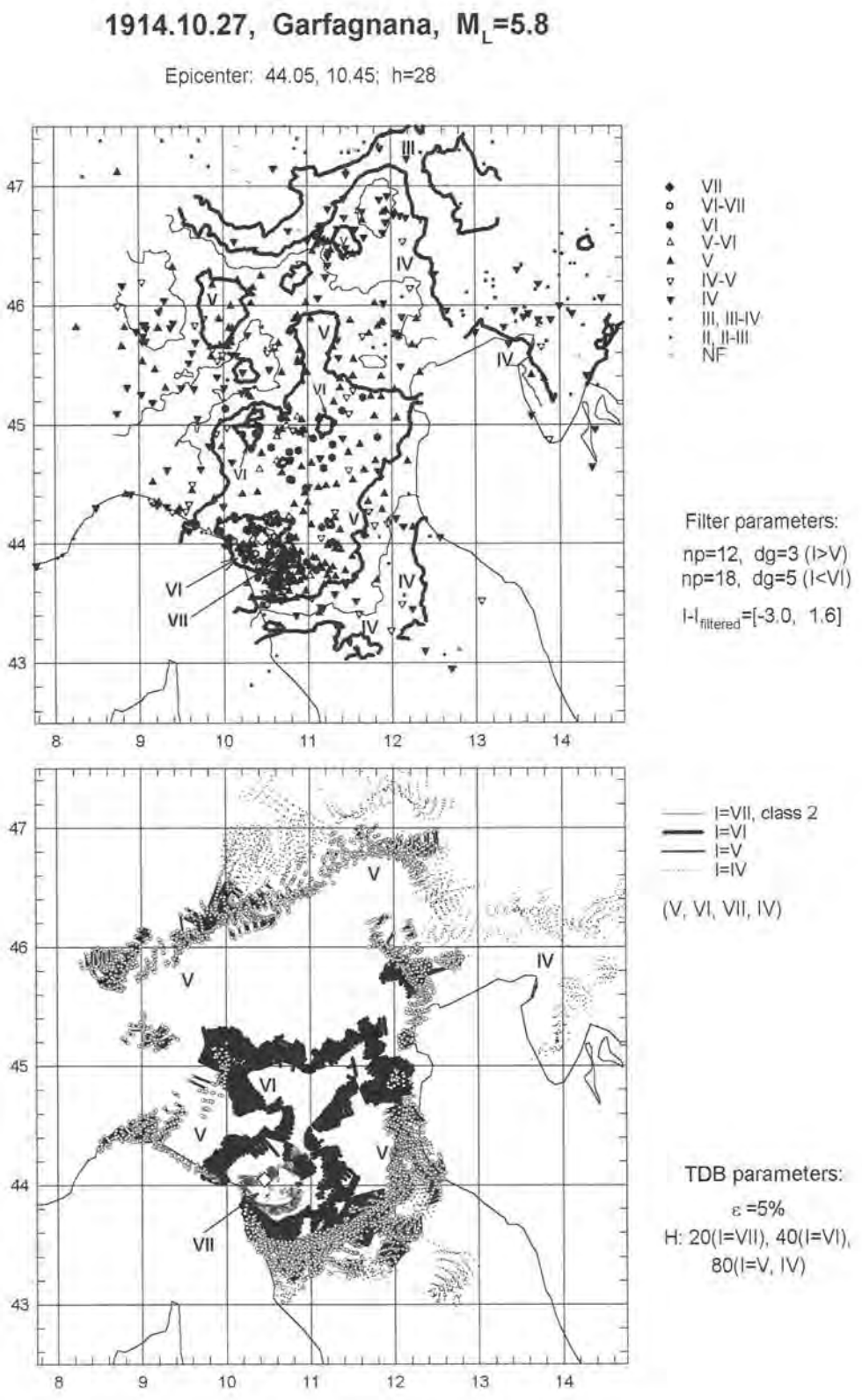
1914.10.27, Garfagnana, M_L=5.8
Epicenter: 44.05, 10.45; h=28
VII
VI-VII
VI
V-VI
V
IV-V
IV
III, III-IV
II, II-III
NF
Filter parameters:
np=12, dg=3 (I>V)
np=18, dg=5 (I<VI)
$I-I_{filtered}$=[-3.0, 1.6]
I=VII, class 2
I=VI
I=V
I=IV
(V, VI, VII, IV)
TDB parameters:
ε =5%
H: 20(I=VII), 40(I=VI),
80(I=V, IV)

Fig. A-22

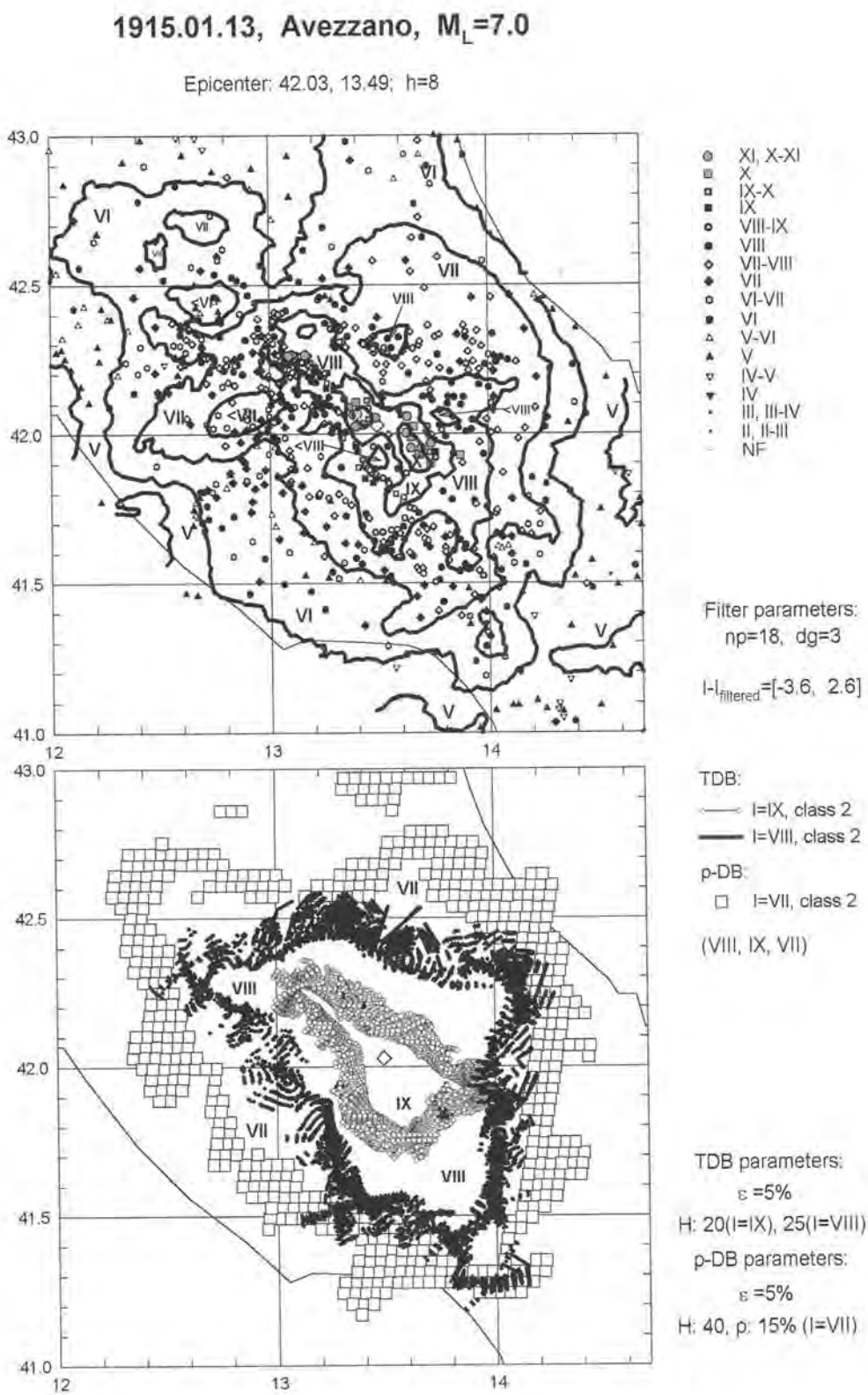
1915.01.13, Avezzano, M_L=7.0
Epicenter: 42.03, 13.49; h=8
XI, X-XI
X
IX-X
IX
VIII-IX
VIII
VII-VIII
VII
VI-VII
VI
V-VI
V
IV-V
IV
III, III-IV
II, II-III
NF
Filter parameters:
np=18, dg=3
$I-I_{filtered}$=[-3.6, 2.6]
TDB:
I=IX, class 2
I=VIII, class 2
p-DB:
I=VII, class 2
(VIII, IX, VII)
TDB parameters:
ε =5%
H: 20(I=IX), 25(I=VIII)
p-DB parameters:
ε =5%
H: 40, p: 15% (I=VII)
43.0
42.5
42.0
41.5
41.0
12
13
14

Fig. A-23

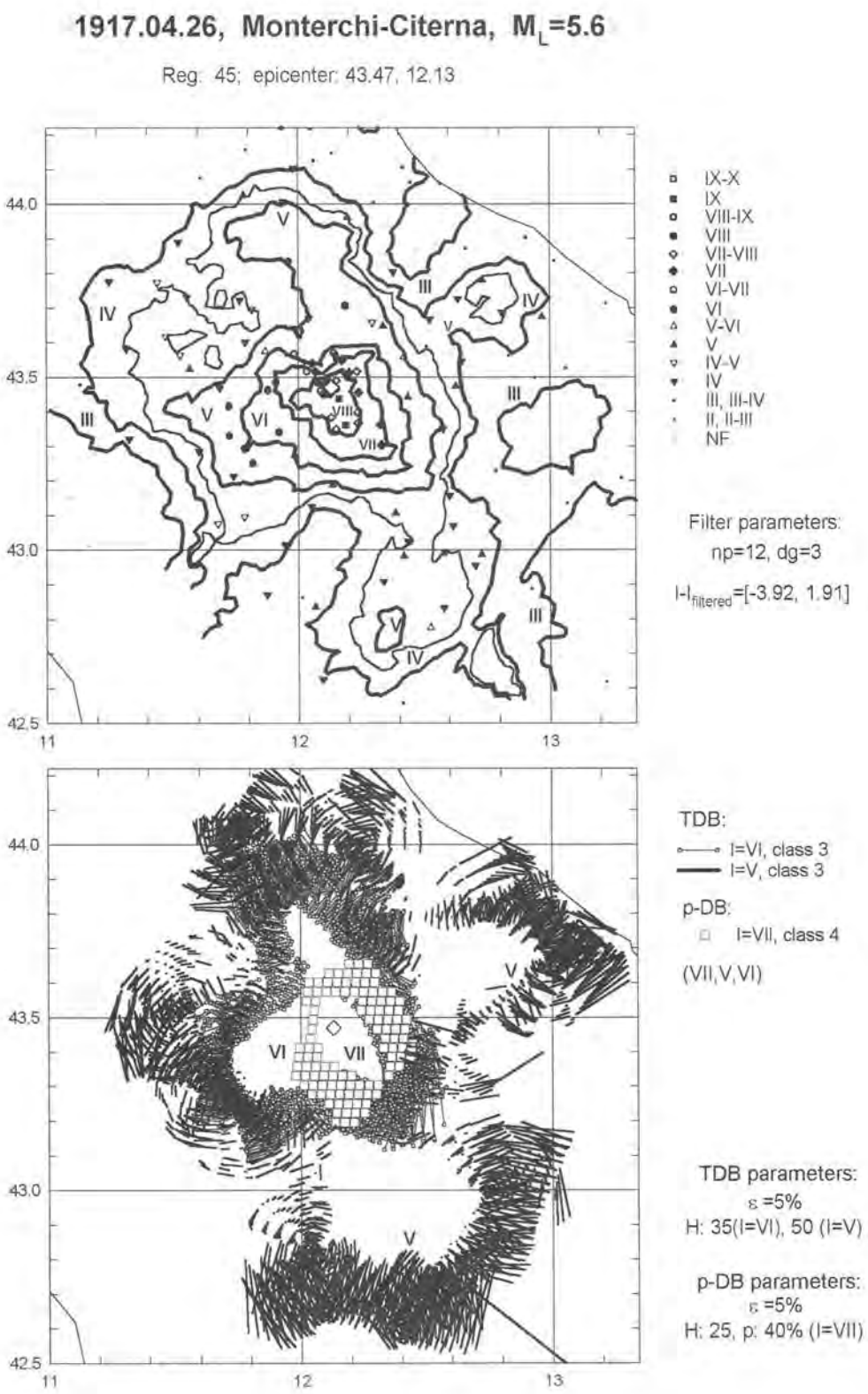
1917.04.26, Monterchi-Citerna, M_L=5.6
Reg: 45; epicenter: 43.47, 12.13
IX-X
IX
VIII-IX
VIII
VII-VIII
VII
VI-VII
VI
V-VI
V
IV-V
IV
III, III-IV
II, II-III
NF
Filter parameters:
np=12, dg=3
$I-I_{filtered}$=[-3.92, 1.91]
TDB:
I=VI, class 3
I=V, class 3
p-DB:
I=VII, class 4
(VII,V,VI)
TDB parameters:
ε =5%
H: 35(I=VI), 50 (I=V)
p-DB parameters:
ε =5%
H: 25, p: 40% (I=VII)
44.0
43.5
43.0
42.5
11
12
13

Fig. A-24

1918.11.10, Appennino romagnolo, S.Sofia, M_L=5.8

Epicenter: 43.95, 11.87; h=12

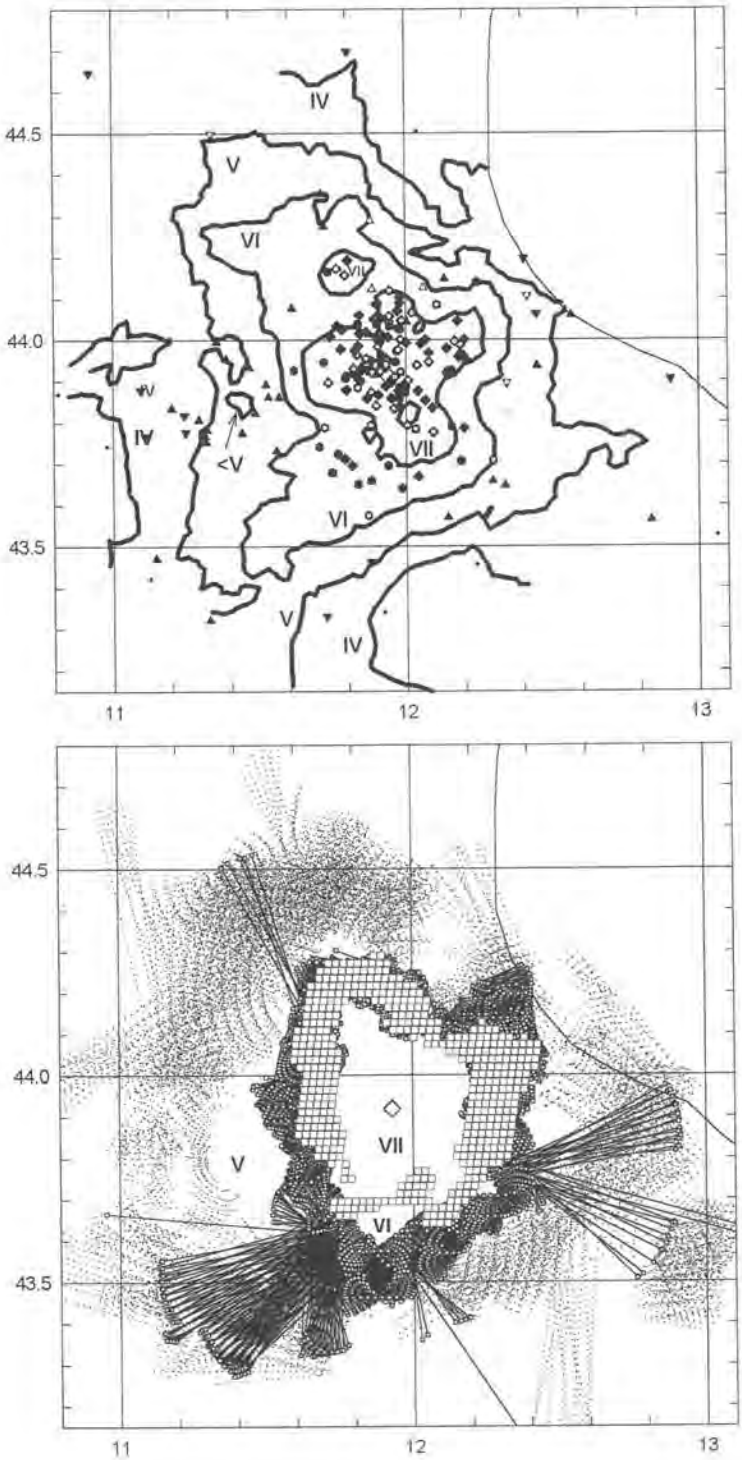

Fig. A-25

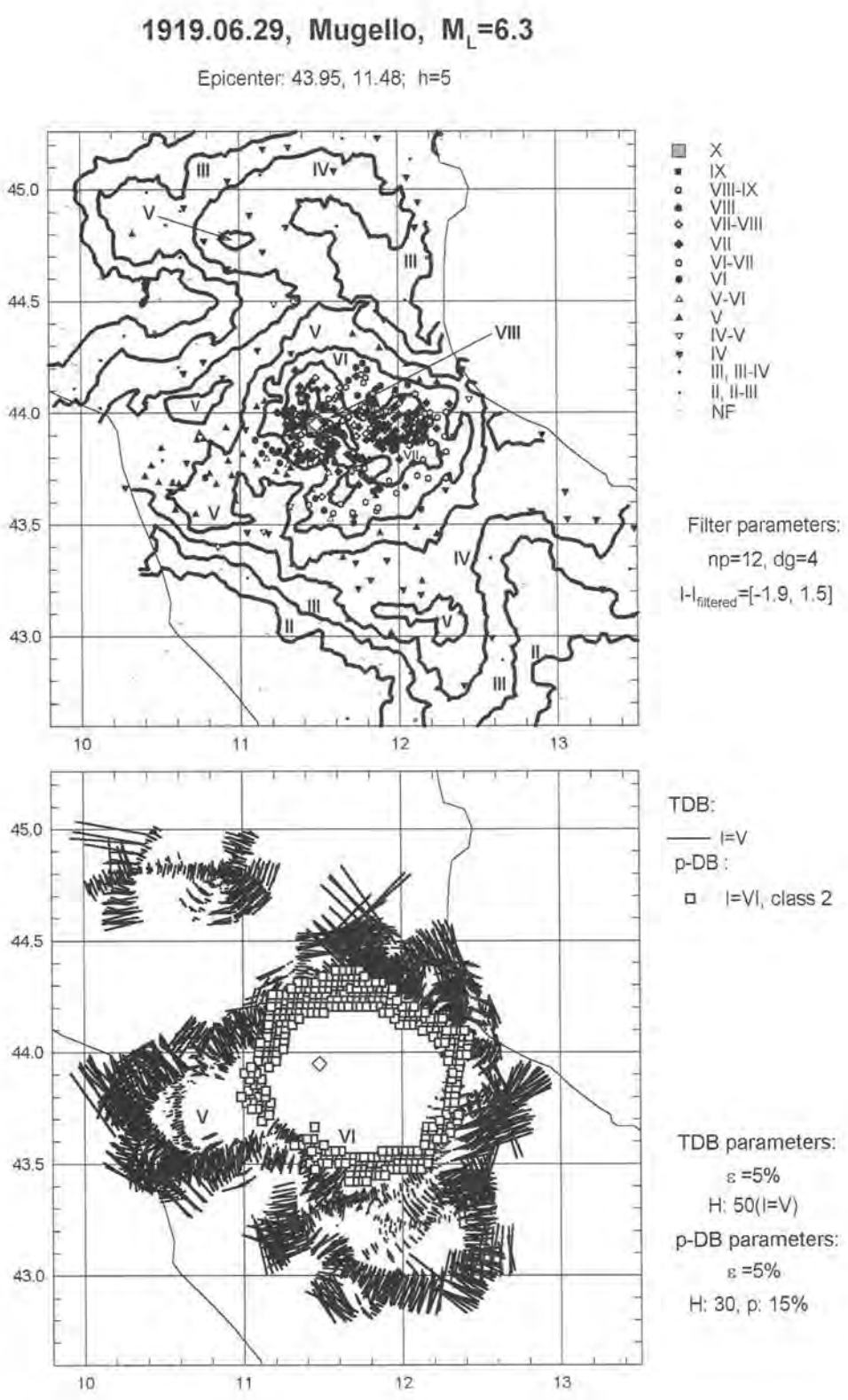
1919.06.29, Mugello, M_L=6.3
Epicenter: 43.95, 11.48; h=5
X
IX
VIII-IX
VIII
VII-VIII
VII
VI-VII
VI
V-VI
V
IV-V
IV
III, III-IV
II, II-III
NF
Filter parameters:
np=12, dg=4
I-I_filtered=[-1.9, 1.5]
TDB:
I=V
p-DB :
I=VI, class 2
TDB parameters:
ε =5%
H: 50(I=V)
p-DB parameters:
ε =5%
H: 30, p: 15%
45.0
44.5
44.0
43.5
43.0
10
11
12
13

Fig. A-26

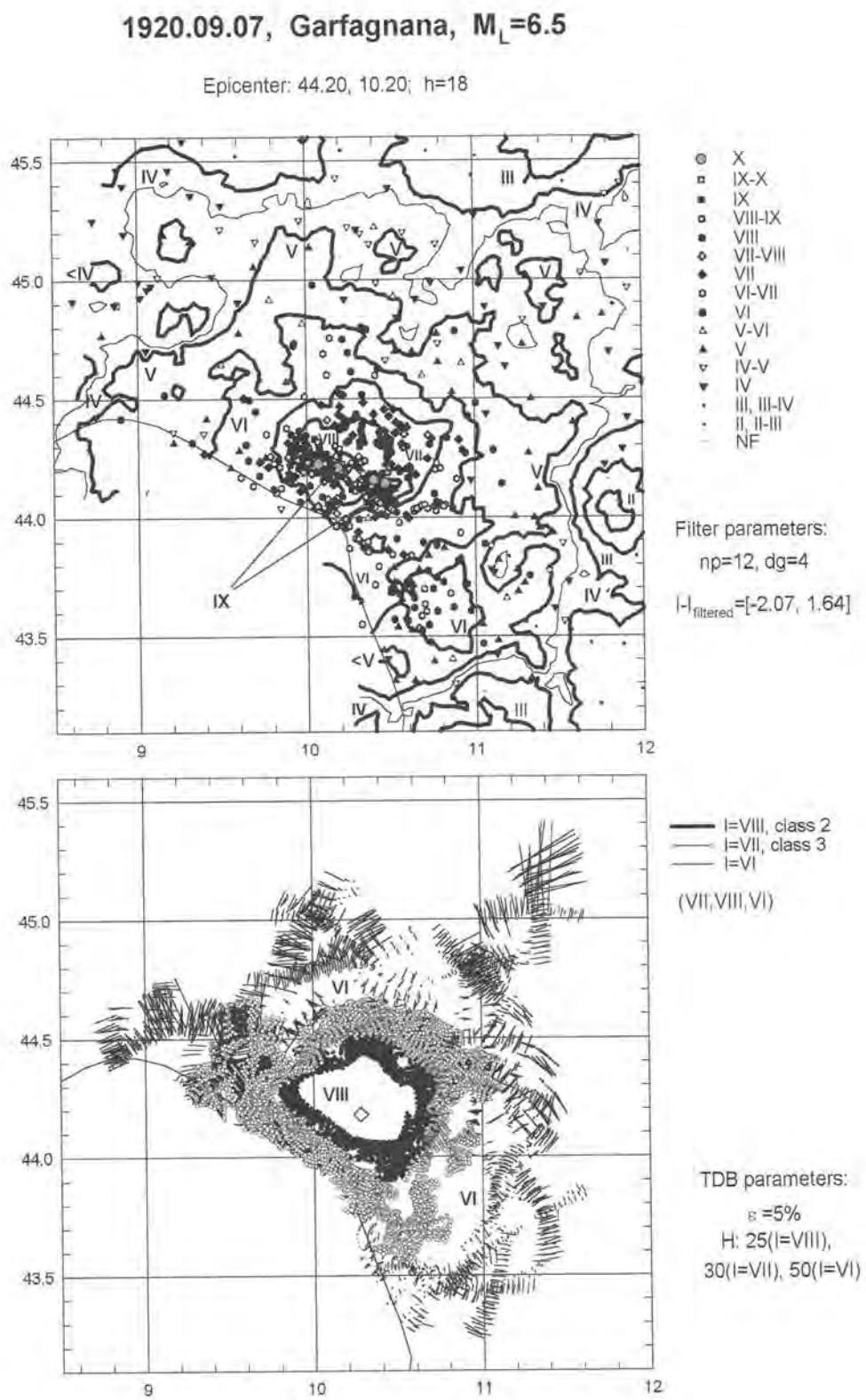
1920.09.07, Garfagnana, M_L=6.5
Epicenter: 44.20, 10.20; h=18
X
IX-X
IX
VIII-IX
VIII
VII-VIII
VII
VI-VII
VI
V-VI
V
IV-V
IV
III, III-IV
II, II-III
NF
Filter parameters:
np=12, dg=4
$I-I_{filtered}$=[-2.07, 1.64]
I=VIII, class 2
I=VII, class 3
I=VI
(VII,VIII,VI)
TDB parameters:
ε =5%
H: 25(I=VIII),
30(I=VII), 50(I=VI)
45.5
45.0
44.5
44.0
43.5
9
10
11
12

Fig. A-27

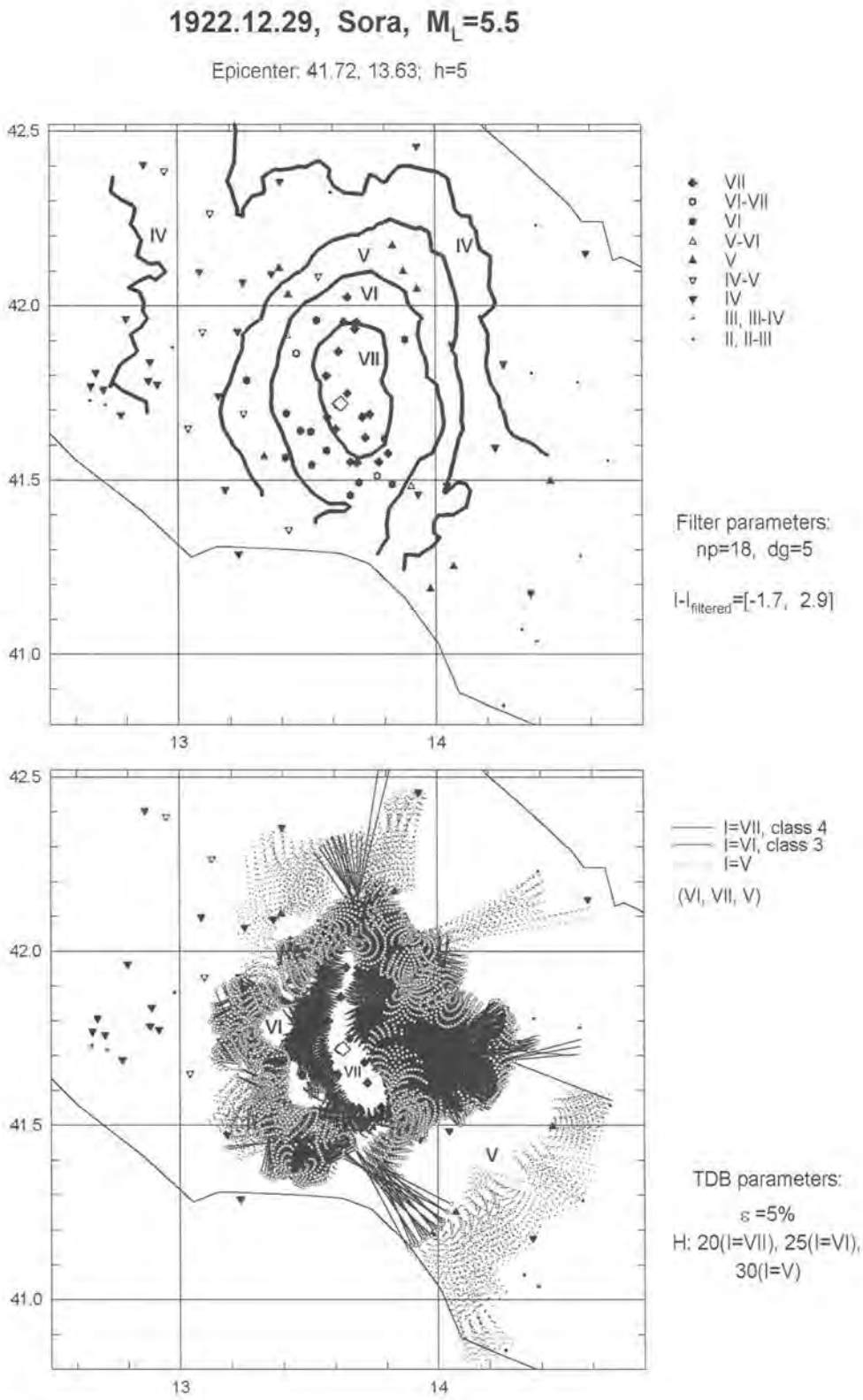
1922.12.29, Sora, M_L=5.5
Epicenter: 41.72, 13.63; h=5
42.5
42.0
41.5
41.0
13
14
IV
V
VI
VII
VII
VI-VII
VI
V-VI
V
IV-V
IV
III, III-IV
II, II-III
Filter parameters:
np=18, dg=5
$I-I_{filtered}$=[-1.7, 2.9]
I=VII, class 4
I=VI, class 3
I=V
(VI, VII, V)
TDB parameters:
ε =5%
H: 20(I=VII), 25(I=VI),
30(I=V)

Fig. A-28

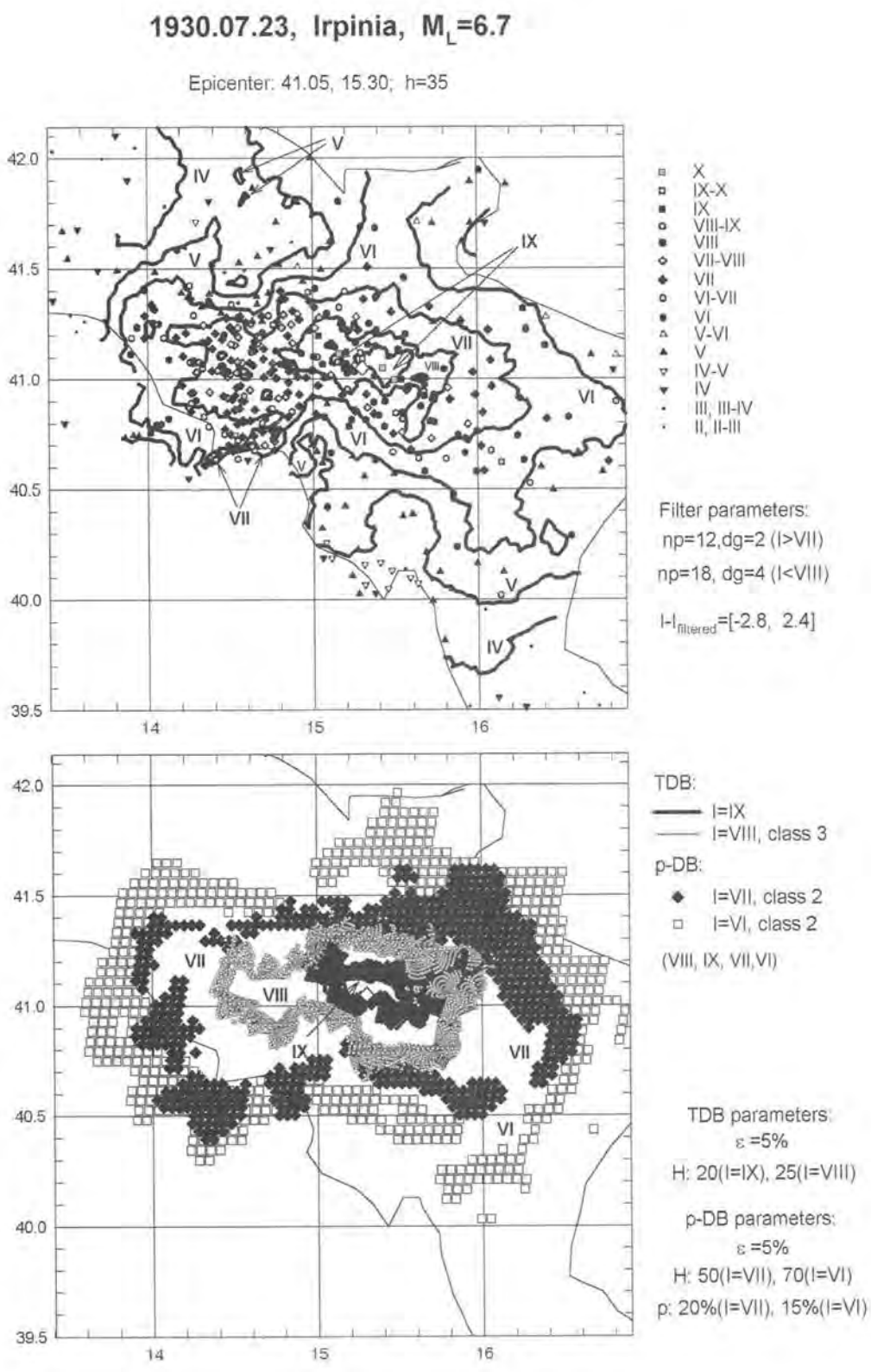
1930.07.23, Irpinia, M_L=6.7
Epicenter: 41.05, 15.30; h=35
X
IX-X
IX
VIII-IX
VIII
VII-VIII
VII
VI-VII
VI
V-VI
V
IV-V
IV
III, III-IV
II, II-III
Filter parameters:
np=12,dg=2 (I>VII)
np=18, dg=4 (I<VIII)
$I-I_{filtered}$=[-2.8, 2.4]
TDB:
I=IX
I=VIII, class 3
p-DB:
I=VII, class 2
I=VI, class 2
(VIII, IX, VII,VI)
TDB parameters:
ε =5%
H: 20(I=IX), 25(I=VIII)
p-DB parameters:
ε =5%
H: 50(I=VII), 70(I=VI)
p: 20%(I=VII), 15%(I=VI)
42.0
41.5
41.0
40.5
40.0
39.5
14
15
16

Fig. A-29

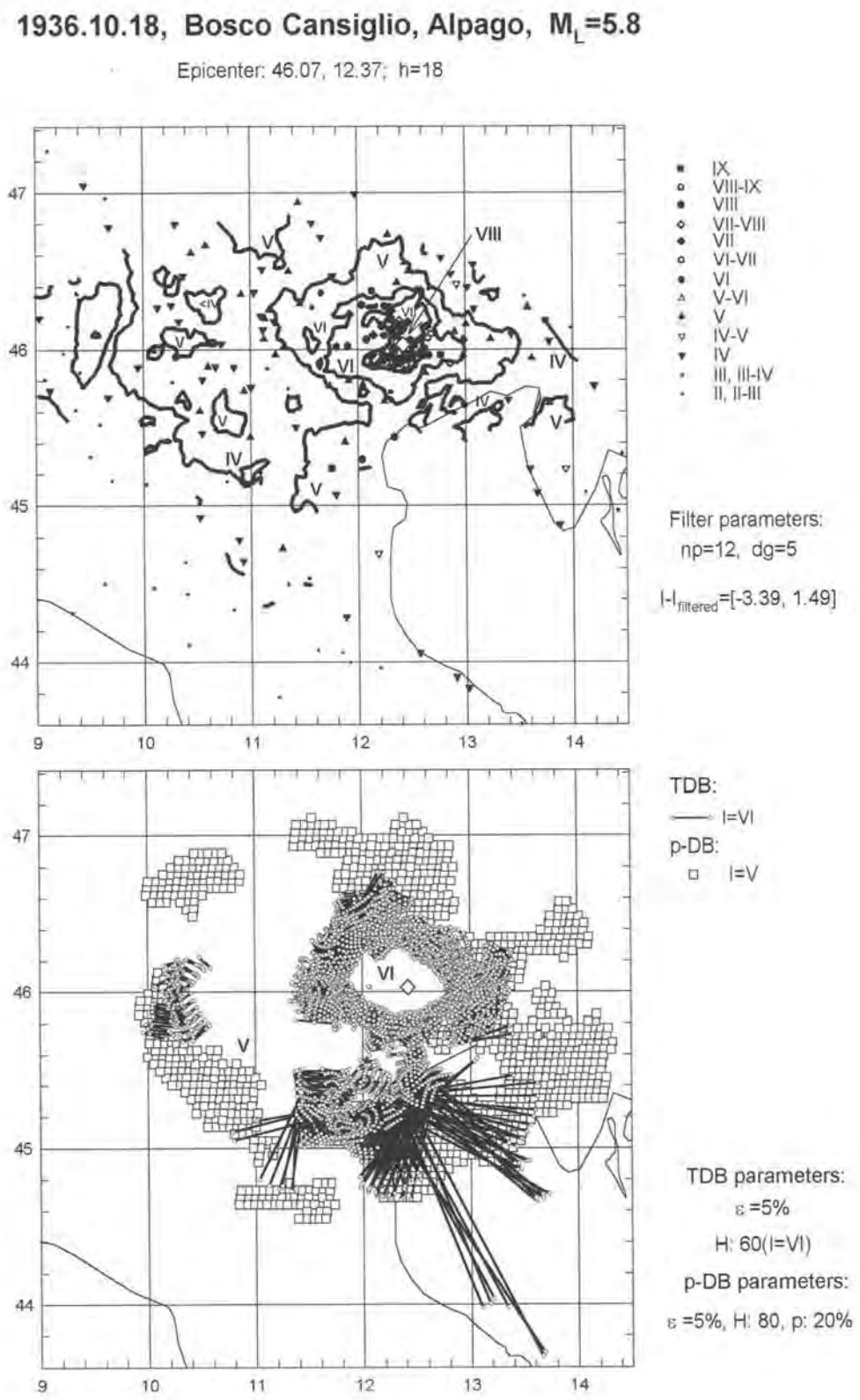
1936.10.18, Bosco Cansiglio, Alpago, M_L=5.8
Epicenter: 46.07, 12.37; h=18
IX
VIII-IX
VIII
VII-VIII
VII
VI-VII
VI
V-VI
V
IV-V
IV
III, III-IV
II, II-III
Filter parameters:
np=12, dg=5
$I-I_{filtered}$=[-3.39, 1.49]
TDB:
I=VI
p-DB:
I=V
TDB parameters:
ε =5%
H: 60(I=VI)
p-DB parameters:
ε =5%, H: 80, p: 20%
47
46
45
44
9
10
11
12
13
14

Fig. A-30

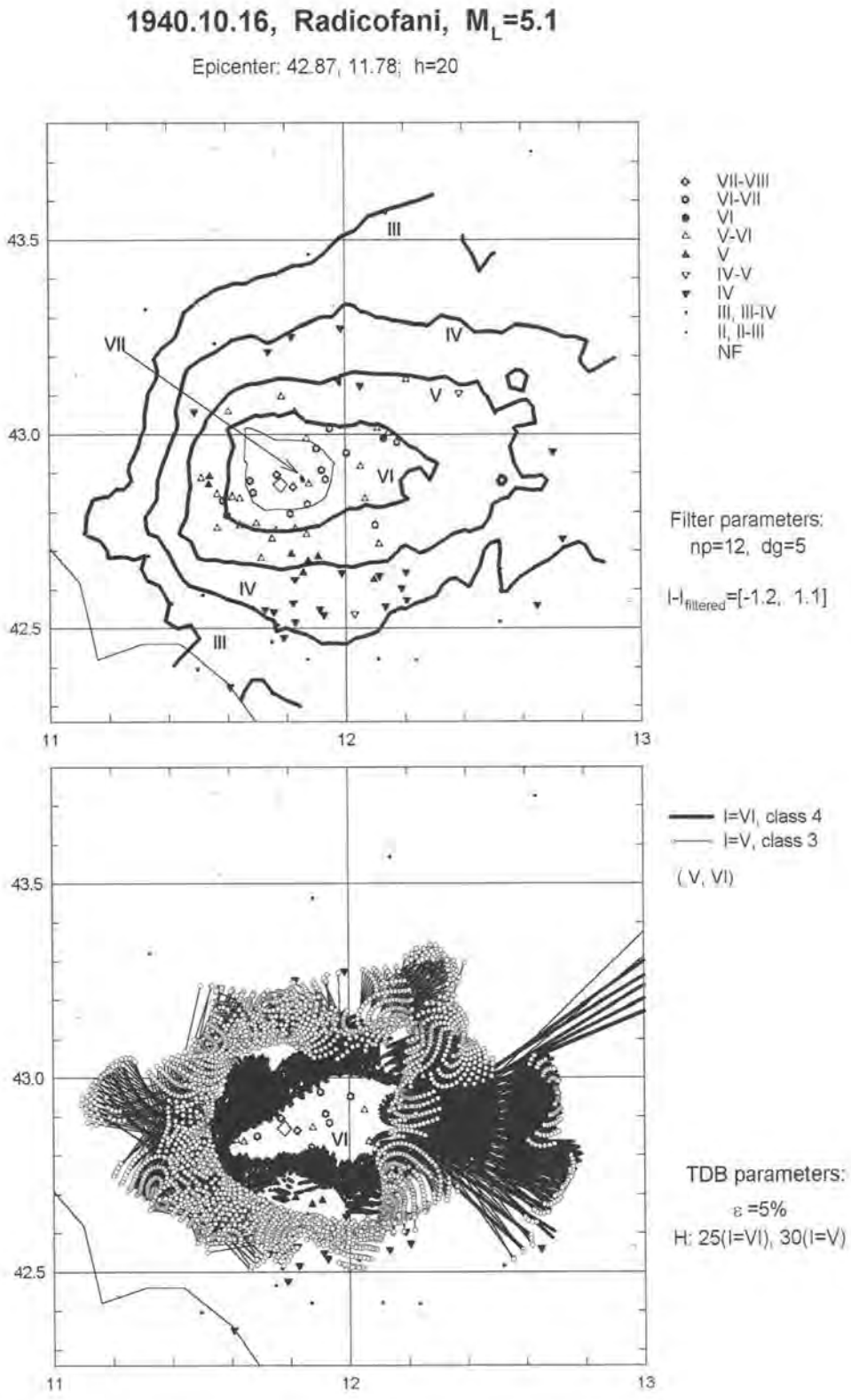
1940.10.16, Radicofani, M_L=5.1
Epicenter: 42.87, 11.78; h=20
VII-VIII
VI-VII
VI
V-VI
V
IV-V
IV
III, III-IV
II, II-III
NF
Filter parameters:
np=12, dg=5
$I-I_{filtered}$=[-1.2, 1.1]
I=VI, class 4
I=V, class 3
(V, VI)
TDB parameters:
ε=5%
H: 25(I=VI), 30(I=V)
43.5
43.0
42.5
11
12
13
III
IV
V
VI
VII

Fig. A-31

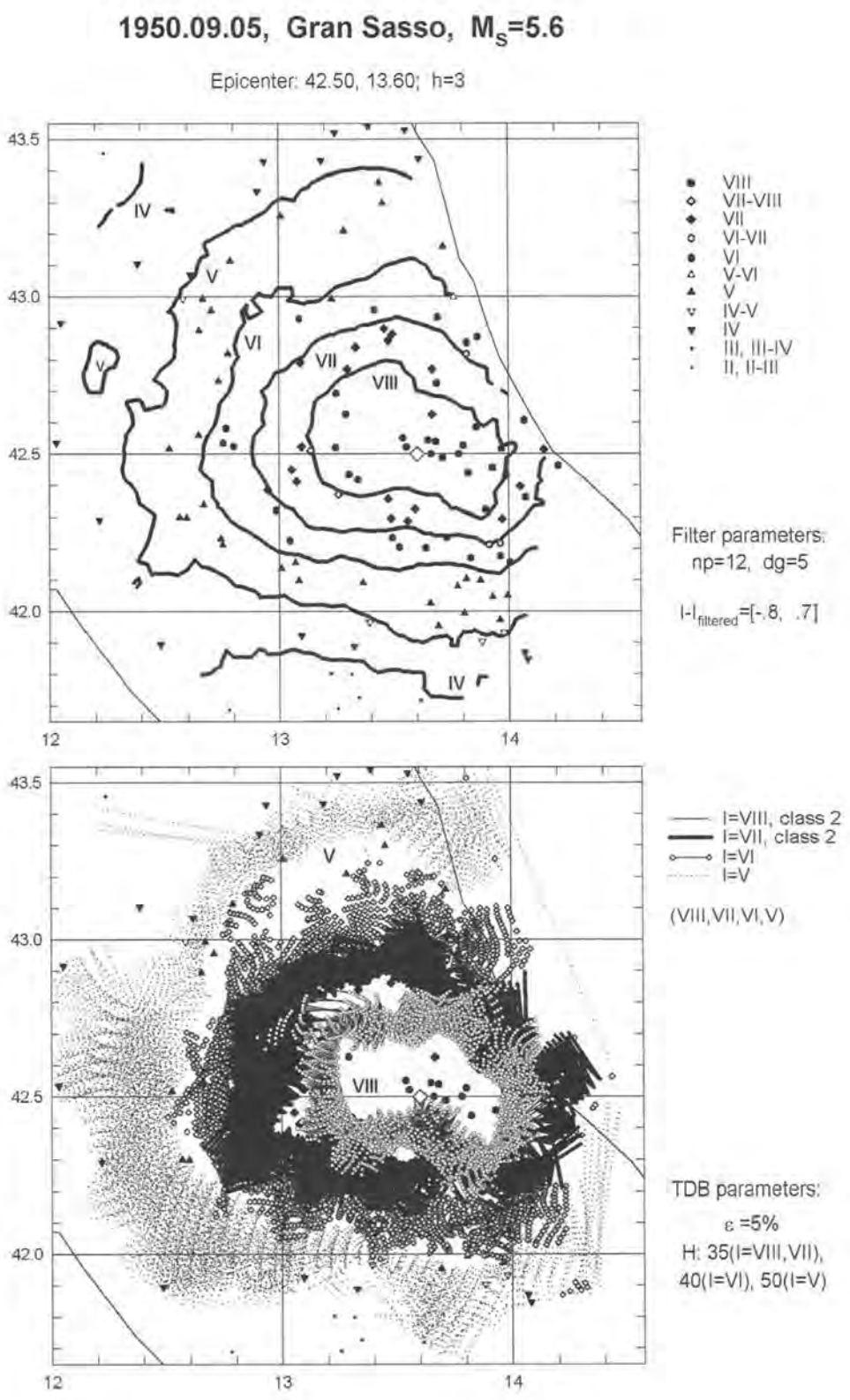
1950.09.05, Gran Sasso, M_S=5.6
Epicenter: 42.50, 13.60; h=3
43.5
43.0
42.5
42.0
12
13
14
IV
V
VI
VII
VIII
VIII
VII-VIII
VII
VI-VII
VI
V-VI
V
IV-V
IV
III, III-IV
II, II-III
Filter parameters:
np=12, dg=5
$I-I_{filtered}$=[-.8, .7]
I=VIII, class 2
I=VII, class 2
I=VI
I=V
(VIII,VII,VI,V)
TDB parameters:
ε =5%
H: 35(I=VIII,VII),
40(I=VI), 50(I=V)

Fig. A-32

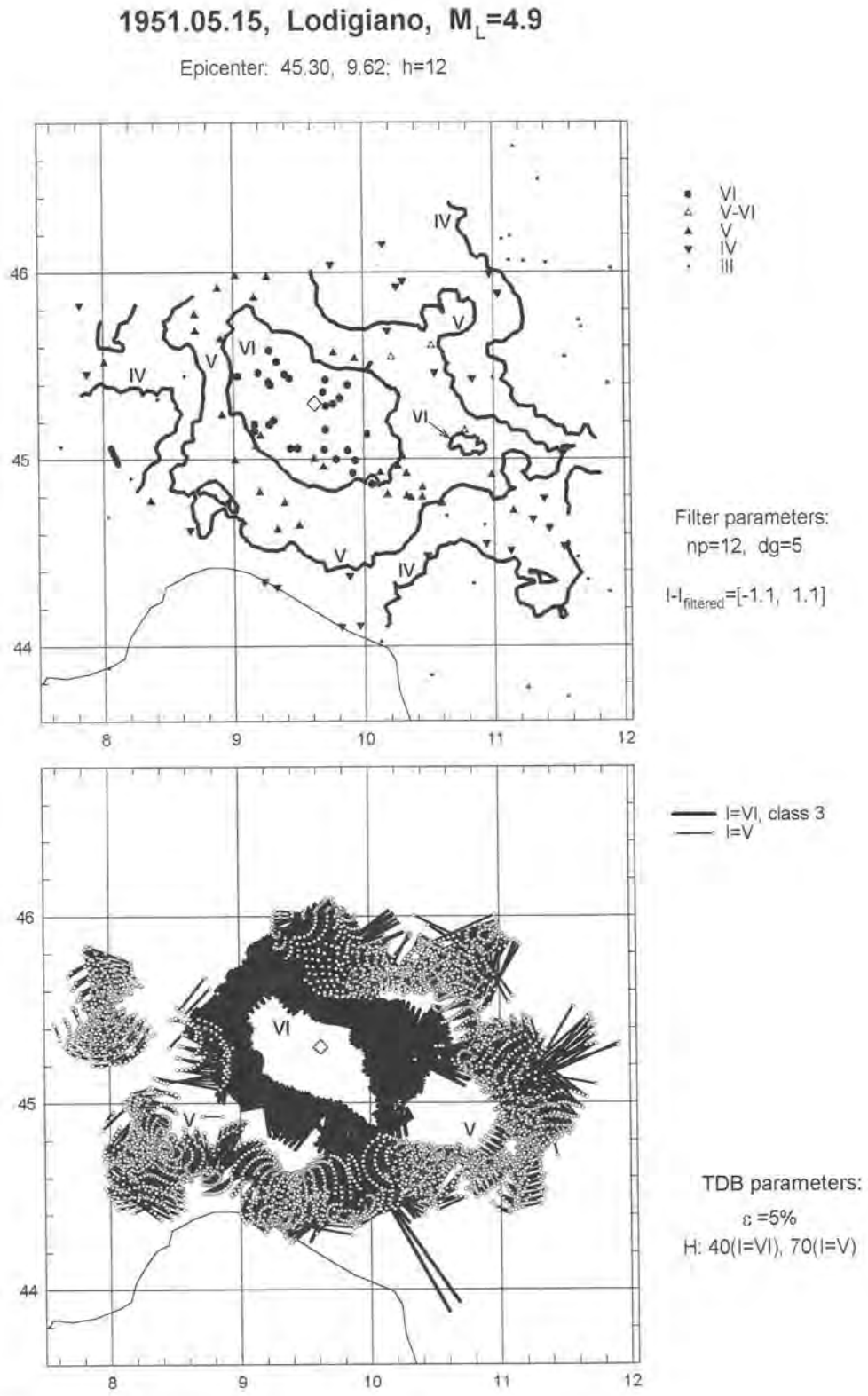
1951.05.15, Lodigiano, M_L=4.9
Epicenter: 45.30, 9.62; h=12
VI
V-VI
V
IV
III
Filter parameters:
np=12, dg=5
$I-I_{filtered}$=[-1.1, 1.1]
I=VI, class 3
I=V
TDB parameters:
ε =5%
H: 40(I=VI), 70(I=V)
46
45
44
8
9
10
11
12

Fig. A-33

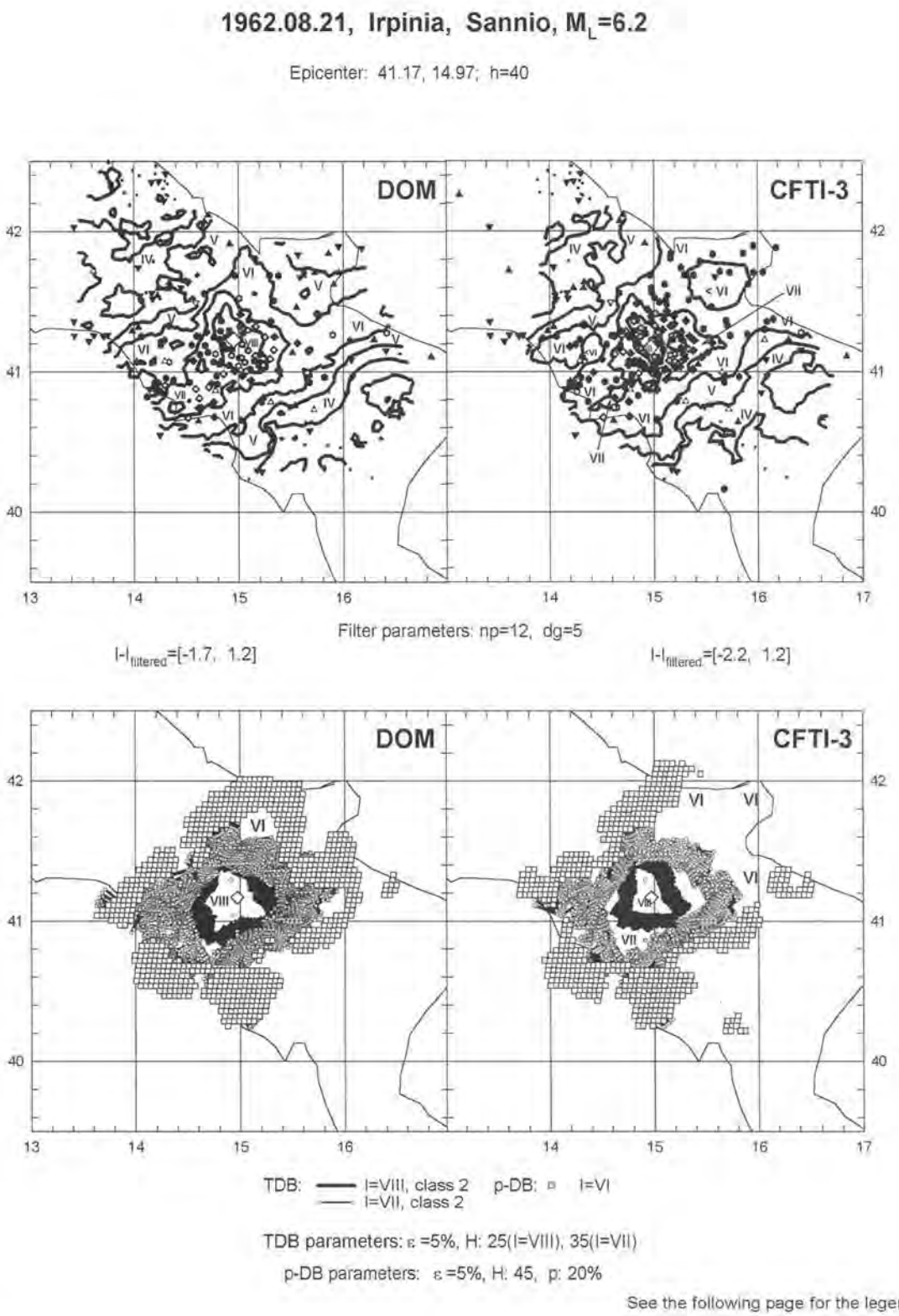

See the following page for the legend

Fig. A-34

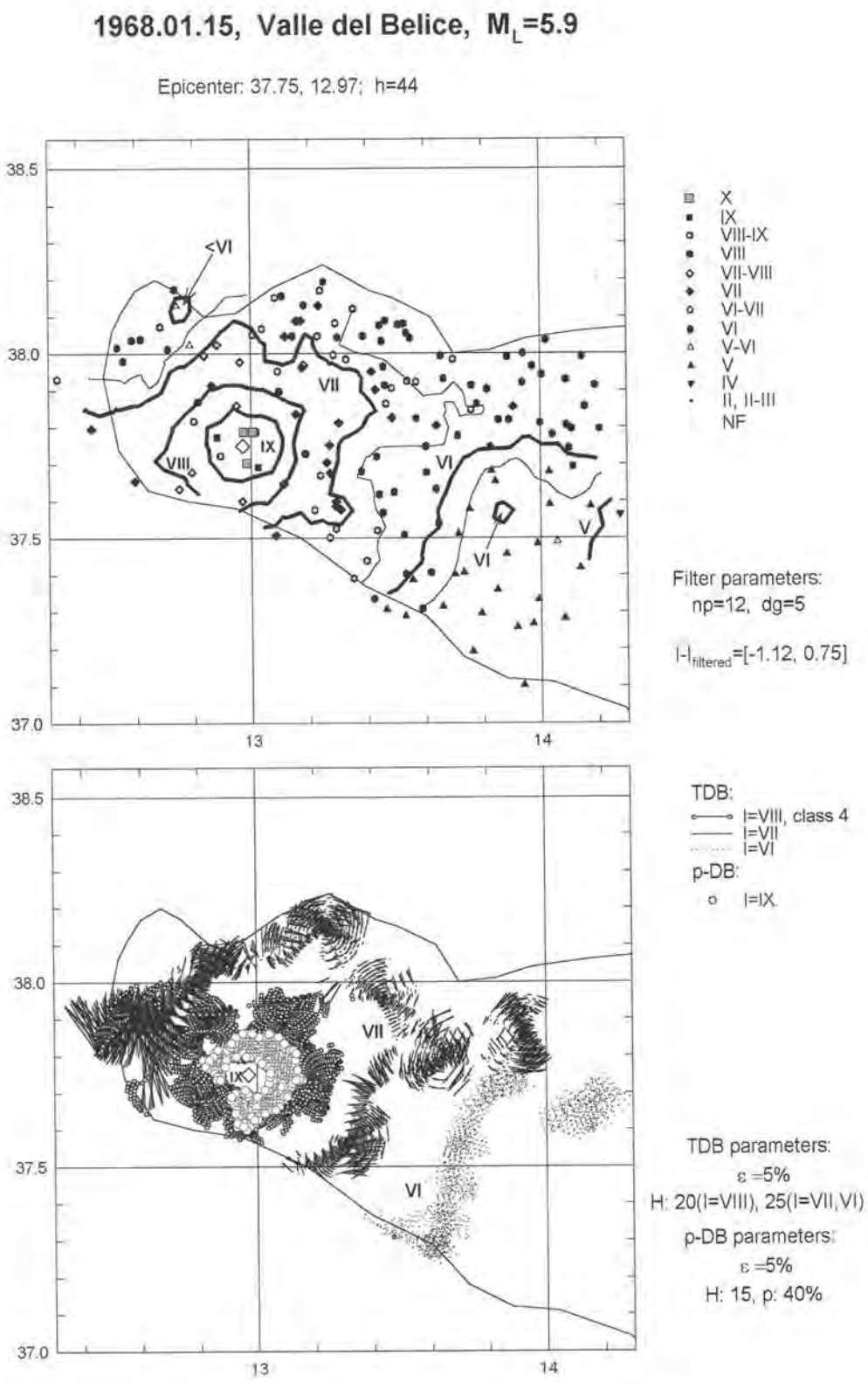
1968.01.15, Valle del Belice, M_L=5.9
Epicenter: 37.75, 12.97; h=44
38.5
38.0
37.5
37.0
13
14
VI
VII
VIII
IX
V
X
IX
VIII-IX
VIII
VII-VIII
VII
VI-VII
VI
V-VI
V
IV
II, II-III
NF
Filter parameters:
np=12, dg=5
$I-I_{filtered}$=[-1.12, 0.75]
TDB:
I=VIII, class 4
I=VII
I=VI
p-DB:
I=IX
TDB parameters:
ε =5%
H: 20(I=VIII), 25(I=VII,VI)
p-DB parameters:
ε =5%
H: 15, p: 40%

Fig. A-35

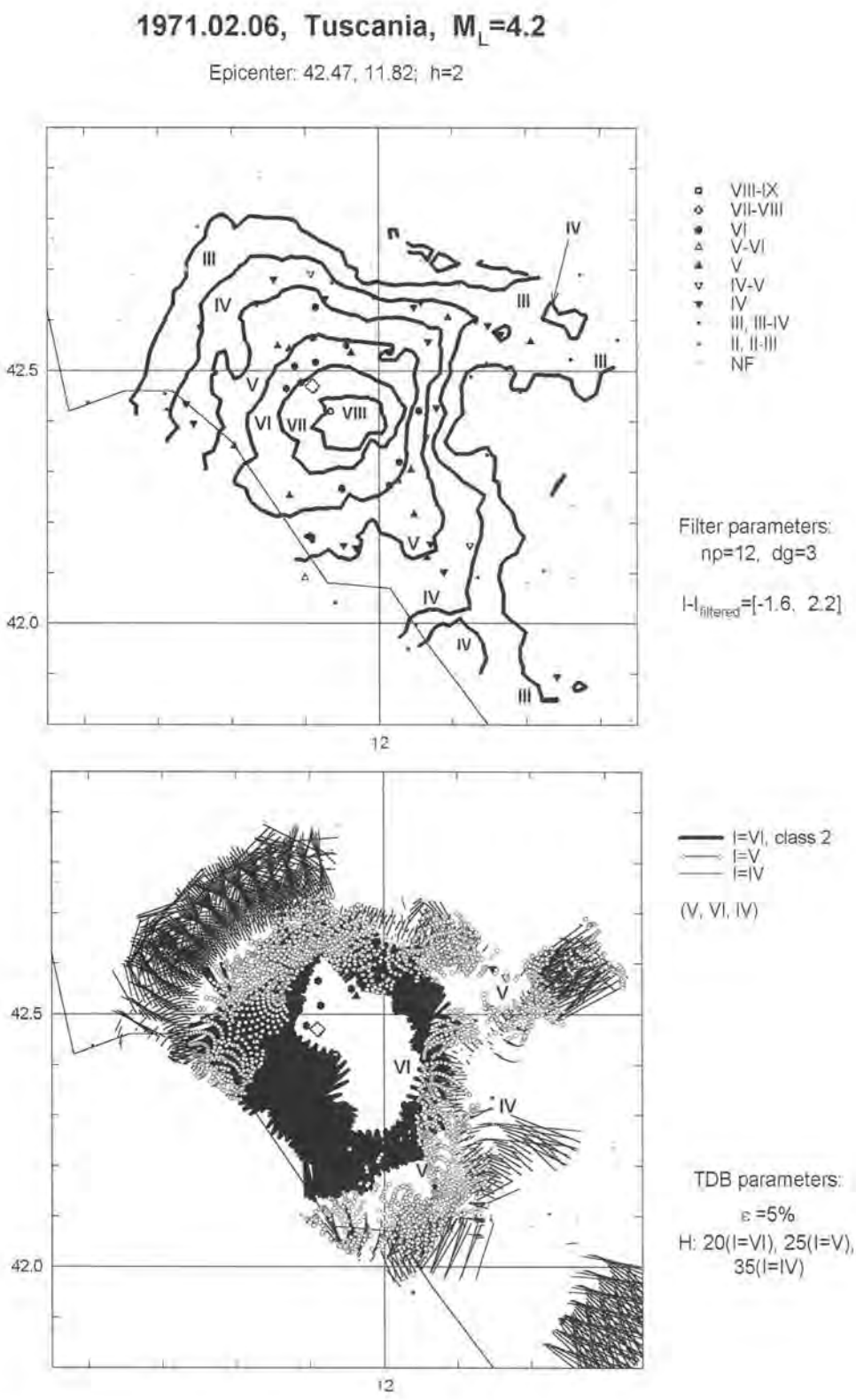
1971.02.06, Tuscania, M_L=4.2
Epicenter: 42.47, 11.82; h=2
VIII-IX
VII-VIII
VI
V-VI
V
IV-V
IV
III, III-IV
II, II-III
NF
Filter parameters:
np=12, dg=3
I-I filtered=[-1.6, 2.2]
I=VI, class 2
I=V
I=IV
(V, VI, IV)
TDB parameters:
ε =5%
H: 20(I=VI), 25(I=V),
35(I=IV)
42.5
42.0
12

Fig. A-36

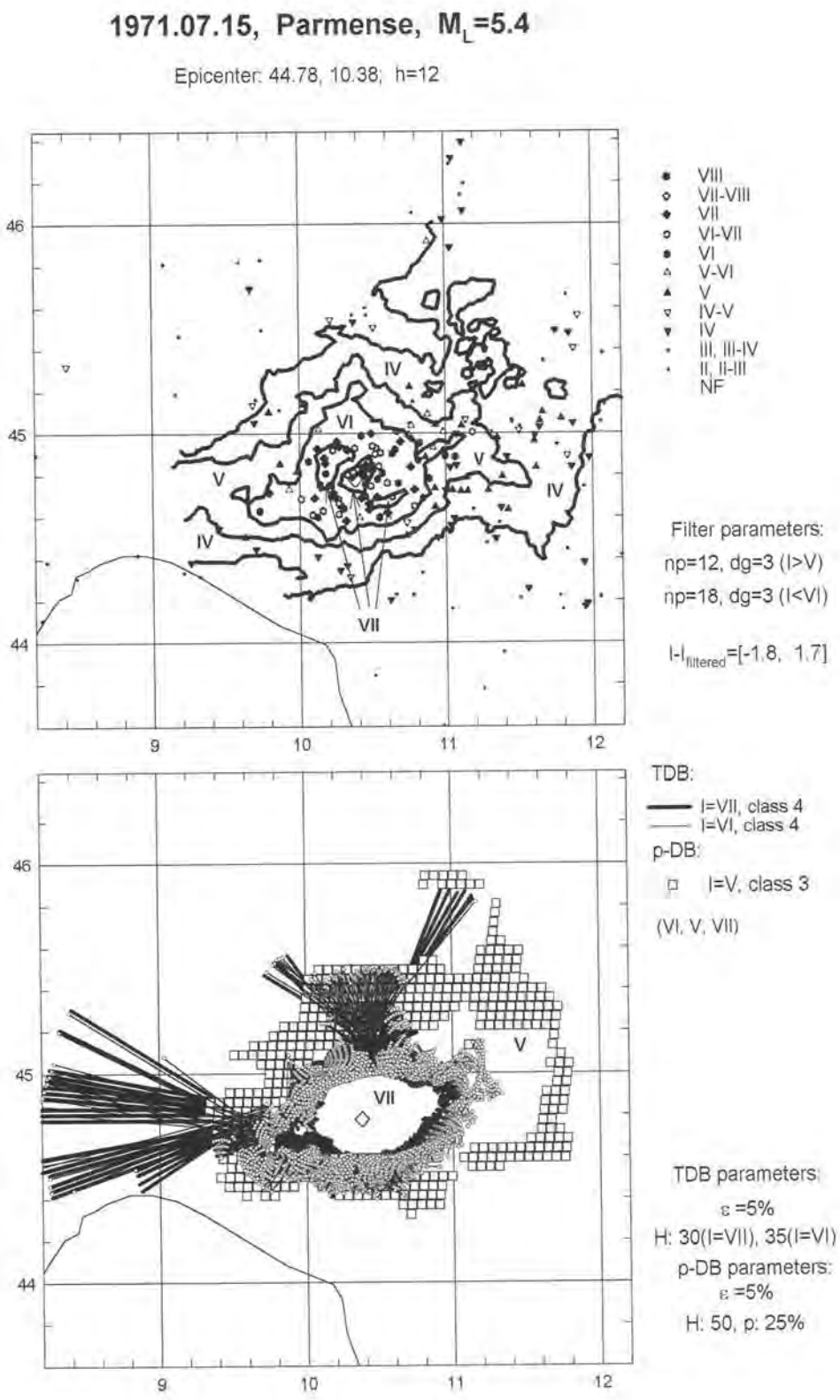
1971.07.15, Parmense, M_L=5.4
Epicenter: 44.78, 10.38; h=12
VIII
VII-VIII
VII
VI-VII
VI
V-VI
V
IV-V
IV
III, III-IV
II, II-III
NF
Filter parameters:
np=12, dg=3 (I>V)
np=18, dg=3 (I<VI)
$I-I_{filtered}$=[-1.8, 1.7]
TDB:
I=VII, class 4
I=VI, class 4
p-DB:
I=V, class 3
(VI, V, VII)
TDB parameters:
ε =5%
H: 30(I=VII), 35(I=VI)
p-DB parameters:
ε =5%
H: 50, p: 25%
46
45
44
9
10
11
12

Fig. A-37

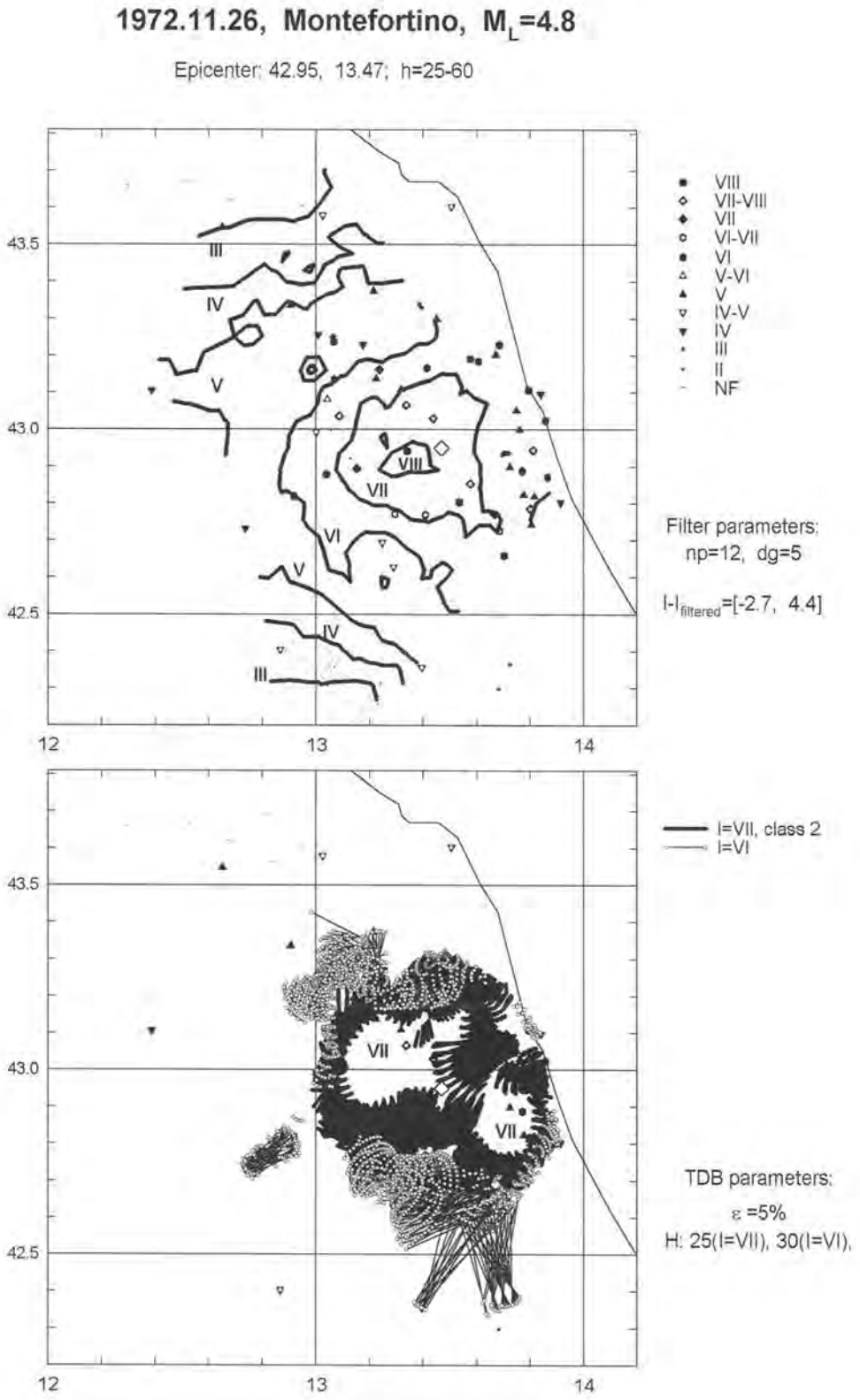
1972.11.26, Montefortino, M_L=4.8
Epicenter: 42.95, 13.47; h=25-60
VIII
VII-VIII
VII
VI-VII
VI
V-VI
V
IV-V
IV
III
II
NF
Filter parameters:
np=12, dg=5
$I-I_{filtered}$=[-2.7, 4.4]
I=VII, class 2
I=VI
TDB parameters:
ε =5%
H: 25(I=VII), 30(I=VI),
43.5
43.0
42.5
12
13
14

Fig. A-38

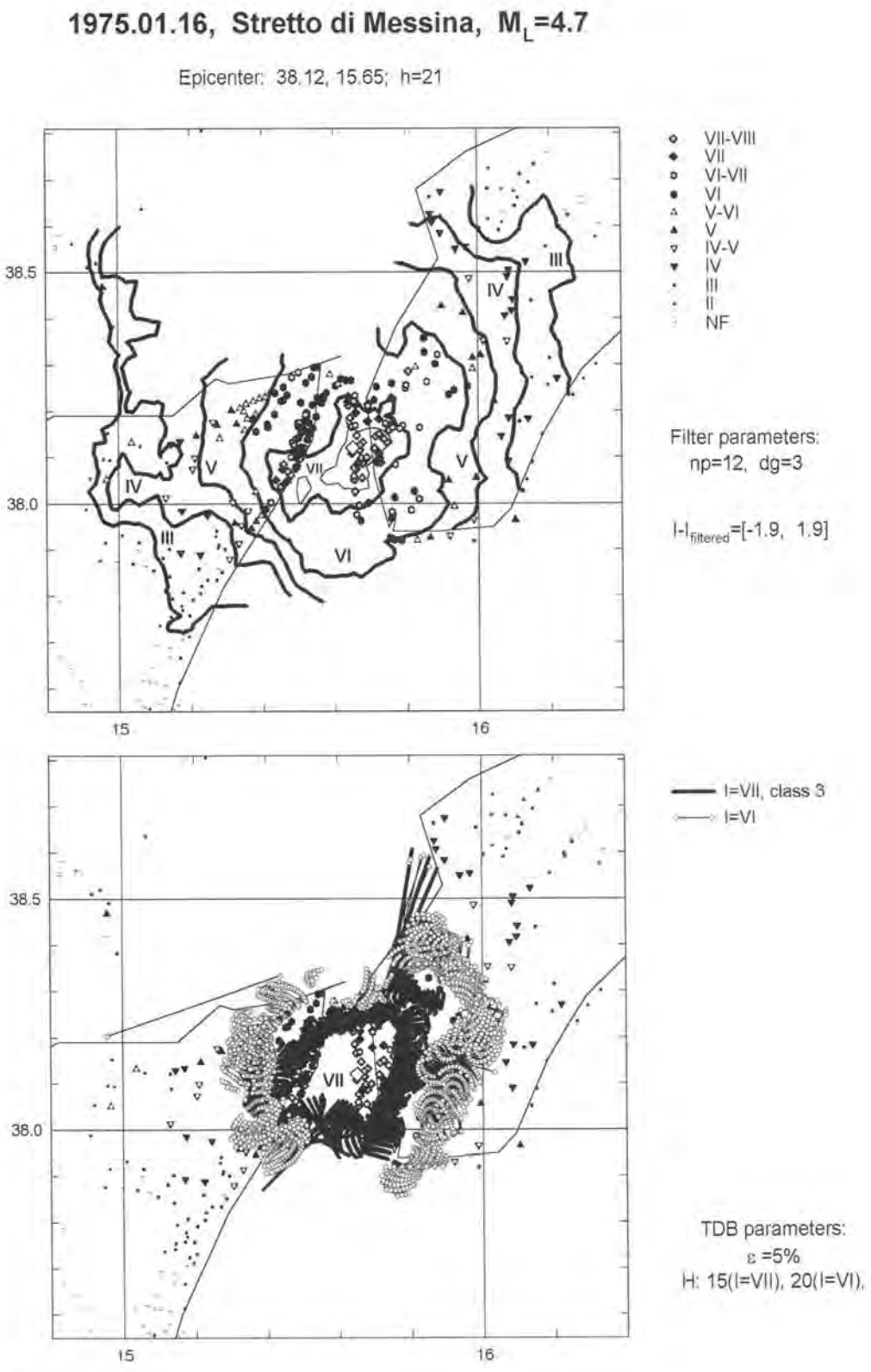
1975.01.16, Stretto di Messina, M_L=4.7
Epicenter: 38.12, 15.65; h=21
VII-VIII
VII
VI-VII
VI
V-VI
V
IV-V
IV
III
II
NF
Filter parameters:
np=12, dg=3
$I-I_{filtered}$=[-1.9, 1.9]
I=VII, class 3
I=VI
TDB parameters:
ε =5%
H: 15(I=VII), 20(I=VI).
38.5
38.0
15
16

Fig. A-39

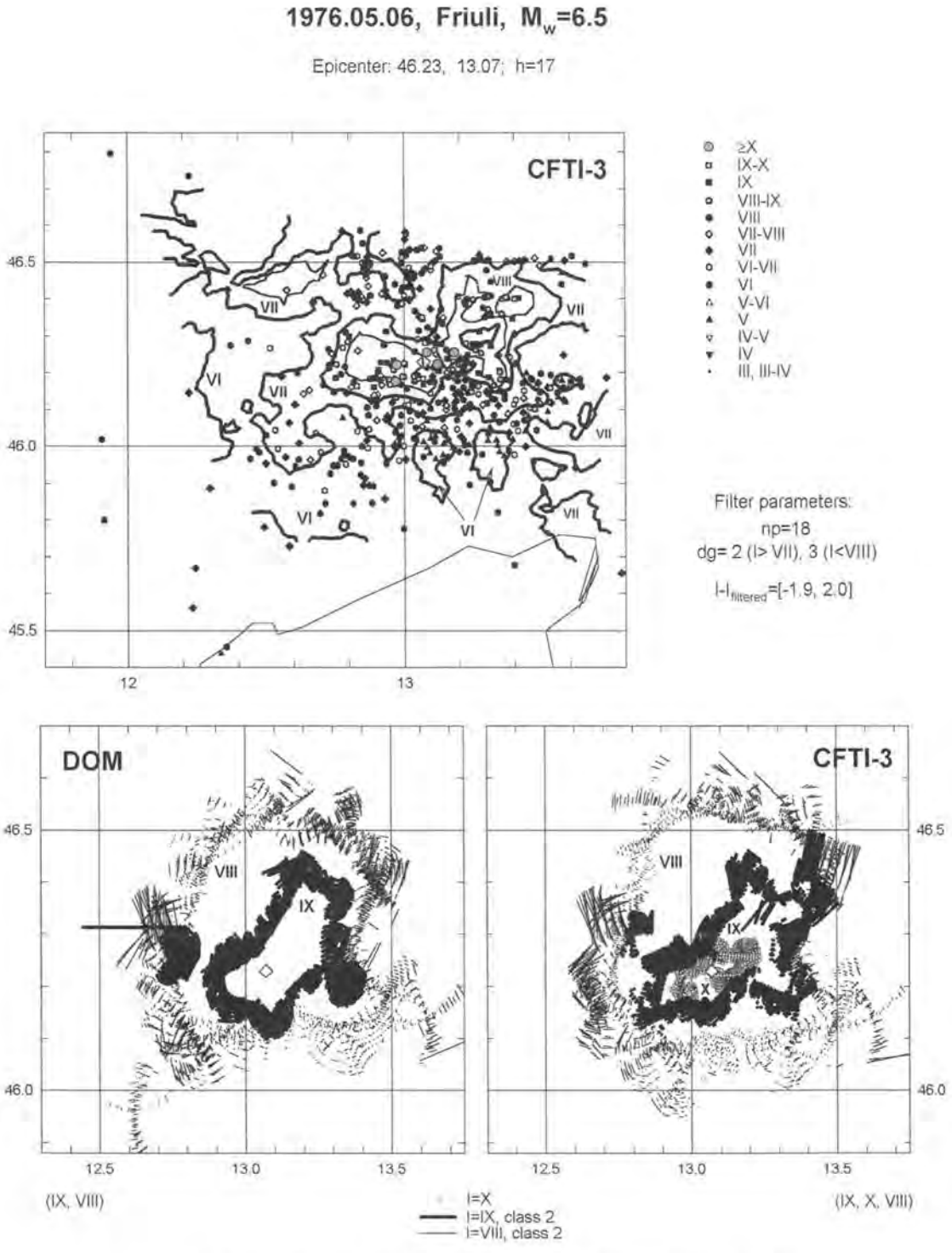
1976.05.06, Friuli, M_w=6.5
Epicenter: 46.23, 13.07; h=17
CFTI-3
≥X
IX-X
IX
VIII-IX
VIII
VII-VIII
VII
VI-VII
VI
V-VI
V
IV-V
IV
III, III-IV
Filter parameters:
np=18
dg= 2 (I> VII), 3 (I<VIII)
$I-I_{filtered}$=[-1.9, 2.0]
46.5
46.0
45.5
12
13
DOM
CFTI-3
12.5
13.0
13.5
(IX, VIII)
(IX, X, VIII)
I=X
I=IX, class 2
I=VIII, class 2
TDB parameters: ε=5% (I=X,IX), 10% (I=VIII), H: 8 (I=X), 10 (I=IX), 20 (I=VIII)

Fig. A-40

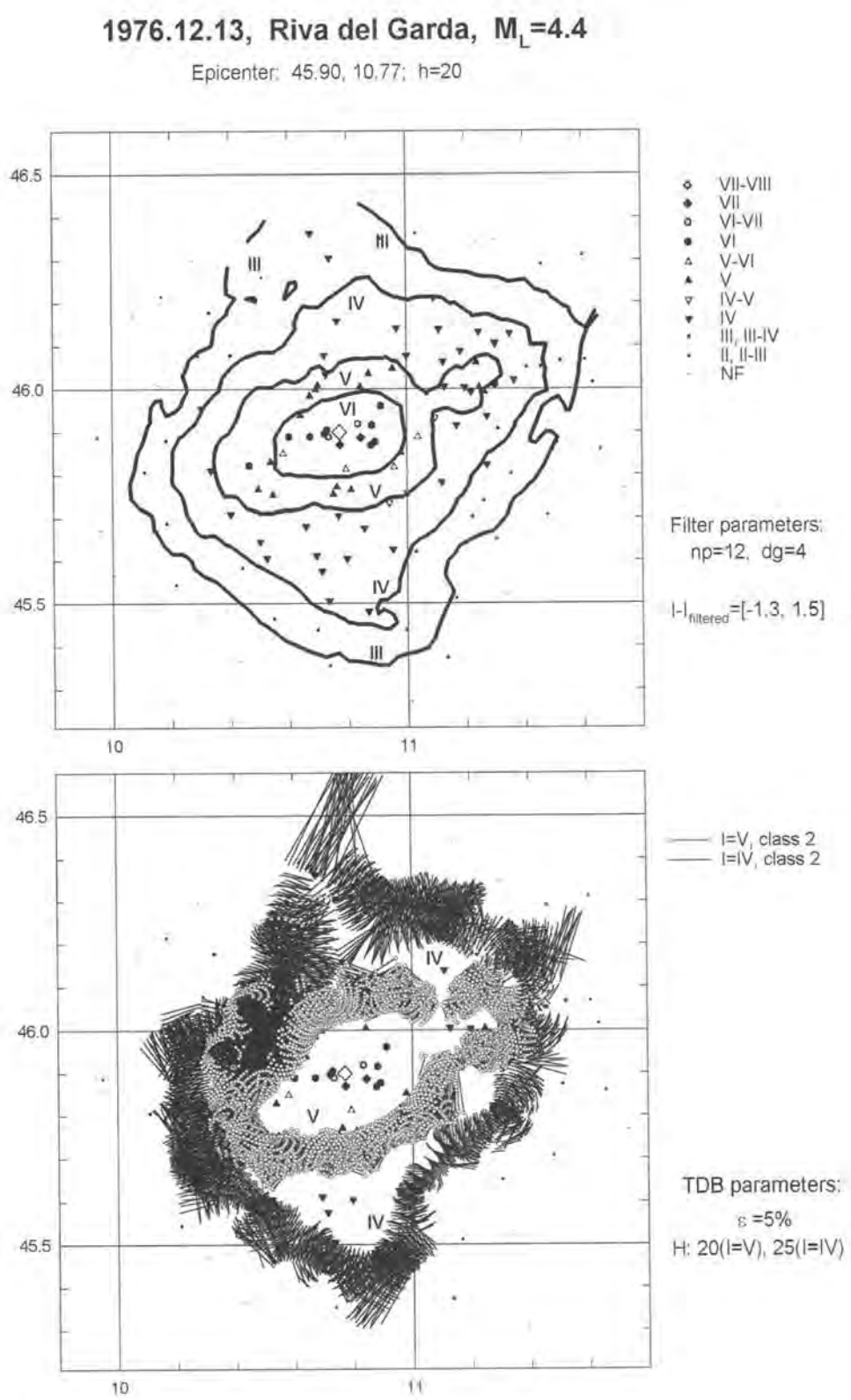
1976.12.13, Riva del Garda, M_L=4.4
Epicenter: 45.90, 10.77; h=20
VII-VIII
VII
VI-VII
VI
V-VI
V
IV-V
IV
III, III-IV
II, II-III
NF
Filter parameters:
np=12, dg=4
$I-I_{filtered}$=[-1.3, 1.5]
I=V, class 2
I=IV, class 2
TDB parameters:
ε =5%
H: 20(I=V), 25(I=IV)
46.5
46.0
45.5
10
11

Fig. A-41

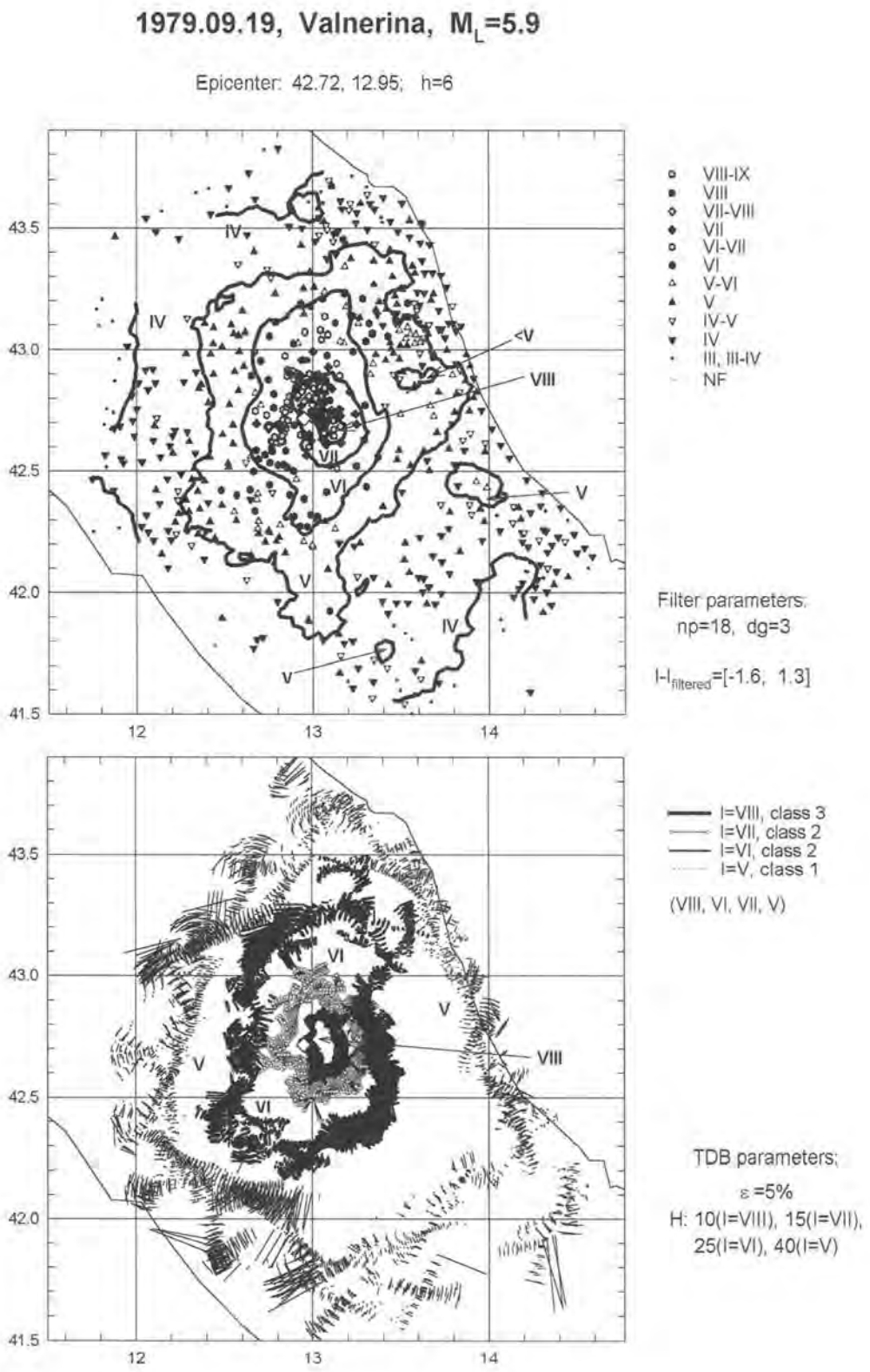
1979.09.19, Valnerina, M_L=5.9
Epicenter: 42.72, 12.95; h=6
VIII-IX
VIII
VII-VIII
VII
VI-VII
VI
V-VI
V
IV-V
IV
III, III-IV
NF
Filter parameters:
np=18, dg=3
$I-I_{filtered}$=[-1.6, 1.3]
I=VIII, class 3
I=VII, class 2
I=VI, class 2
I=V, class 1
(VIII, VI, VII, V)
TDB parameters:
ε=5%
H: 10(I=VIII), 15(I=VII),
25(I=VI), 40(I=V)
43.5
43.0
42.5
42.0
41.5
12
13
14

Fig. A-42

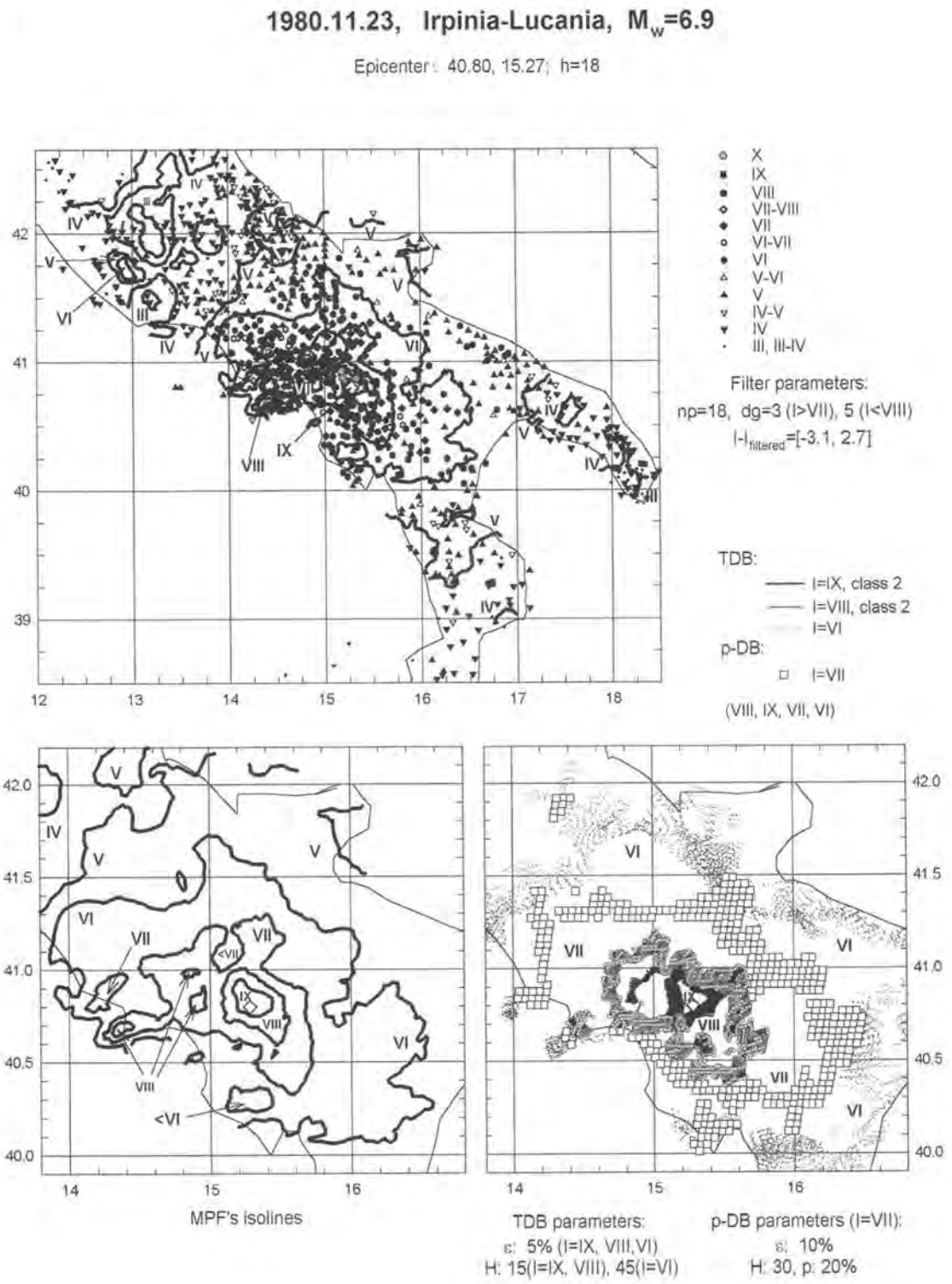
1980.11.23, Irpinia-Lucania, M_w=6.9
Epicenter: 40.80, 15.27; h=18
X
IX
VIII
VII-VIII
VII
VI-VII
VI
V-VI
V
IV-V
IV
III, III-IV
Filter parameters:
np=18, dg=3 (I>VII), 5 (I<VIII)
$I-I_{filtered}$=[-3.1, 2.7]
TDB:
I=IX, class 2
I=VIII, class 2
I=VI
p-DB:
I=VII
(VIII, IX, VII, VI)
MPF's isolines
TDB parameters:
ε: 5% (I=IX, VIII,VI)
H: 15(I=IX, VIII), 45(I=VI)
p-DB parameters (I=VII):
ε: 10%
H: 30, p: 20%

Fig. A-43

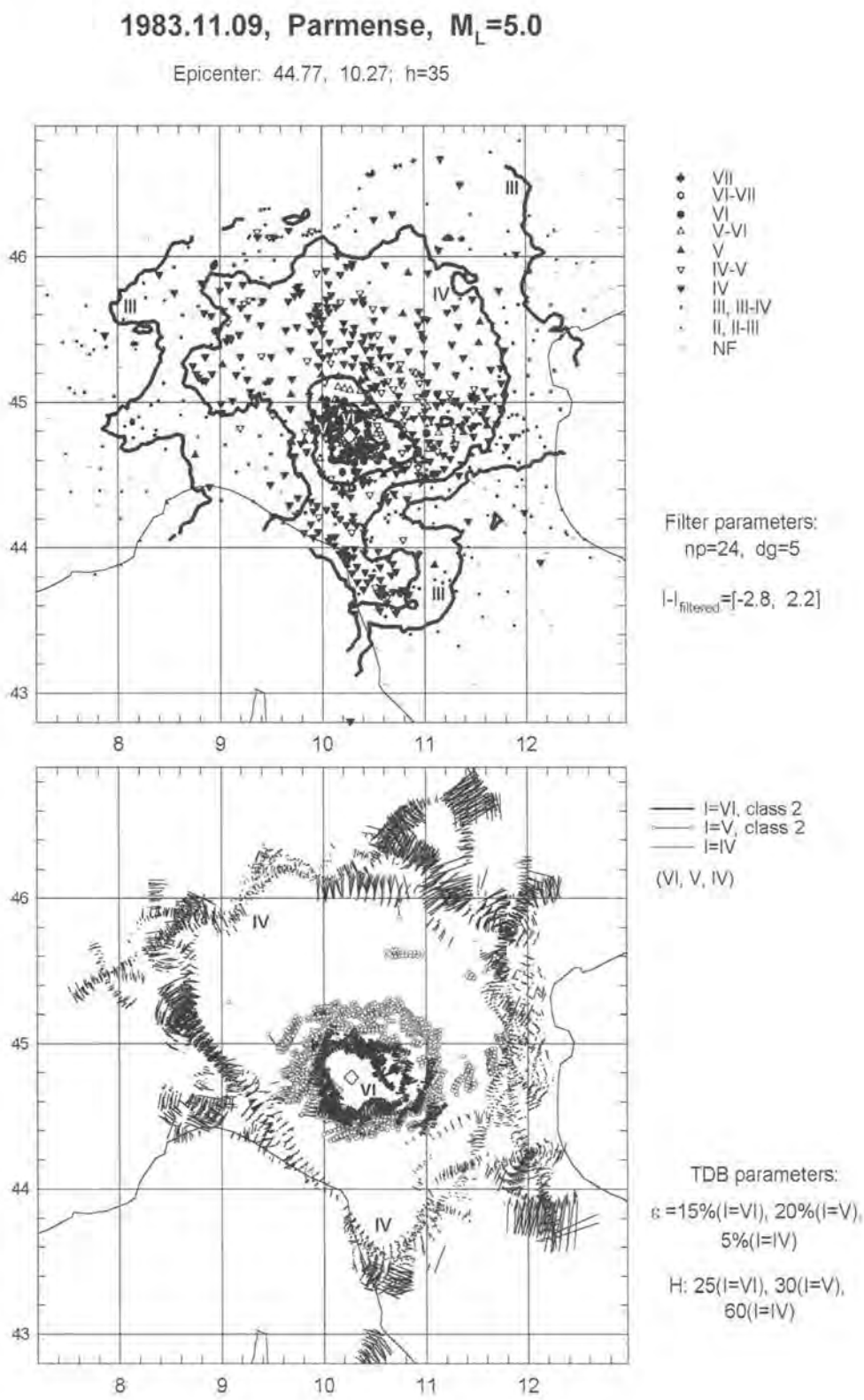
1983.11.09, Parmense, M_L=5.0
Epicenter: 44.77, 10.27; h=35
VII
VI-VII
VI
V-VI
V
IV-V
IV
III, III-IV
II, II-III
NF
Filter parameters:
np=24, dg=5
$I-I_{filtered}$=[-2.8, 2.2]
I=VI, class 2
I=V, class 2
I=IV
(VI, V, IV)
TDB parameters:
ε =15%(I=VI), 20%(I=V), 5%(I=IV)
H: 25(I=VI), 30(I=V), 60(I=IV)
46
45
44
43
8
9
10
11
12

Fig. A-44

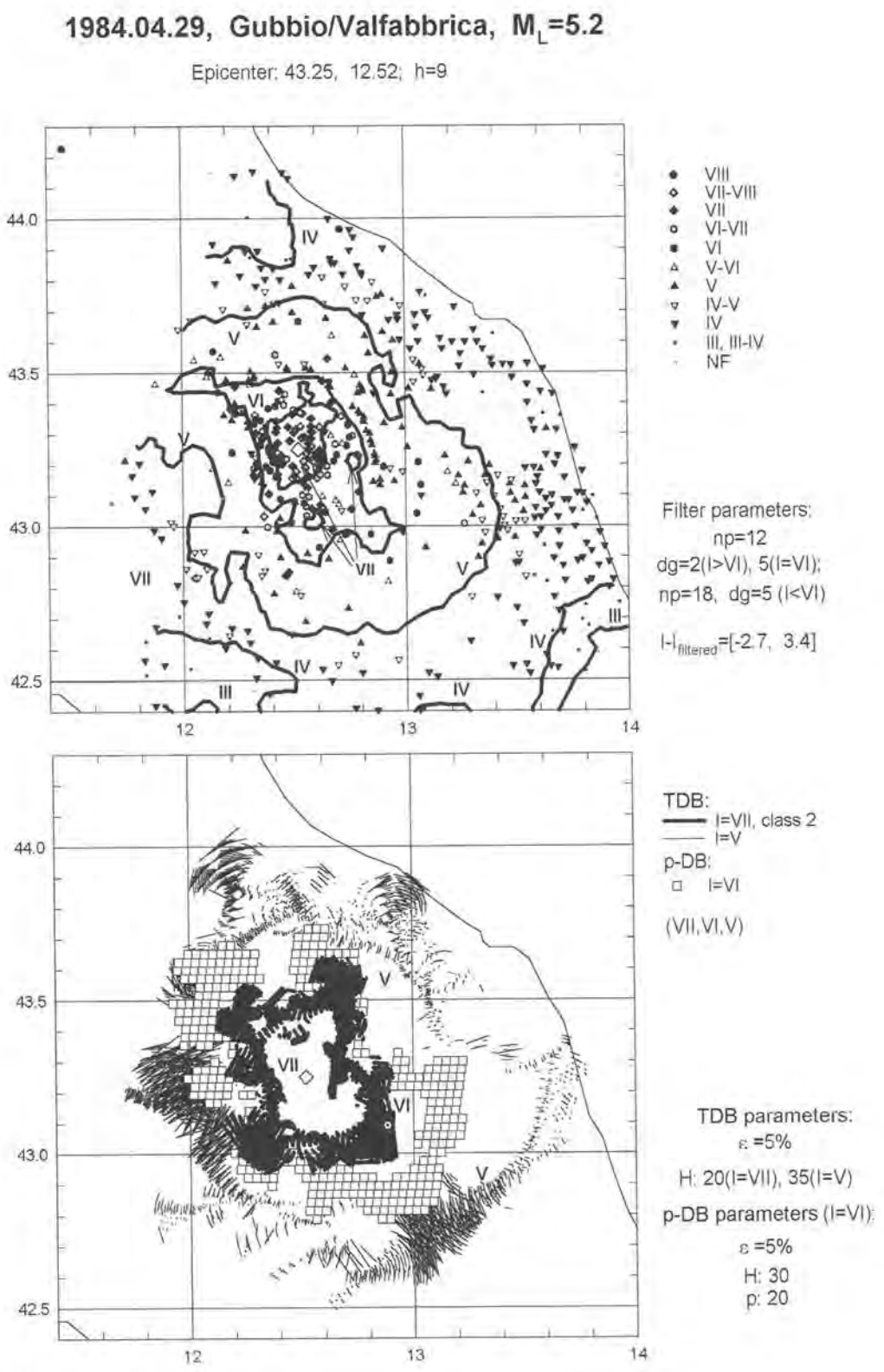
1984.04.29, Gubbio/Valfabbrica, M_L=5.2
Epicenter: 43.25, 12.52; h=9
VIII
VII-VIII
VII
VI-VII
VI
V-VI
V
IV-V
IV
III, III-IV
NF
Filter parameters:
np=12
dg=2(I>VI), 5(I=VI);
np=18, dg=5 (I<VI)
$I-I_{filtered}$=[-2.7, 3.4]
TDB:
I=VII, class 2
I=V
p-DB:
I=VI
(VII,VI,V)
TDB parameters:
ε =5%
H: 20(I=VII), 35(I=V)
p-DB parameters (I=VI):
ε =5%
H: 30
p: 20
44.0
43.5
43.0
42.5
12
13
14

Fig. A-45

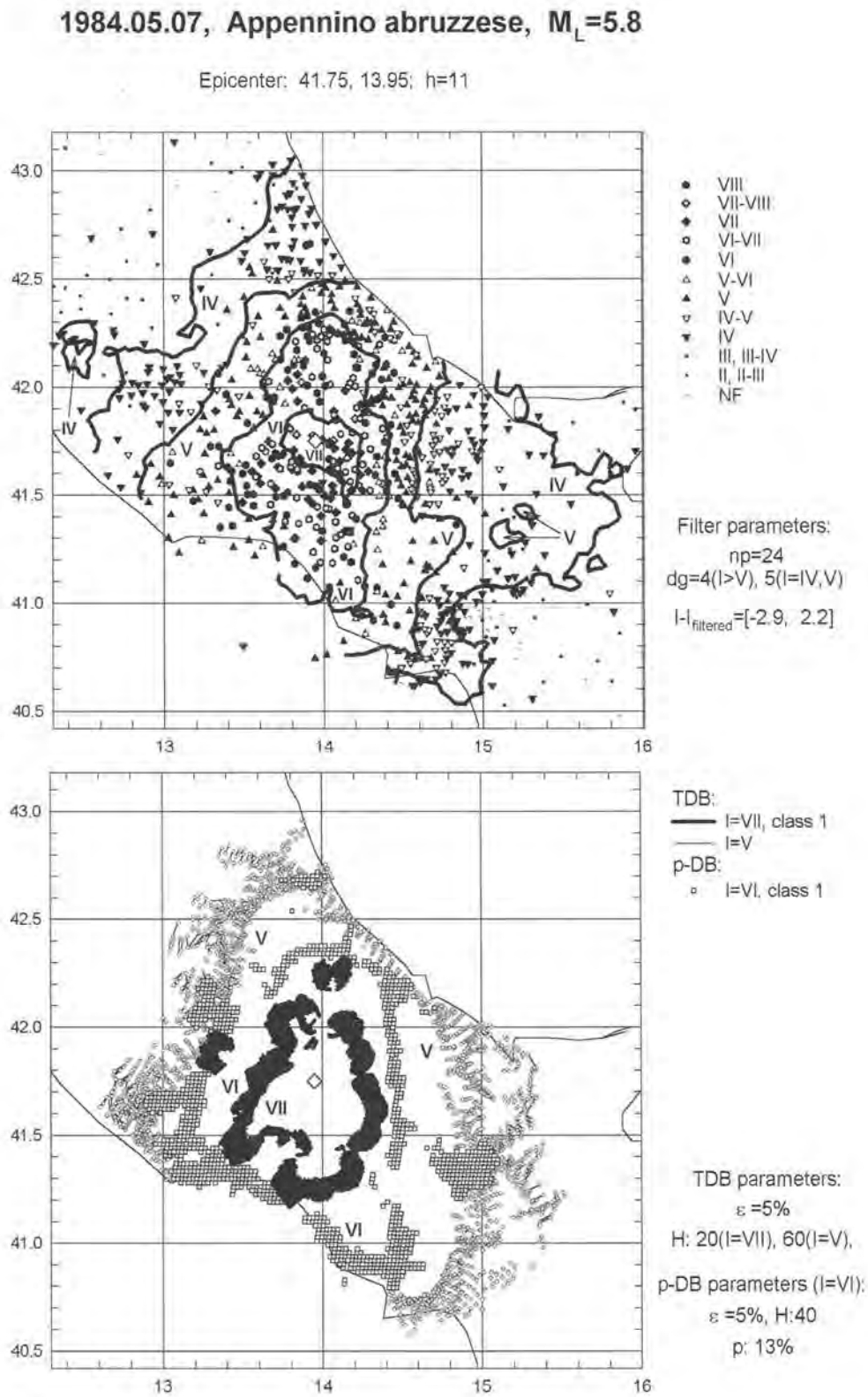
1984.05.07, Appennino abruzzese, M_L=5.8
Epicenter: 41.75, 13.95; h=11
VIII
VII-VIII
VII
VI-VII
VI
V-VI
V
IV-V
IV
III, III-IV
II, II-III
NF
Filter parameters:
np=24
dg=4(I>V), 5(I=IV,V)
$I-I_{filtered}$=[-2.9, 2.2]
TDB:
I=VII, class 1
I=V
p-DB:
I=VI, class 1
TDB parameters:
ε =5%
H: 20(I=VII), 60(I=V),
p-DB parameters (I=VI):
ε =5%, H:40
p: 13%
43.0
42.5
42.0
41.5
41.0
40.5
13
14
15
16

Fig. A-46

1984.05.11, Appennino abruzzese (aftershock), M_L=5.3

Epicenter: 41.70, 14.03; h=10

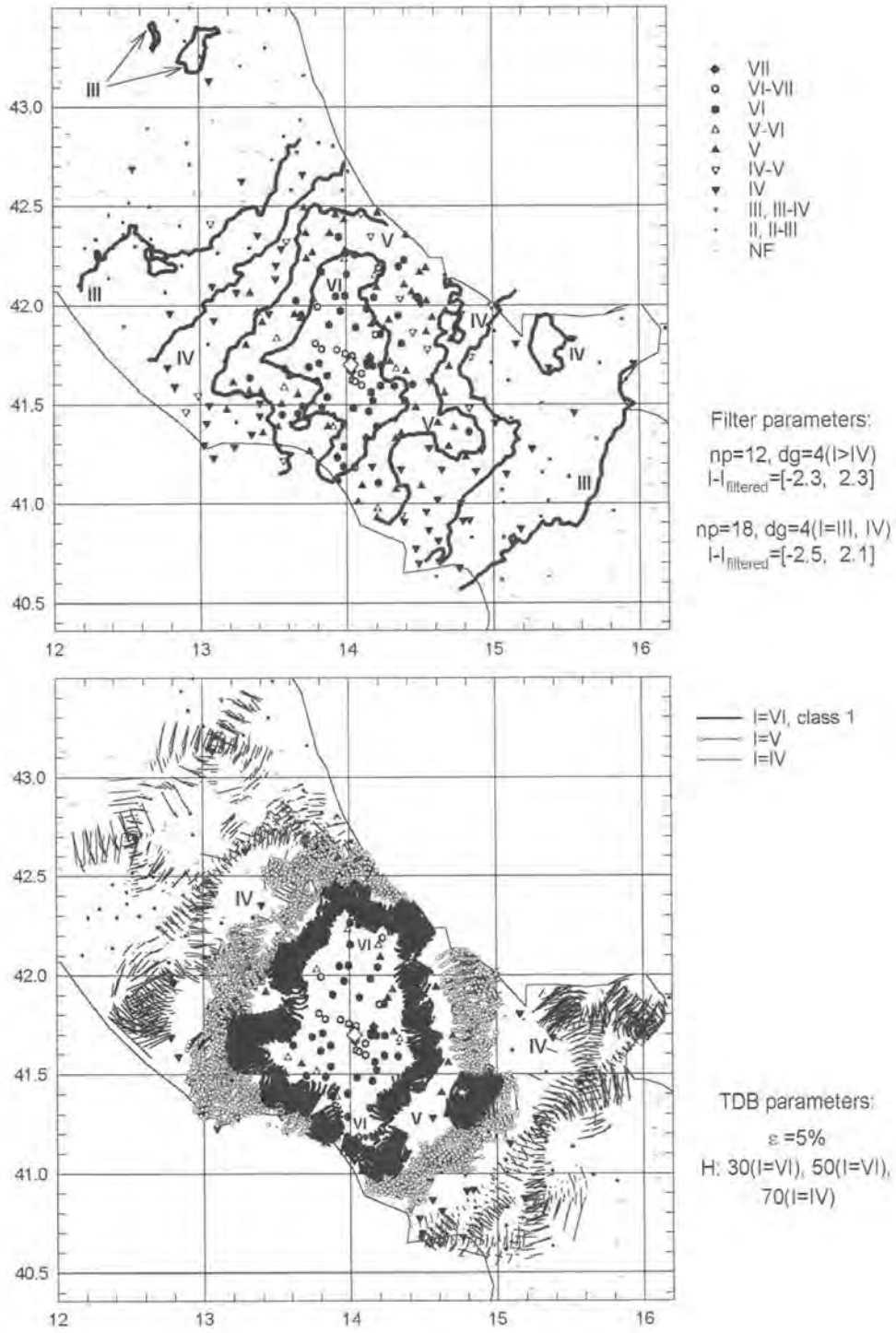

Fig. A-47

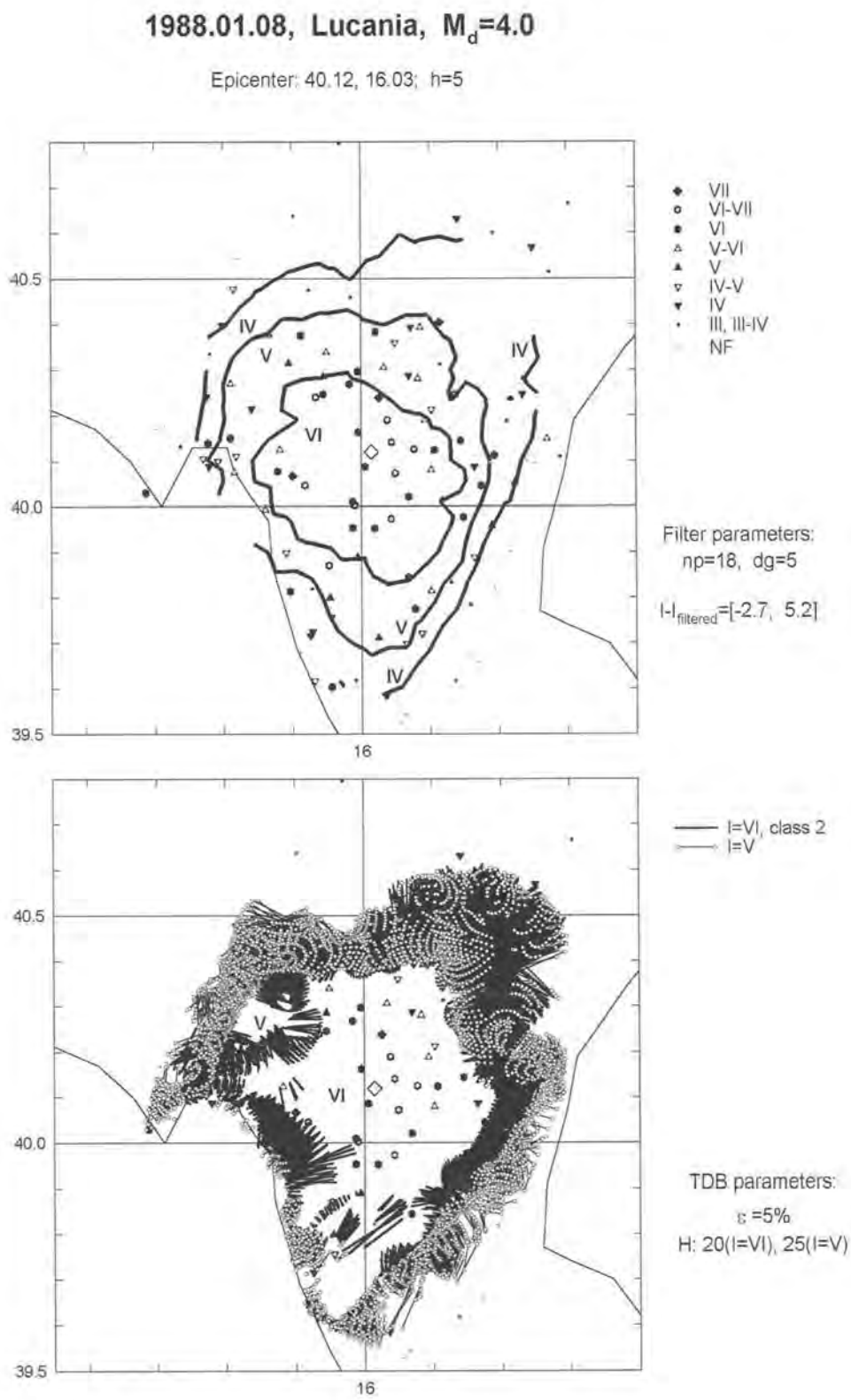
1988.01.08, Lucania, M_d=4.0
Epicenter: 40.12, 16.03; h=5
VII
VI-VII
VI
V-VI
V
IV-V
IV
III, III-IV
NF
Filter parameters:
np=18, dg=5
$I-I_{filtered}$=[-2.7, 5.2]
I=VI, class 2
I=V
TDB parameters:
ε =5%
H: 20(I=VI), 25(I=V)
40.5
40.0
39.5
16

Fig. A-48

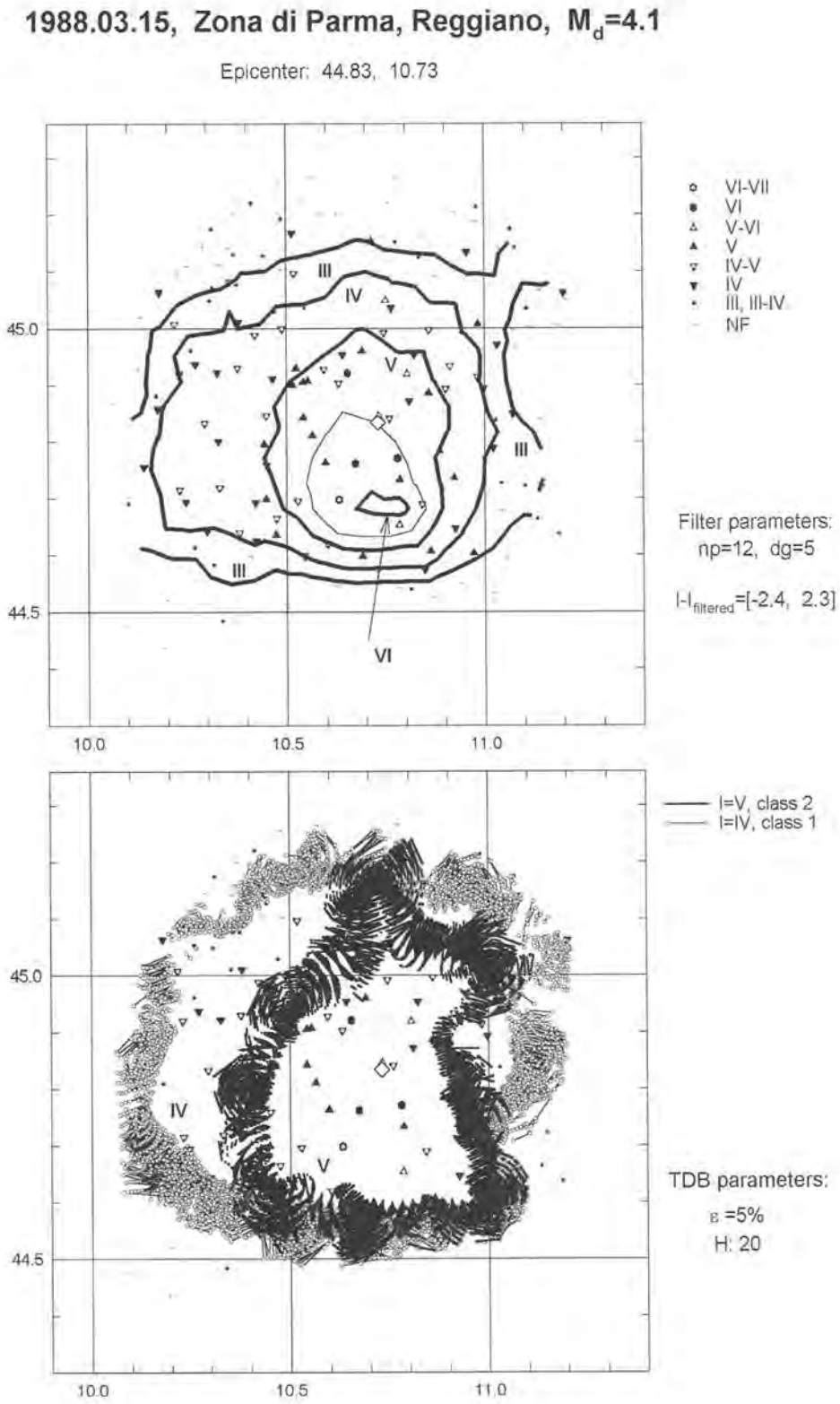
1988.03.15, Zona di Parma, Reggiano, M_d=4.1
Epicenter: 44.83, 10.73
VI-VII
VI
V-VI
V
IV-V
IV
III, III-IV
NF
III
IV
V
III
III
VI
45.0
44.5
10.0
10.5
11.0
Filter parameters:
np=12, dg=5
$I-I_{filtered}$=[-2.4, 2.3]
I=V, class 2
I=IV, class 1
IV
V
TDB parameters:
ε =5%
H: 20

Fig. A-49

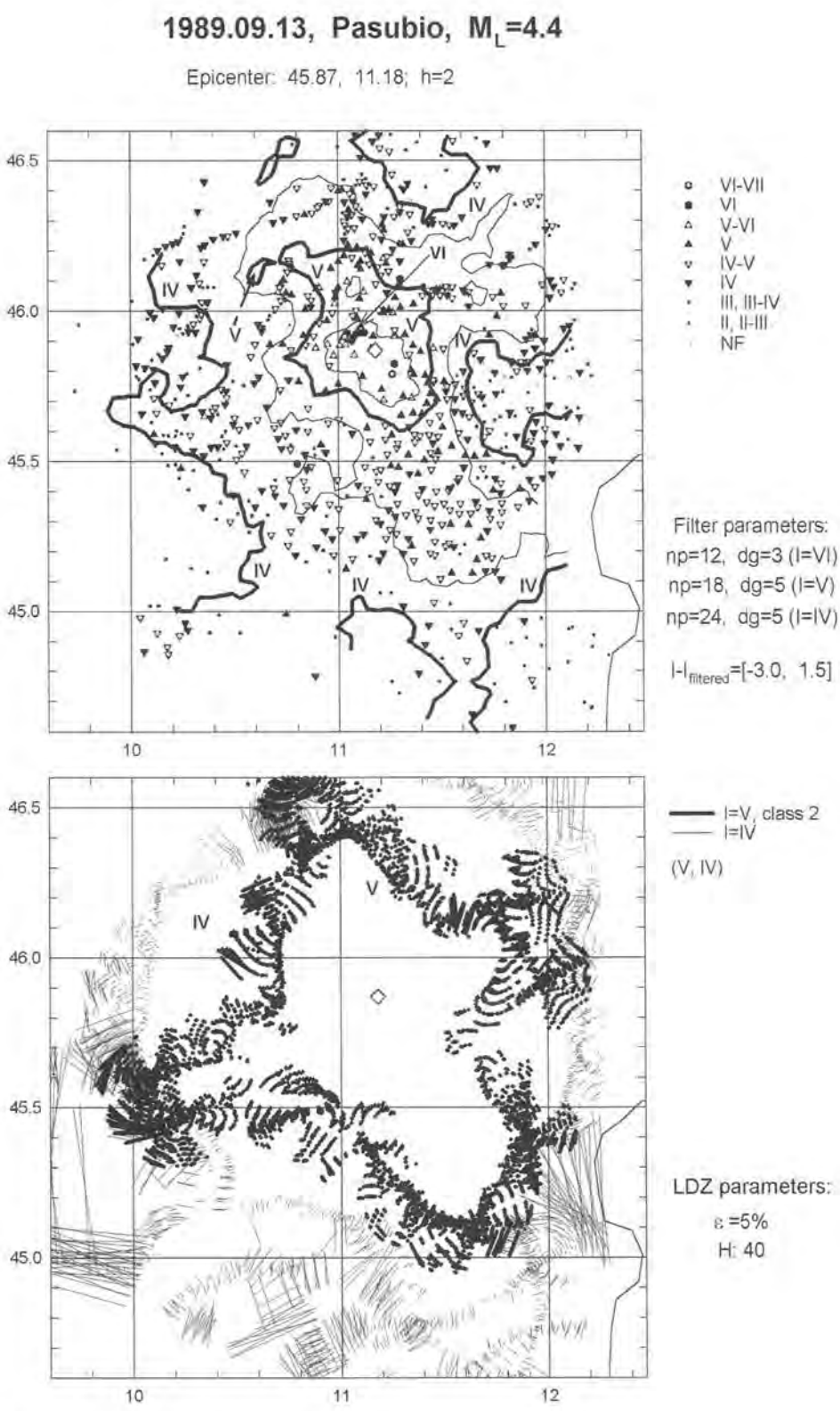
1989.09.13, Pasubio, M_L=4.4
Epicenter: 45.87, 11.18; h=2
VI-VII
VI
V-VI
V
IV-V
IV
III, III-IV
II, II-III
NF
Filter parameters:
np=12, dg=3 (I=VI)
np=18, dg=5 (I=V)
np=24, dg=5 (I=IV)
$I-I_{filtered}$=[-3.0, 1.5]
I=V, class 2
I=IV
(V, IV)
LDZ parameters:
ε =5%
H: 40
46.5
46.0
45.5
45.0
10
11
12

Fig. A-50

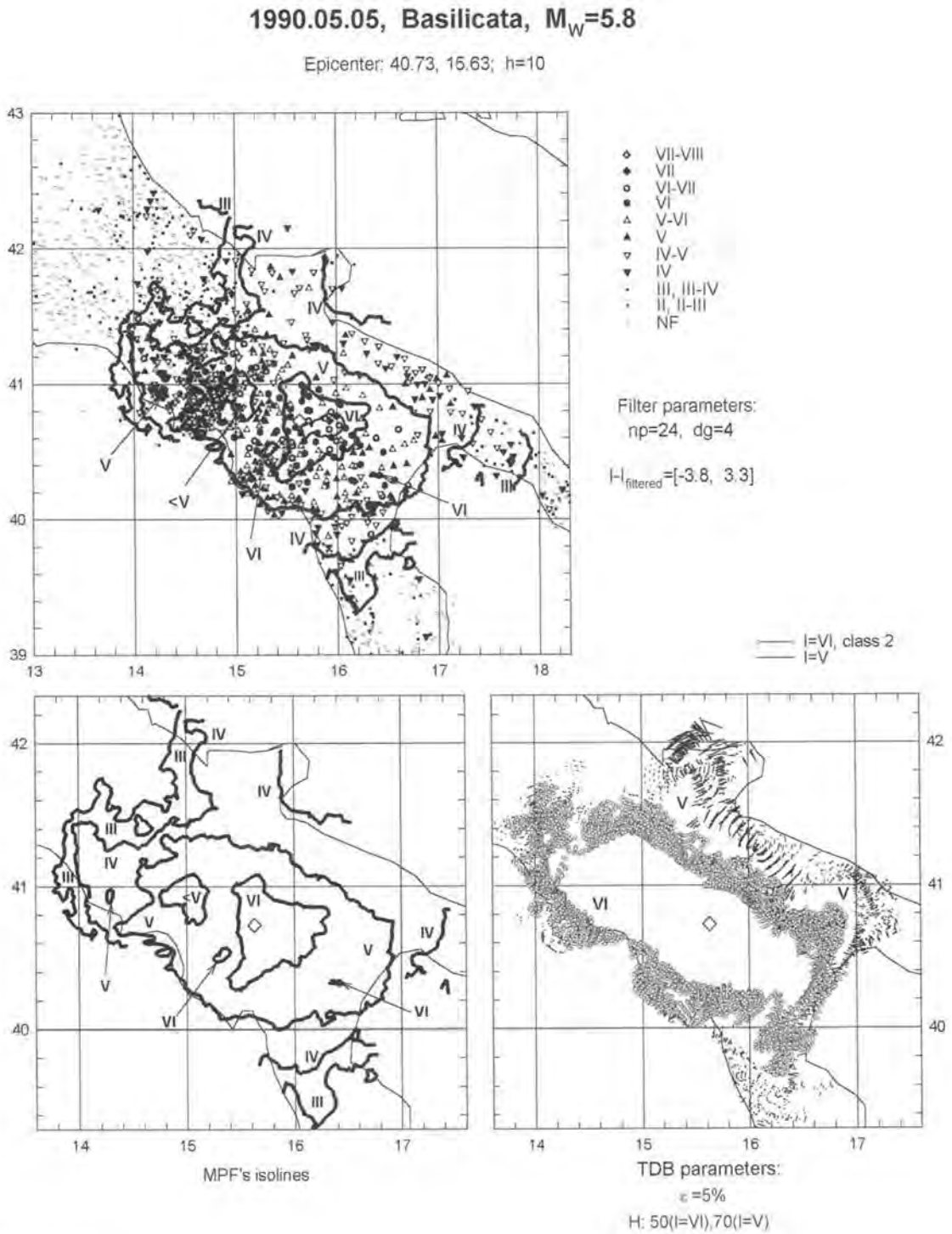
1990.05.05, Basilicata, M_W=5.8
Epicenter: 40.73, 15.63; h=10
VII-VIII
VII
VI-VII
VI
V-VI
V
IV-V
IV
III, III-IV
II, II-III
NF
Filter parameters:
np=24, dg=4
$I-I_{filtered}$=[-3.8, 3.3]
I=VI, class 2
I=V
MPF's isolines
TDB parameters:
ε=5%
H: 50(I=VI),70(I=V)

Fig. A-51

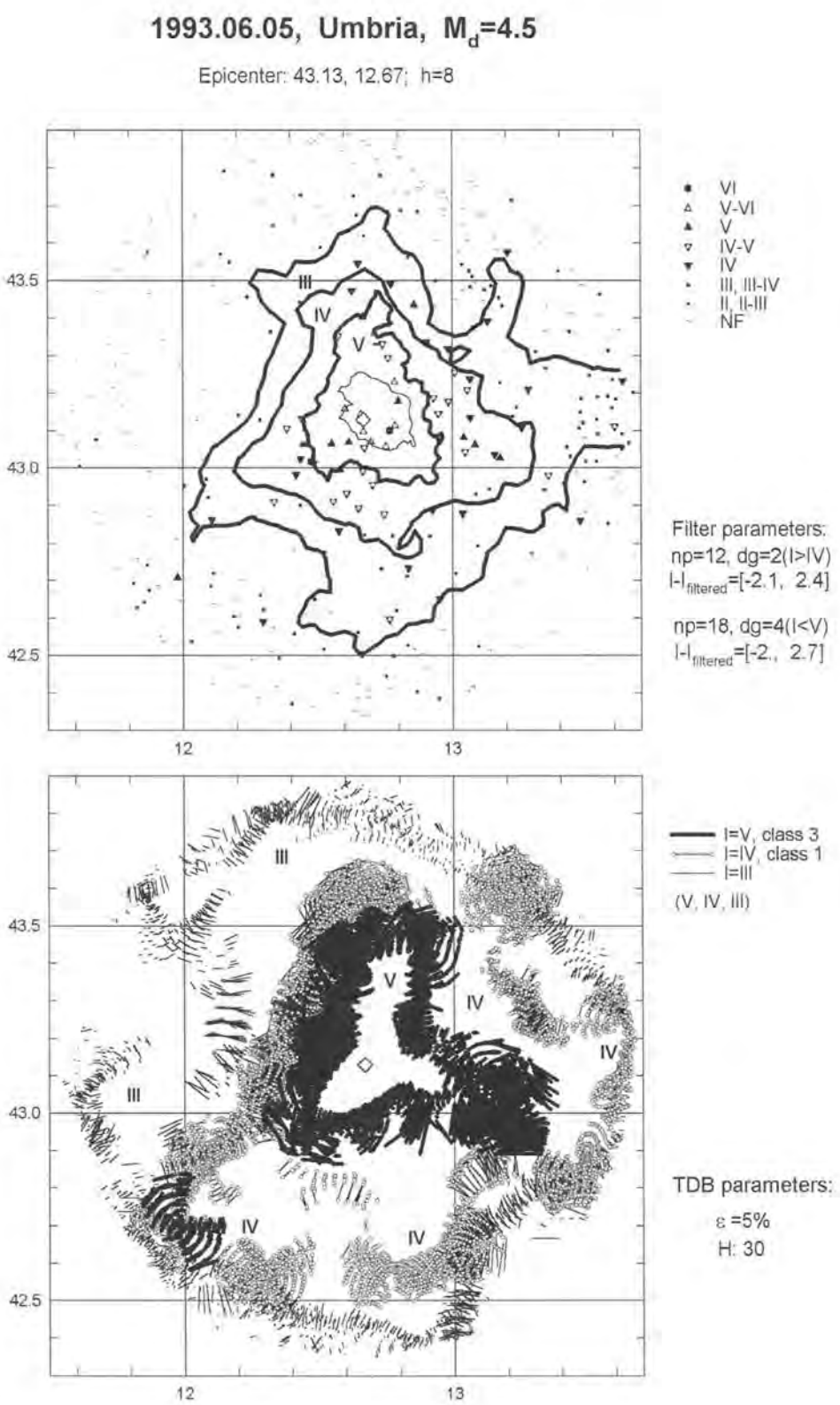
1993.06.05, Umbria, M_d=4.5
Epicenter: 43.13, 12.67; h=8
VI
V-VI
V
IV-V
IV
III, III-IV
II, II-III
NF
Filter parameters:
np=12, dg=2(I>IV)
$I-I_{filtered}$=[-2.1, 2.4]
np=18, dg=4(I<V)
$I-I_{filtered}$=[-2., 2.7]
I=V, class 3
I=IV, class 1
I=III
(V, IV, III)
TDB parameters:
ε =5%
H: 30
43.5
43.0
42.5
12
13

Fig. A-52

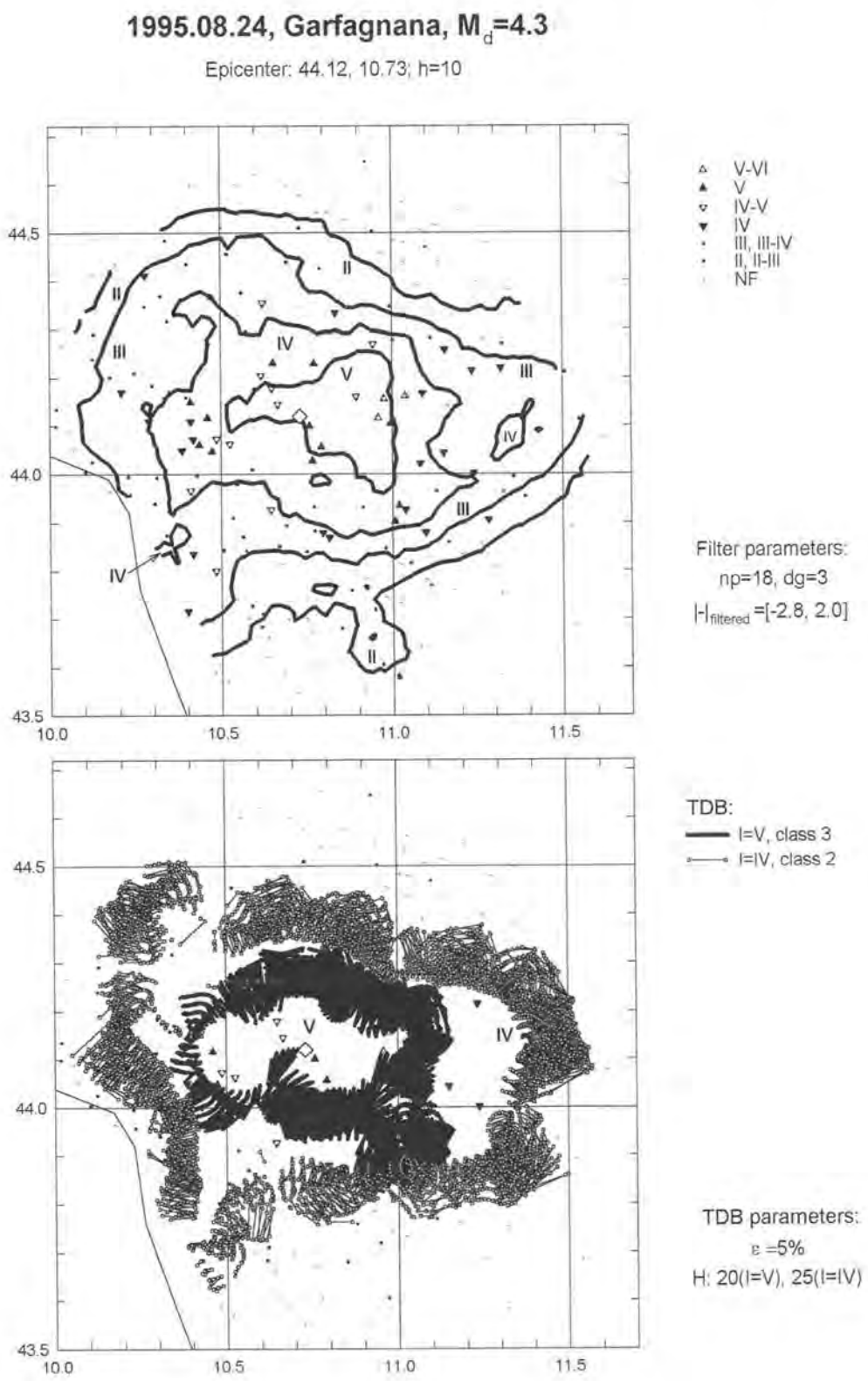
1995.08.24, Garfagnana, M_d=4.3
Epicenter: 44.12, 10.73; h=10
V-VI
V
IV-V
IV
III, III-IV
II, II-III
NF
Filter parameters:
np=18, dg=3
$I-I_{filtered}$=[-2.8, 2.0]
TDB:
I=V, class 3
I=IV, class 2
TDB parameters:
ε =5%
H: 20(I=V), 25(I=IV)
44.5
44.0
43.5
10.0
10.5
11.0
11.5

Fig. A-53

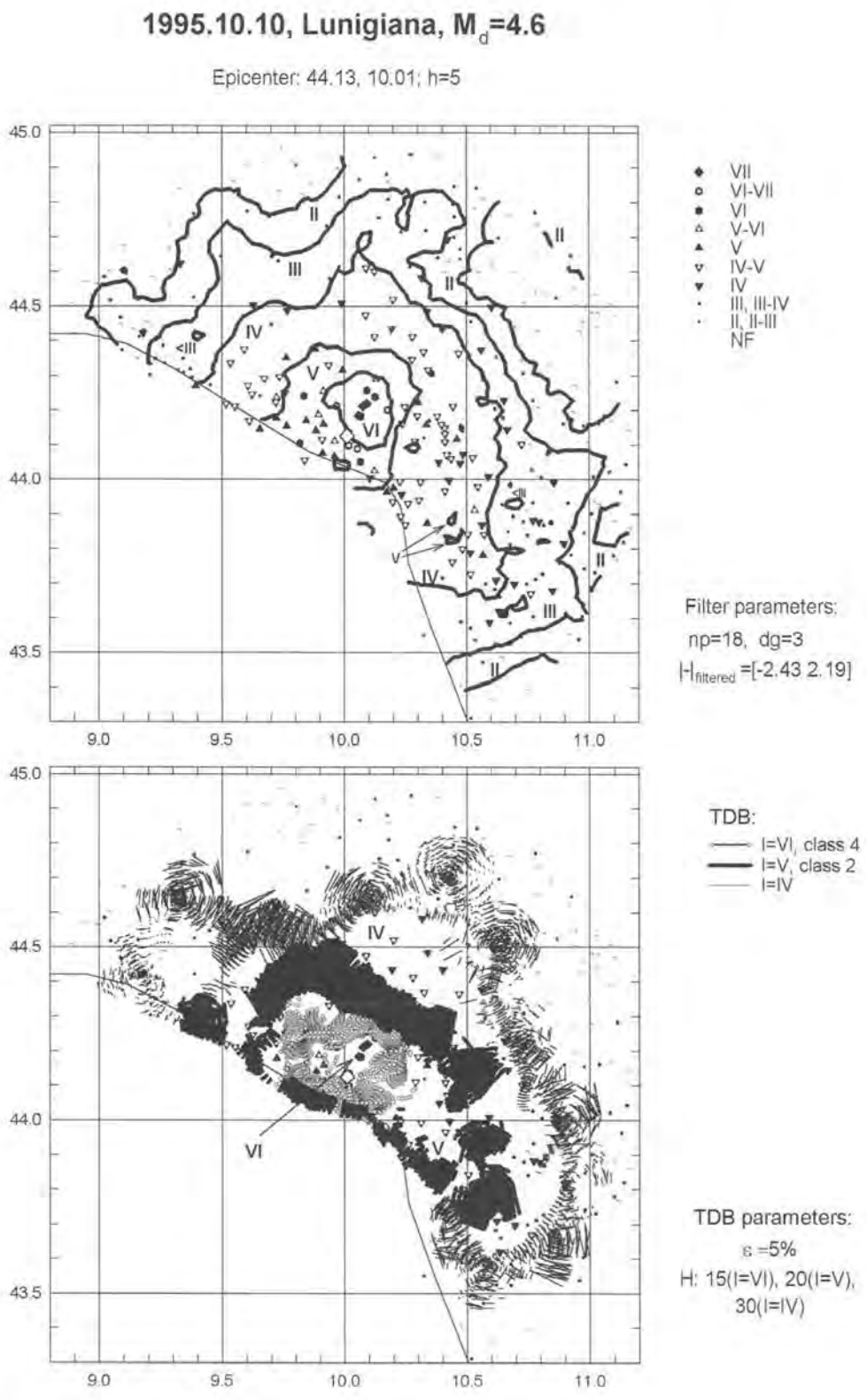
1995.10.10, Lunigiana, M_d=4.6
Epicenter: 44.13, 10.01; h=5
VII
VI-VII
VI
V-VI
V
IV-V
IV
III, III-IV
II, II-III
NF
Filter parameters:
np=18, dg=3
$I_{filtered}$=[-2.43 2.19]
TDB:
I=VI, class 4
I=V, class 2
I=IV
TDB parameters:
ε =5%
H: 15(I=VI), 20(I=V), 30(I=IV)
45.0
44.5
44.0
43.5
9.0
9.5
10.0
10.5
11.0

Fig. A-54

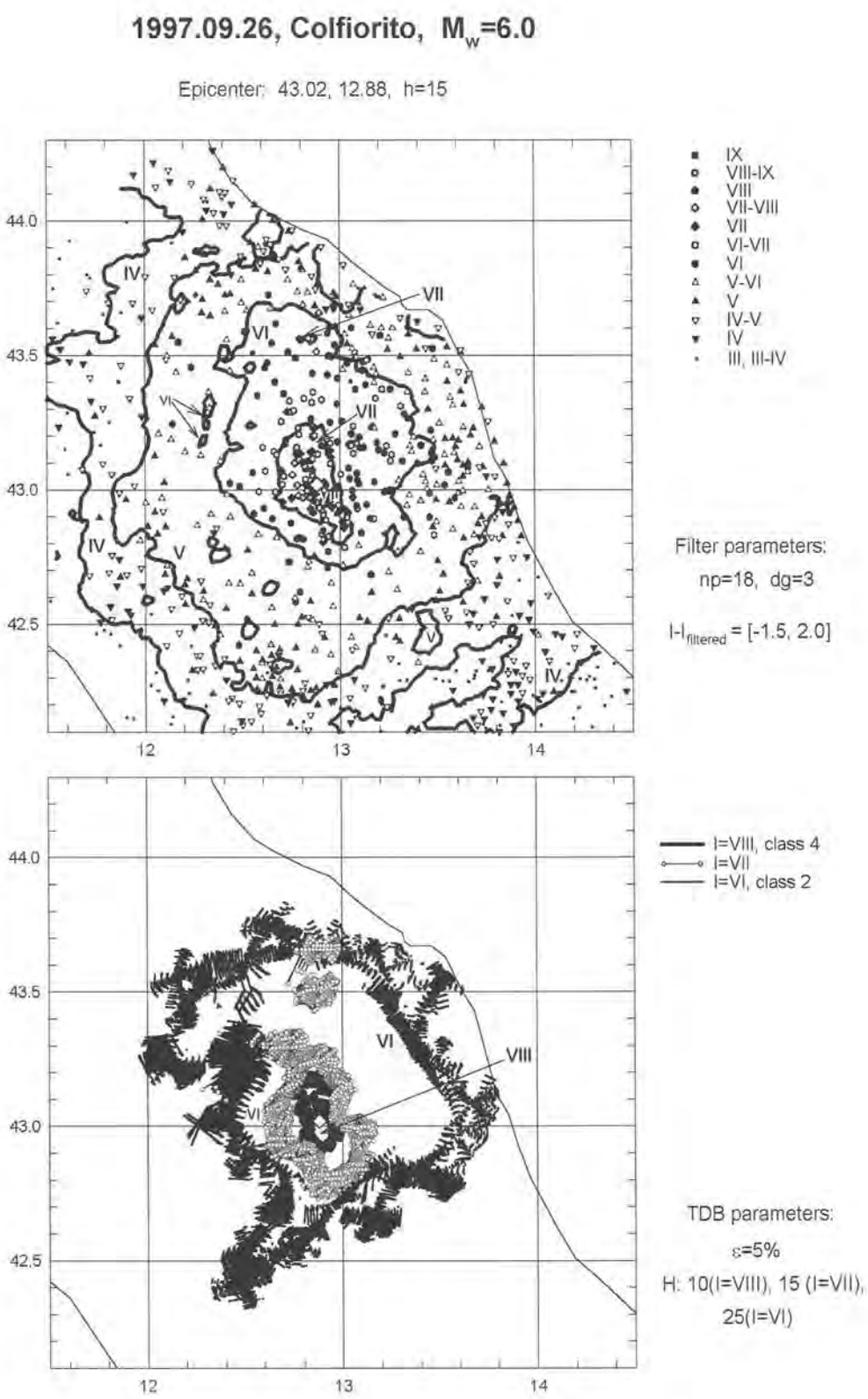
1997.09.26, Colfiorito, M_w=6.0
Epicenter: 43.02, 12.88, h=15
IX
VIII-IX
VIII
VII-VIII
VII
VI-VII
VI
V-VI
V
IV-V
IV
III, III-IV
Filter parameters:
np=18, dg=3
$I-I_{filtered}$ = [-1.5, 2.0]
I=VIII, class 4
I=VII
I=VI, class 2
TDB parameters:
ε=5%
H: 10(I=VIII), 15 (I=VII),
25(I=VI)
44.0
43.5
43.0
42.5
12
13
14

Fig. A-55

References

[BM]: *Bolletino Macrosismico*; 1988-1993. Instituto di Geoficica, Unita Operativa Geodinamica, Roma

Burger R. W., Somerville P. G., Barker J. S., Herrmann R. B. and Helmberger D. V.; 1987: *The Effect of Crustal Structure on Strong Ground Motion Attenuation Relations in Eastern North America.* Bull. Seismol. Soc. Am., **77**, 420-439.

Caputo M., Keilis-Borok V. I., Kronrod T. L., Molchan G. M., Panza G. F., Piva A. and Postpishl D.; 1973: *Models of earthquake occurrence and isoseismals in Italy.* Annali di Geofisica, **26**, 421-444.

Caputo M., Keilis-Borok V. I., Kronrod T. L., Molchan G. M., Panza G. F., Piva A. and Postpishl, D.; 1974: *The estimation of seismic risk for central Italy.* Annali di Geofisica, **27**, 349-365.

[CFTI-2]: Boschi E., Guidoboni E., Ferrari G., Valensise G. and Gasperini P.; 1997: *Catalogo dei Forti Terremoti in Italia dal 461 a.C. al 1990.* ING-SGA, Bologna. 644 pp.

[CFTI-3]: Boschi E., Guidoboni E., Ferrari G., Margotti D., Valensise G. and Gasperini P. (eds); 2000: *Catalogue of strong Italian earthquakes from 461 B.C. to 1997.* Introductory texts and CD-ROM. Annali di Geofisica, **43**, 609-868.

[CMT]: *Harvard Centroid Moment Tensor database,* Harvard Seismology: http://www.seismology. harvard.edu

[CS]: Augliera P., Cattaneo H., Di Giovambattista R., Duri G., Frapiccini M., Gasperini P., Geravasi A., Govoni A., Guerra I., Marchetti A., Marsan P., Milana G., Monachesi G., Moretti A., Moroncelli L., Orlanducci L., Parolai S., Renner G., Spallarossa D., Trojani L. and Vannucci G.; 2001: *Catalogo strumentali dei terremoti 'italiani' dal 1981 al 1996.* CD ROM. INGV-GNDT.

De Rubeis V., Gasparini C. and Tosi P.; 1992: *Determination of the macroseismic field by means of trend and multivariate analysis of questionnaire data.* Bull. Seismol. Soc. Am., **82**, 1206-1222.

[DOM]: Monachesi G. and Stucchi M.; 1997: *DOM 4.1, an intensity data base of damaging earthquakes in the Italian area.* GNDT, http://emidius.itim.mi.cnr.it/DOM/home.html.

Florsch N., Faeh D., Suhadolc P. and Panza G. F.; 1991: *Complete synthetic seismograms for high-frequency multimode Love waves.* Pure Appl. Geophys., **136**, 529-560.

Gasperini P., Bernardini F., Valensise G. and Boschi E.; 1999: *Defining Seismogenic Sources from Historical Earthquake Felt Reports.* Bull. Seism. Soc. Am., **89**, 94-110.

Gusev A. A. and Shumilina L. S.; 2000: *Modeling the intensity-magnitude-distance relation based on the concept of an incoherent extended earthquake source.* Volc. Seis., **21**, 443-463.

Johnston A. C.; 1996:, *Seismic moment assessment of earthquakes in stable continental regions –II. Historical seismicity.* Geophys. J. Int., **129**, 639-678.

Karnik V.; 1969: *Seismicity of the European Area,* Part 1. Reid Publishing Company, Holland.

Molchan G. M., Kronrod T. L. and Panza G. F.; 2002: *Shape analysis of isoseismals based on empirical and synthetic data.* Pure Appl.Geophys. **159** (in press). (See also ICTP, IC/2000/2, Trieste).

[NT411]: Camassi R. and Stucchi M.; 1997, 1998: NT4.1, *un catalogo parametrico di terremoti di area italiana al di sopra della soglia del danno: a parametric catalogue of damaging earthquakes in the Italian area.* http://emidius.itim. mi.cnr.it/NT/home.html

Panza G. F.; 1985: *Synthetic seismograms: the Rayleigh waves modal summation.* J. Geophys., **58**, 125-145.

Panza G., Craglietto A. and Suhadolc P.; 1991: *Source geometry of historical events retrieved by syntethic isoseismals.* Tectonophysics, **193**, 173-184.

[P]; Postpischl D.; 1985: *Catalogo dei terremoti italiani dall'anno 1000 al 1980.* Quaderni della Ricerca Scientifica, 114, 2B, Bologna 1985, 239 pp.

Shebalin N. V.; 1972: *Macroseismic data as information on source parameters of large earthquakes.* Phys. Earth. Planet. Inter., **6**, 316-323.

Sirovich L. and Pettenati F.; 1999: *Seismotectonic outline of South-Eastern Sicily: an evaluation of available options for the earthquake fault rupture scenario.* J. Seismology, **3**, 213-233.

Tosi P., De Rubeis V. and Gasparini C.; 1995: *An analytic method for separating local from regional effects on macroseismic intensity.* Annali di Geofisica, **38**, 55-65.

Wilks S. S.; 1962: *Mathematical statistics.* Wiley, New York, 644 pp.